Naval Oceanographic and
Atmospheric Research Laboratory

Technical Note 50

July 1990

Sea Ice Lead Statistics from Satellite Imagery of the Lincoln Sea during the ICESHELF Acoustic Exercise, Spring 1990

AD-A228 735

DTIC
ELECTE
OCT.2 2 1990
S B D

F. M. Fetterer
A. E. Pressman
Remote Sensing Branch
Ocean Sensing and Prediction Division
Ocean Science Directorate

R. L. Crout
Planning Systems Incorporated
Slidell, Louisiana

These working papers were prepared for the timely dissemination of information; this document does not represent the official position of NOARL.

Abstract

During March and April of 1990, the Naval Oceanographic and Atmospheric Research Laboratory's (NOARL) Remote Sensing Branch collected Advanced Very High Resolution Radiometer (AVHRR) satellite imagery of the Lincoln Sea and Fram Strait in support of the ICESHELF and ICEX acoustic exercises. The Lincoln Sea imagery was analyzed for sea ice lead statistics using a new method based on the Hough transform. Products of the analysis such as lead orientation rose diagrams, lead spacing statistics, and the area covered by leads, are presented here along with the imagery from which the products were derived. Ice motion vectors for three time periods produced by an automated ice motion algorithm are also shown. Imagery of the Fram Strait is included in the appendix.

Acknowledgments

Contents

Accession For

NTIS GRA&I	✓
DTIC TAB	☐
Unannounced	☐
Justification	

By_____
Distribution/

Availability Codes

| Dist | Avail and/or Special |
| | |

A-1

Sea Ice Lead Statistics from Satellite Imagery of the Lincoln Sea during the ICESHELF Acoustic Exercise, Spring 1990

1. Introduction

During March and April of 1990, the Naval Oceanographic and Atmospheric Research Laboratory's (NOARL) Remote Sensing Branch collected satellite imagery of sea ice in the Lincoln Sea and Fram Strait. The collection and analysis of the Lincoln Sea imagery was undertaken in support of the ICESHELF acoustic exercise. This exercise, conducted by the Arctic Acoustics Branch, took place on the ice north of Ellesmere Island, Canada, from approximately 21 March through 21 April. Figure 1 shows the area for which imagery was acquired. The area is approximately 1024 km^2. A 512 km^2 subsection of each image was analyzed for lead statistics.

The involvement of the Remote Sensing Branch in the ICESHELF acoustic exercise is twofold: First, during the exercise, imagery was acquired over the exercise area and facsimiles of the imagery were sent to ICESHELF investigators at Alert, Ellesmere Island, on each day for which a cloud-free image was available. This gave investigators an indication of ice conditions over a broad area surrounding the ice camp. The imagery is presented here along with analysis of the imagery for lead statistics and ice motion. Second, acoustic data acquired during the exercise will be compared with ice parameters derived from the satellite imagery in order to determine if correspondences exist between ice parameters observable in National Oceanic and Atmospheric Administration (NOAA) polar orbiting satellite imagery and acoustic parameters. This will be the subject of a future report.

Another acoustic exercise, ICEX, was under way in April 1990. At the request of ICEX Principal Investigator Dr. Nancy Bedford, the Remote Sensing Branch acquired imagery in the Fram Strait. The imagery was processed at NOARL on the Interactive Digital Satellite Image Processing System (IDSIPS), and then sent via phone link to a PC-based image processing system in Thule, Greenland. Dr. Bedford used the imagery to assist in planning flights for the deployment of sonobuoys. Figure 2 shows the area within which imagery was acquired. The imagery is included in this technical note, although no analysis of the imagery for lead statistics was performed. Flight lines are drawn on the imagery in cases where flight line positions are available.

2. Image processing and analysis method

Satellite imagery from the NOAA polar orbiter's Advanced Very High Resolution Radiometer (AVHRR) was acquired for several weeks both preceding and during the ICESHELF acoustic exercise. AVHRR imagery is available at two resolutions: Local Area

1

Coverage (LAC) imagery has a resolution of 1.1 km at nadir, while Global Area Coverage (GAC) imagery has a resolution about 4 times larger than that of LAC. The acquisition of LAC imagery over an area must be scheduled through NOAA and may not be available on short notice. GAC imagery is available without scheduling, but the relatively poor resolution of GAC imagery makes it unsuitable for resolving small features such as most leads. Coincident LAC and GAC imagery was acquired on 30 March in order to have an example of the degradation in image quality and lead statistics which can be expected if GAC instead of LAC imagery is used. GAC imagery may, however, provide acceptable input for ice motion algorithms. The ice motion algorithm used here was not tested with GAC data because of difficulties in receiving GAC data at NOARL during the experiment time frame.

After the conclusion of ICESHELF, Defense Meteorological Satellite Program (DMSP) Operational Line Scan (OLS) film data were obtained at NOARL for the time period, 09-14 April 1990. A cursory analysis of the data indicated total cloud cover in the ICESHELF area. This analysis supports the results of the NOAA survey which also indicated no useful imagery during the same time period due to cloudy conditions.

During the acoustic exercise, a hard copy of each day's LAC image was examined to see if the image was sufficiently cloud free to warrant processing. Processing on IDSIPS entails mapping the image to a polar stereographic projection and calibrating the image. Most images then received further analysis for lead statistics. Table 1 is a list of all Lincoln Sea imagery examined for possible use with the date and time of acquisition, data type (LAC or GAC), an indication of whether the image was processed for lead statistics, and some comments concerning image quality. All imagery is NOAA AVHRR channel 4 infrared imagery.

Analysis for lead orientation is performed using a Hough transform technique presently under development. The technique is described briefly in a following section and more thoroughly in the appendix. In addition to lead orientation, an analysis is made of lead spacing and the area covered by leads (fractional area coverage) in each image using software developed at NOARL.

The lead analysis products depend upon the preliminary creation of a binary image in which lead pixels are white and all other pixels are black. The pixels are classified by applying a brightness threshold which is chosen interactively. Open water or thin ice in leads causes leads to appear brighter or warmer than the surrounding ice. There are several difficulties with this technique for classifying lead pixels. First, because the resolution of LAC imagery is 1.1 km at best, only the largest leads will be resolved. There are many more small leads than there are large leads. The distribution and orientation of small leads may follow that of large leads, but further research into this issue is necessary. Furthermore, the radiometric signature of a narrow lead with open water may be identical to that of a

2

wider lead with thin ice. Therefore the width of a lead and whether or not it is ice covered cannot be judged by this method. Also, a threshold chosen for one image may not be ideal for another image. This is because in some scenes transparent clouds through which leads are visible make it necessary to boost the threshold. Most importantly, choosing a threshold interactively means that results will depend to some extent upon the operator. For these reasons, the lead analysis products in this technical note are not suitable for studies such as heat flux calculations in which precise measurements are necessary. However, information on gross lead orientation, spacing, and area coverage is given by the products. Efforts are under way to find an automated method of creating a binary lead image, and to determine the error inherent in each product.

The products which can be derived from each image are described below in the order in which they are presented in section 3. A brief explanation of how each product is created is included. All images are processed on the International Imaging Systems (IIS) image processor. Products created from the Lincoln Sea imagery for this data report are:

1. Enhanced image with latitude, longitude grid and land mask;
2. Binary image of leads;
3. Binary image with land and cloudy areas removed;
4. Rose plots of lead size versus lead orientation;
5. Table of lead size versus lead orientation;
6. Table of lead spacing and width for compass directions between 0 and 180°;
7. Grey level image in which brightness represents the area covered by leads.

Enhanced image with latitude, longitude grid and land mask

Each image is mapped to a polar stereographic projection with the position of least distortion at the 512 km^2 area center. The Central Intelligence Agency world coastline data base is used to create a land mask for the northern parts of Greenland and Ellesmere Island which appear in the area. The CIA data base is inaccurate by several km in this area. The land mask is applied to match the coast of Ellesmere Island, which results in the mask being shifted several km to the east of its proper position over north Greenland. Images are enhanced through the application of a Wallis filter. The Wallis filter modifies the image by normalizing the histogram of image intensity within a window which is moved across the image. The result is improved contrast and the enhancement of leads.

Binary image of leads

A binary image is created by first applying a Wallis filter to the original image using a 5 x 5 pixel window. This enhances the contrast between leads and background, and removes overall

differences in image brightness from one part of the image to another, making the application of a global (single) threshold possible. A threshold is then chosen interactively by lowering the threshold until most of the visible leads are included. Lowering the threshold too far results in the inclusion of spurious single pixel points or "noise" over much of the image.While the technique used to obtain lead orientation is relatively insensitive to noise, lead area coverage is obtained by simply counting the number of white or "lead" pixels. Therefore lead area results can be substantially biased by the inaccurate classification of lead pixels in the binary image. To minimize inconsistency in results, a single person created all binary images. An automated method of creating binary images is under development.

Binary image with land and cloudy areas removed

Methods commonly used for masking clouds in infrared images of the ocean (e.g., removing all pixels cooler than some threshold) are not successful over ice-covered seas, where clouds may be either warmer or cooler than underlying ice. Clouds are often distinguishable from leads only by their shape. Clouds and land are therefore removed from binary images by applying a 64 x 64 pixel grid to the image, and simply making blank those grid elements (or blocks) in which clouds or land appear. Figure 3 shows the grid blocks. One advantage of this method is that lead statistics within a given block on different days can be compared. It is also clear exactly what part of each image is being analyzed, since there is no ambiguity between a cloudy area and an area with no leads, as there would be if clouds were masked in their irregular form. A function, CLOUDMASK, was written to allow cloudy blocks to be removed interactively with a trackball on the IIS image processor. The original and the binary image can be flickered underneath the grid. Grid size can be varied if desired.

Rose plots of lead size vs. orientation

Lead orientation is obtained within each 64 x 64 pixel block of a cloud-free binary image using the Hough transform. It is assumed that leads can be represented by straight lines. The Hough transform technique automatically finds lines and their orientation, as well as the number of pixels along each line. A FORTRAN program computes the Hough transform of each lead point in each binary 64 x 64 pixel grid block. Results are stored in an accumulator array in which the columns represent lead orientation in degrees from vertical, and rows represent the normal distance from a lead line to the image origin. The value of an element in the accumulator array is equal to the number of pixels in a lead line, where the line is defined by orientation and normal distance. Because each column in the accumulator array has the size of a lead with that column's orientation, the accumulator array can be used to create a rose plot of lead size for orientations between 0 and $180°$. The length of the

4

vector on the rose plot indicates the size of a lead with the given orientation. If there are two or more leads with the same orientation, the length of the vector will be the sum of their areas. On the rose plots, the outer-most ring is equal to 200 km^2. An inclination of 0° with respect to vertical in the image is at the top of the rose plot, and that of 90° or horizontal is at the right of the rose plot. The appendix contains more information on the Hough transform and its application here.

Table of lead size vs. lead orientation

The IIS function 64PROSE, which produces the rose plots described in the previous paragraph, also produces a data file or table of lead size vs. orientation. The table includes only those leads covering an area greater than 50 km^2. The table is arranged by block number, where the block number refers to the 64 x 64 pixel blocks shown in figure 3.

Table of lead spacing and width for compass directions between 0 and 180°

Lead spacing and width statistics are obtained for each cloud-free binary image by passing a "comb" of 64 lines through the image, and finding the average spacing between encounters with leads along each line of the comb, after the method of Arctic Analysts Inc. (1988). The comb is rotated through 180° in steps of 15°, in order to obtain lead spacing as a function of compass direction (Fig. 4). Results are presented in a table which shows the number of times leads are crossed by the lines in the comb at a given comb orientation, the mean spacing between leads for that orientation in km, the standard deviation for that orientation, the mean lead width, and the standard deviation of the width. Because of the relatively coarse resolution of the AVHRR, most leads appear either 1 or 2 km wide. Therefore the width measurement is somewhat meaningless. A FORTRAN program entitled Leadstats creates the table of spacing and width statistics.

Grey level image in which brightness represents area covered by leads

This product gives a quick visual impression of the areas of an image in which lead density or lead size is greatest. It is obtained using IIS function GREYLEADS, which simply finds the percentage of each 64 x 64 pixel block which is covered by white pixels in the cloud-free binary image. That block in which the area covered is greatest is then given a grey level intensity of 512, and all other blocks are mapped to an intensity between 0 and 512 depending upon the fractional area coverage of leads within each block.

3. Imagery and products

The figures and tables beginning with figure 5 show imagery and derived products for the dates listed below:

    18 Mar 90
    19 Mar 90
    20 Mar 90
    20 Mar 90 GAC
    30 Mar 90
    30 Mar 90 GAC
    03 Apr 90
    07 Apr 90
    15 Apr 90
    17 Apr 90

Imagery is LAC unless noted as GAC.

4. Products for subareas of images

Lead spacing and orientation can be obtained for distinct areas within a binary image. Figure 45 shows two areas within the 19 March 90 binary image. Area 1 has more small leads than area 2. This is reflected in the spacing statistics for areas 1 and 2 shown in Table 23. The mean spacing between leads is, on average, somewhat less in area 1. Rose plots of lead size vs. orientation for the two areas are shown in Figures 46a and 46b. Note that there are fewer leads in area 2 and almost none have a near-horizontal orientation.

5. Ice motion

Ice motion vectors are obtained automatically for an image pair using a cross correlation technique. The ice motion algorithm is based on the work of Ninnis et al. (1986). Vectors are computed on a 10 km grid. Confidence in a resulting vector is given by its correlation coefficient. If the coefficient falls under a set value, the vector is not drawn. The algorithm does not distinguish between clouds, ice, and land. Vectors which differ from their neighbors in magnitude or orientation by more than a given amount are filtered from the result.

Three sets of image pairs are appropriate for the ice motion algorithm. Ice motion in the Lincoln Sea, as elsewhere in the Arctic basin, depends to a large extent upon wind speed and direction. On average, the pack ice moves from west to east along the north coast of Greenland and exits the Arctic basin through the Fram Strait. The 30 March to 03 April image pair reflects this (Fig. 47), as does the 03 to 07 April pair (Fig. 48). Shorefast ice extends from the coast about 80 km; north of the shorefast ice motion is to the east at about 5 km per day. The 15 to 17 April image pair (Fig. 49) shows little or no ice motion. This is consistent with the Polar Ice Prediction System (PIPS) model wind and ice motion vector output for this time frame (see next section). Vector error of a few pixels may be caused by errors in mapping images to a projection. This leads to inaccurate registration of an image pair.

6. PIPS model wind and ice velocity vectors

PIPS is an operational, dynamic/thermodynamic ice forecasting mouel run daily at the Fleet Numerical Oceanography Center. The PIPS model is forced by geostrophic winds computed from surface pressure fields, by geostrophic ocean currents, and by ocean heat fluxes. For more information on PIPS, see Preller and Posey (1989). PIPS model ice and wind velocity vectors provided by Dr. Ruth Preller, NOARL Code 322, are included here as a supplement to motion vectors from AVHRR images. Plots (Figs. 50, 51, and 52) show predicted wind and current velocity on each day within intervals over which AVHRR motion vectors were computed.

While the difference in grid size prevents the direct comparison of motion vectors from PIPS with AVHRR ice motion vectors, the PIPS output puts the AVHRR motion vectors in the larger context of basin-wide conditions. The PIPS model output shows that most of the ice motion to the east during the period between 30 March to 03 April occurs on the first day (Fig. 50a - 50f), as ice in the Lincoln Sea responds to westerly winds. From 03 to 07 April (Figs. 50e - 50f, and 51a - 51h) wind and ice motion is more constantly to the east. Between 15 and 17 April (Figs. 52a - 52f), slight ice motion to the east in the Lincoln Sea on the 15th is reversed by easterly winds on the 16th. The change in the wind pattern on the 17th results in little ice motion within the Lincoln Sea and much of the Arctic basin.

7. Conclusion

A first attempt at lead analysis from AVHRR imagery using new software developed at NOARL was made during the ICESHELF acoustic experiment. Comments on the suitability of the lead analysis method and products for comparison with acoustic data or for operational ice analysis would be appreciated.

References

Arctic Analysts Inc. (1988). Statistical Analysis of Lead Data in the Eastern Arctic based upon NOAA AVHRR Satellite Imagery. Naval Ocean Research and Development Activity, Stennis Space Center, MS, Contract Report N00014-86-C-0829.

Ninnis, R.M., W.J. Emery, and M.J. Collins (1986). Automated extraction of pack ice motion from Advanced Very High Resolution Radiometer imagery. Journal of Geophysical Research 91:10725-10734.

Preller, R.H. and P.G. Posey (1989). The Polar Ice Prediction System - A Sea Ice Forecasting System. Naval Ocean Research and Development Activity, Stennis Space Center, MS, NORDA Report 212.

Table 1. ICESHELF '90 image summary.

Date	Data Type	Time	Processed	Comments
12 Mar 90	LAC	1519Z		Some clouds, subarea 50/50
13 Mar 90	LAC	1508Z		Min clouds
15 Mar 90	LAC	1442Z		Some clouds
18 Mar 90	LAC	1553Z	x	Excellent, clear
19 Mar 90	LAC	1445Z	x	Excellent, clear
20 Mar 90	GAC	1211Z	x	Clouds to north
20 Mar 90	LAC	1530Z	x	Clouds to north
21 Mar 90	LAC	1522Z		Cloudy, few visible leads
22 Mar 90	LAC	1512Z		Cloudy, visible to north, SA 90% Clouds
23 Mar 90	LAC	1501Z		Leads N and NE of subarea
25 Mar 90	LAC			> 90% cloudy
26 Mar 90	LAC			100% cloudy
27 Mar 90	LAC	1559Z		Leads to north, no registration
28 Mar 90	LAC			Hardware problems
29 Mar 90	LAC	1537Z		· North okay, coast is cloudy
30 Mar 90	LAC	1522Z	x	Pretty good
30 Mar 90	GAC	1522Z	x	Pretty good
31 Mar 90	LAC	1515Z		80% clouds, leads north
01 Apr 90	LAC	1500Z		50% clouds
03 Apr 90	LAC	1442Z	x	Clear
04 Apr 90	LAC	1432Z		Clear, coastal clouds
05 Apr 90	LAC			No pass received
06 Apr 90	LAC			100% cloudy
07 Apr 90	LAC	1530Z	x	Clear
08 Apr 90	LAC	1526Z		Cloudy, leads to NE
09 Apr 90	LAC			100% clouds
12 Apr 90	LAC	1445Z		100% clouds
15 Apr 90	LAC	1409Z	x	Haze over shelf, else good
16 Apr 90	LAC	1540Z		Fair in NW of box
17 Apr 90	LAC	1533Z	x	Haze, but okay, more breakup at outlet
19 Apr 90	LAC	1511Z		Clouds over most of area
22 Apr 90	LAC	1434Z		NE box clear, else clouds

Thule

Date	Time	Comments
01 Apr 90	0957Z	Very good
03 Apr 90	0953Z	Very good
04 Apr 90	0924Z	Very good
05 Apr 90	1055Z	Good, hazy north of Fram Strait
06 Apr 90	1045Z	Many clouds
07 Apr 90	1034Z	Clouds
08 Apr 90	1023Z	Good in Fram and North
09 Apr 90	0852Z	Some clouds
11 Apr 90	0949Z	Very good
12 Apr 90	0936Z	Okay
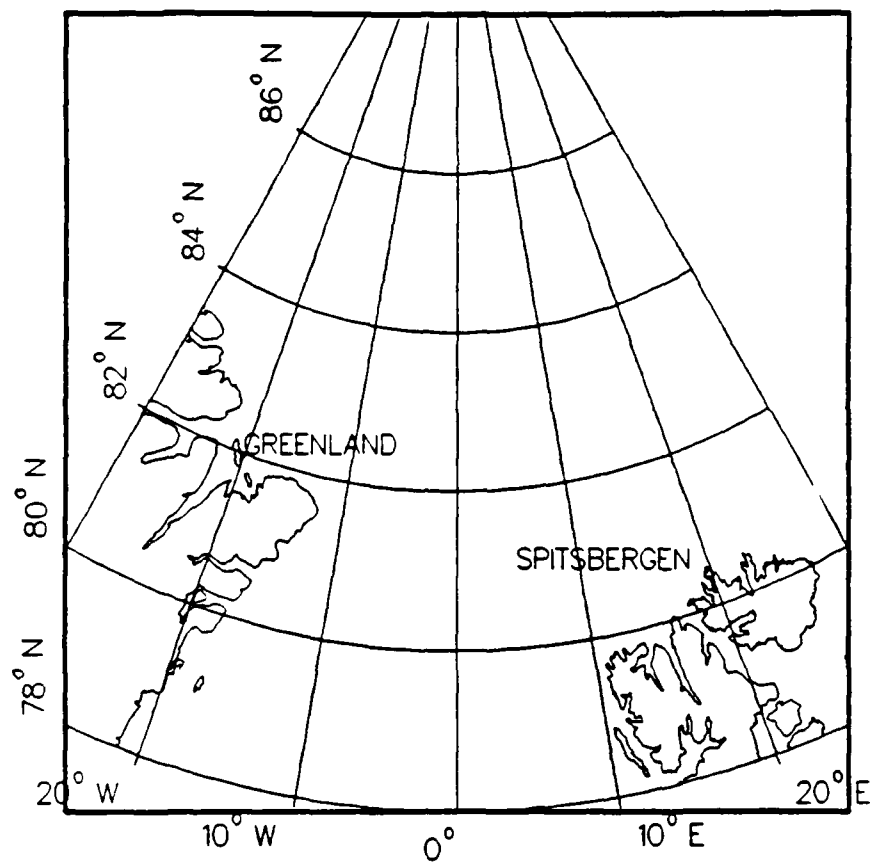
Figure 2. Area over which satellite imagery was acquired by NOARL for the ICEX acoustics exercise.

IMAGE BLOCKS

1	2	3	4	5	6	7	8
9	10	11	12	13	14	15	16
17	18	19	20	21	22	23	24
25	26	27	28	29	30	31	32
33	34	35	36	37	38	39	40
41	42	43	44	45	46	47	48
49	50	51	52	53	54	55	56
57	58	59	60	61	62	63	64

IMAGE ROW — rows marked 0, 64, 128, 192, 256, 320, 384, 448, 512

IMAGE COLUMN — columns marked 0, 64, 128, 192, 256, 320, 384, 448, 512

Figure 3. Image grid blocks used in removing cloudy areas and in determining lead orientation.
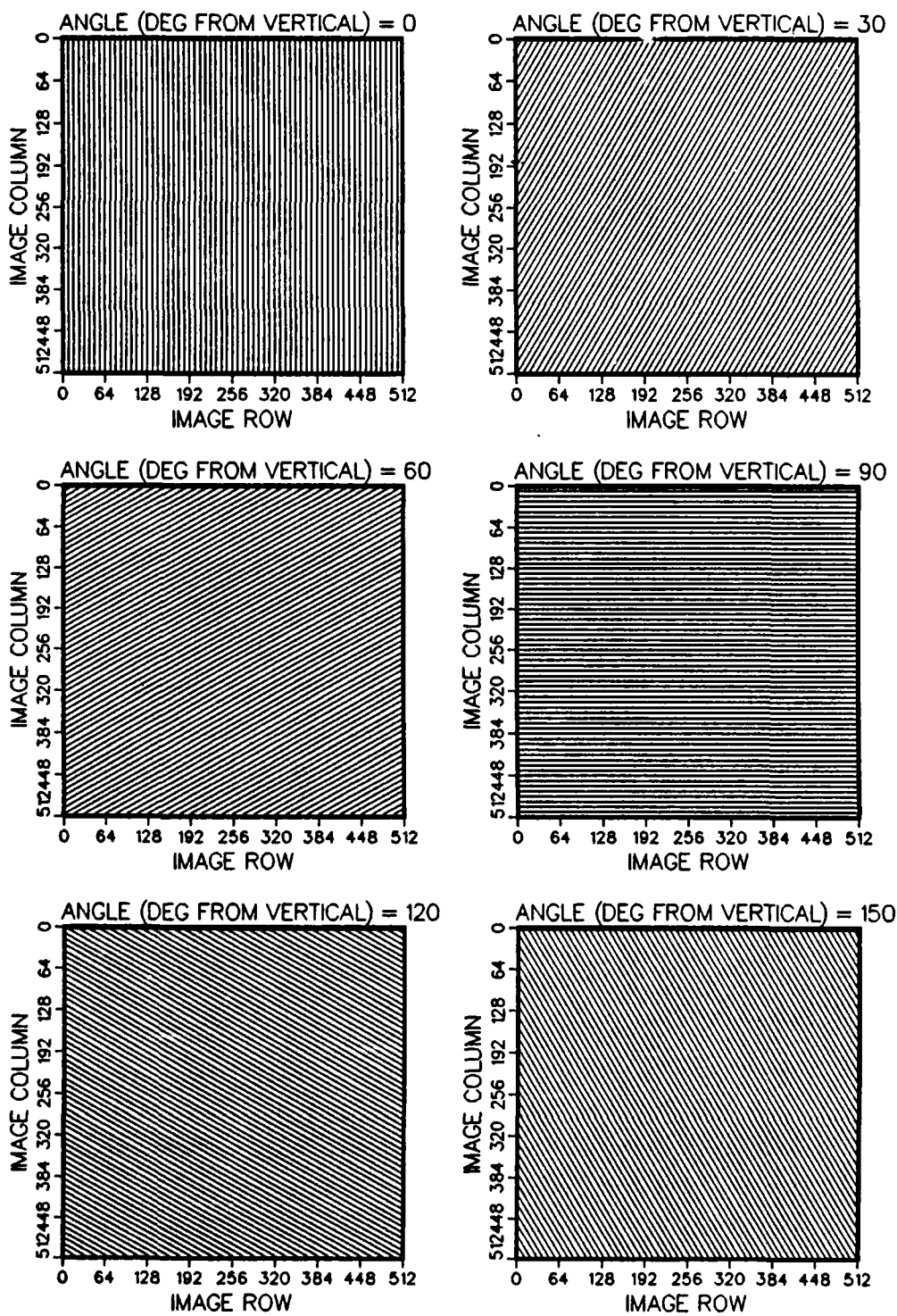
Figure 4. Comb of 64 lines (at vertical orientation). The average distance along all lines between intersections with leads gives average lead spacing. The comb is rotated to give spacing as a function of comb orientation.

Figure 5. 18 March 90 enhanced image with grid and land mask.
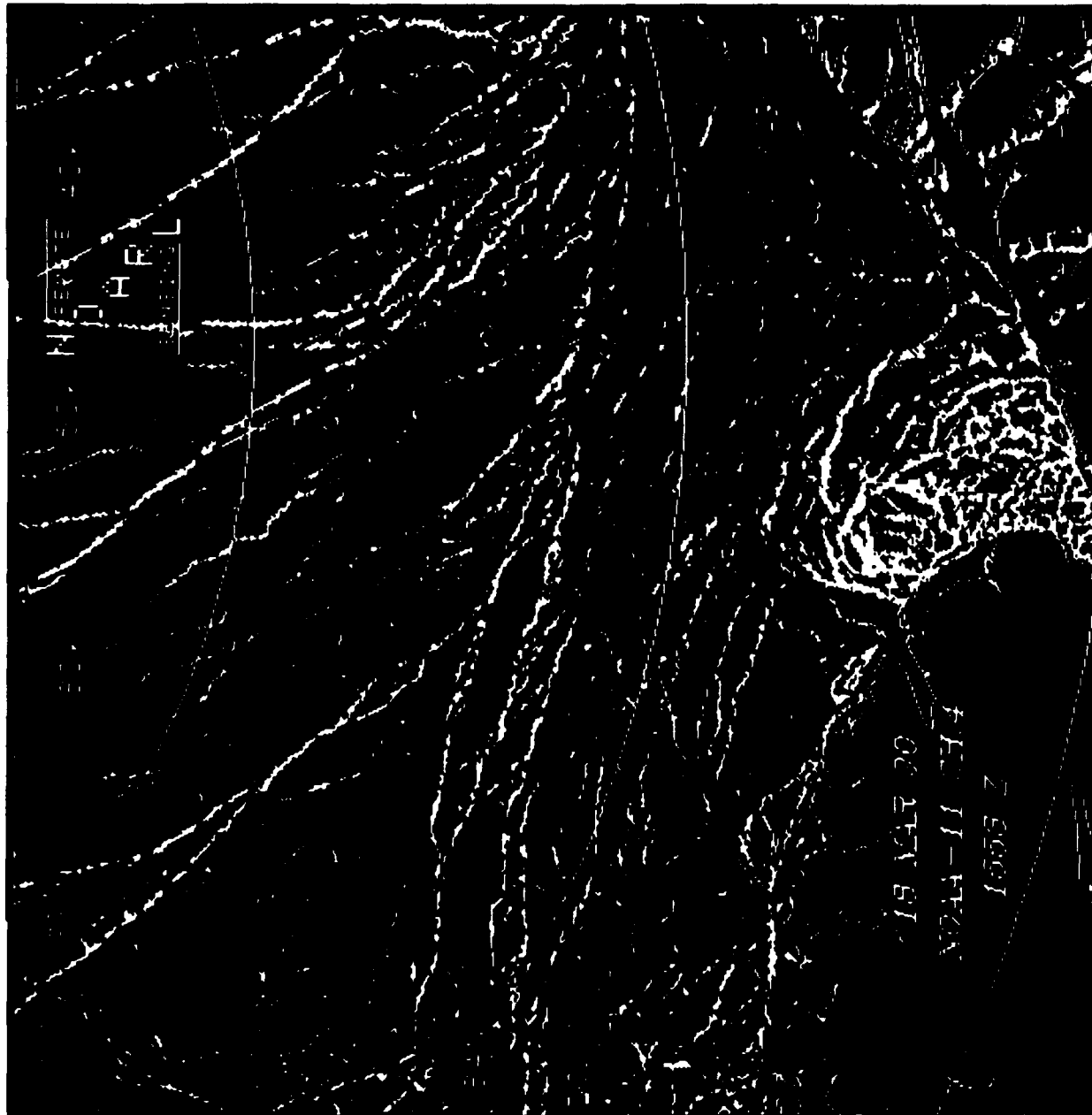
Figure 6. 18 March 90 binary image of leads.
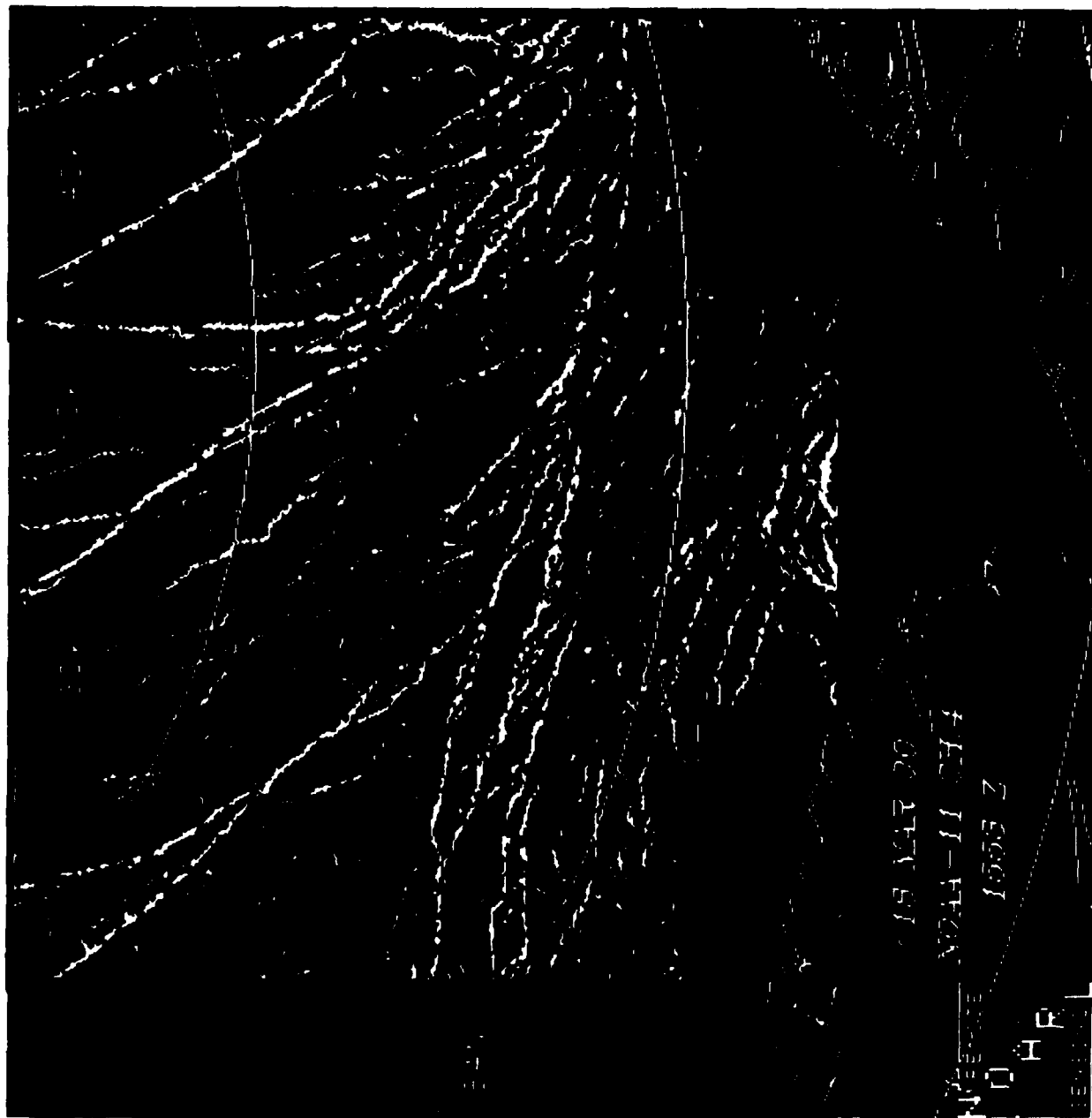
Figure 7a. 18 March 90 binary image of leads with land and cloud blocks removed.
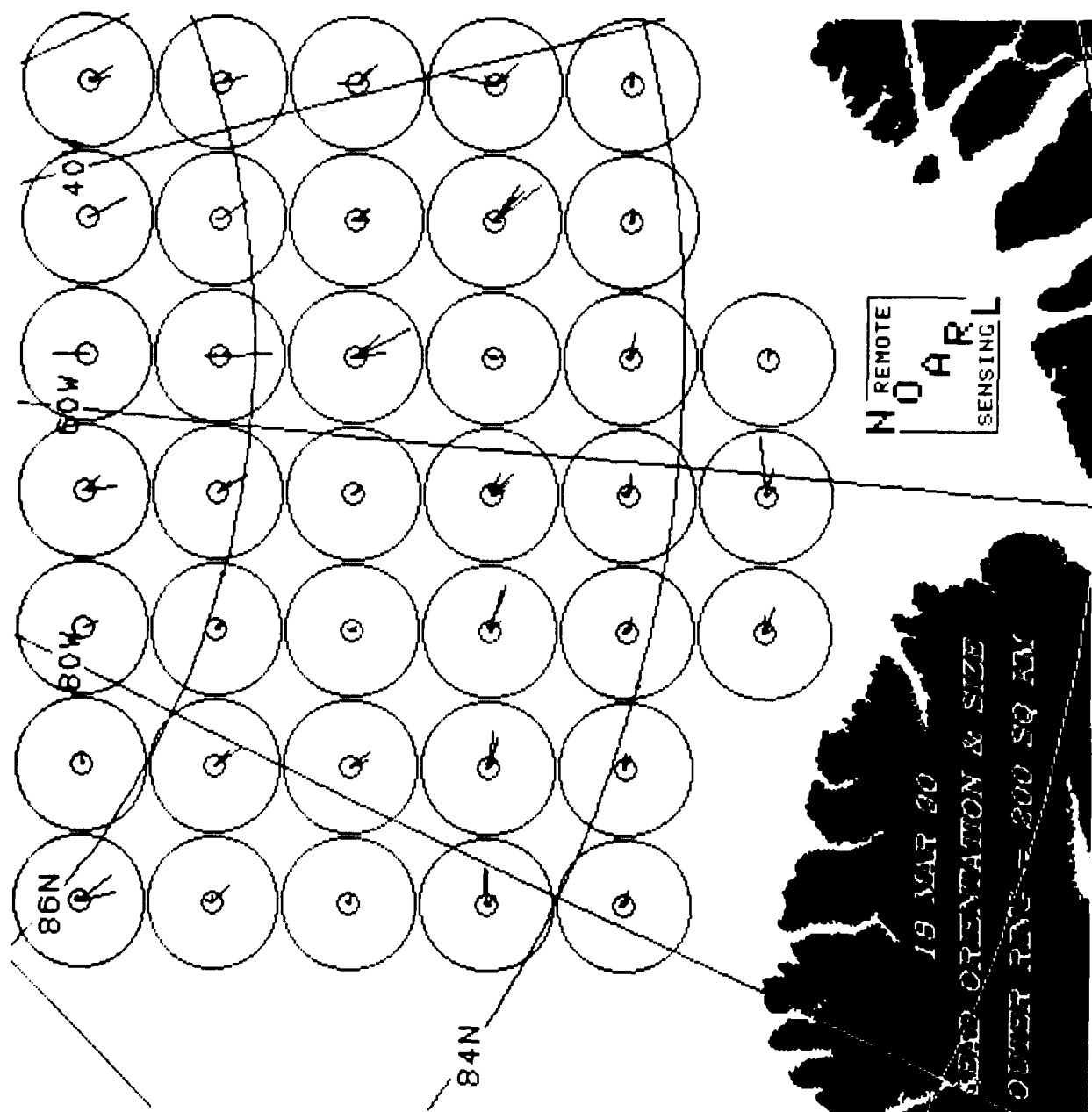
Figure 7b. 18 March 90 rose plots of lead size vs. orientation.

Table 3. 18 March 90 lead size and orientation.

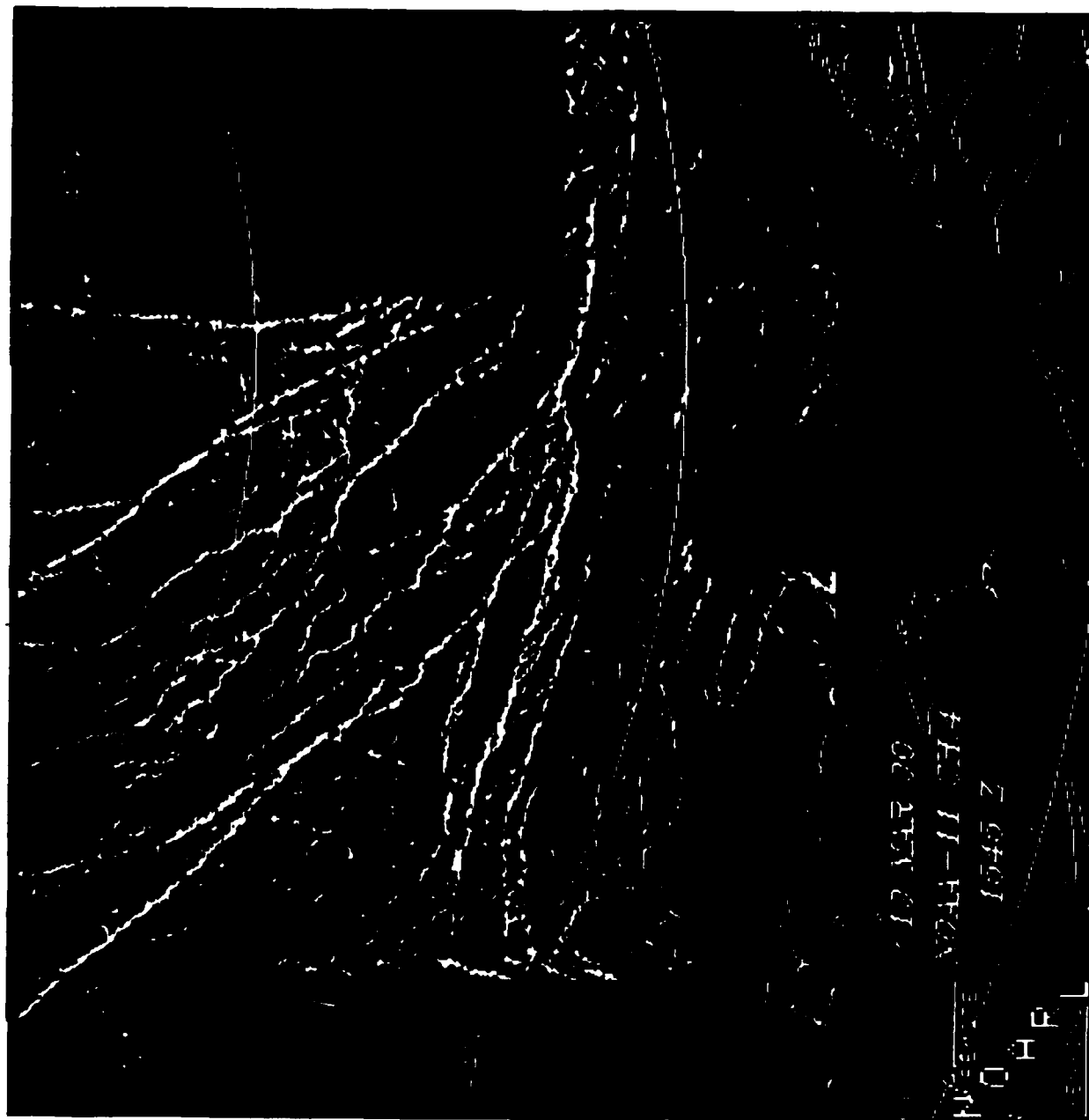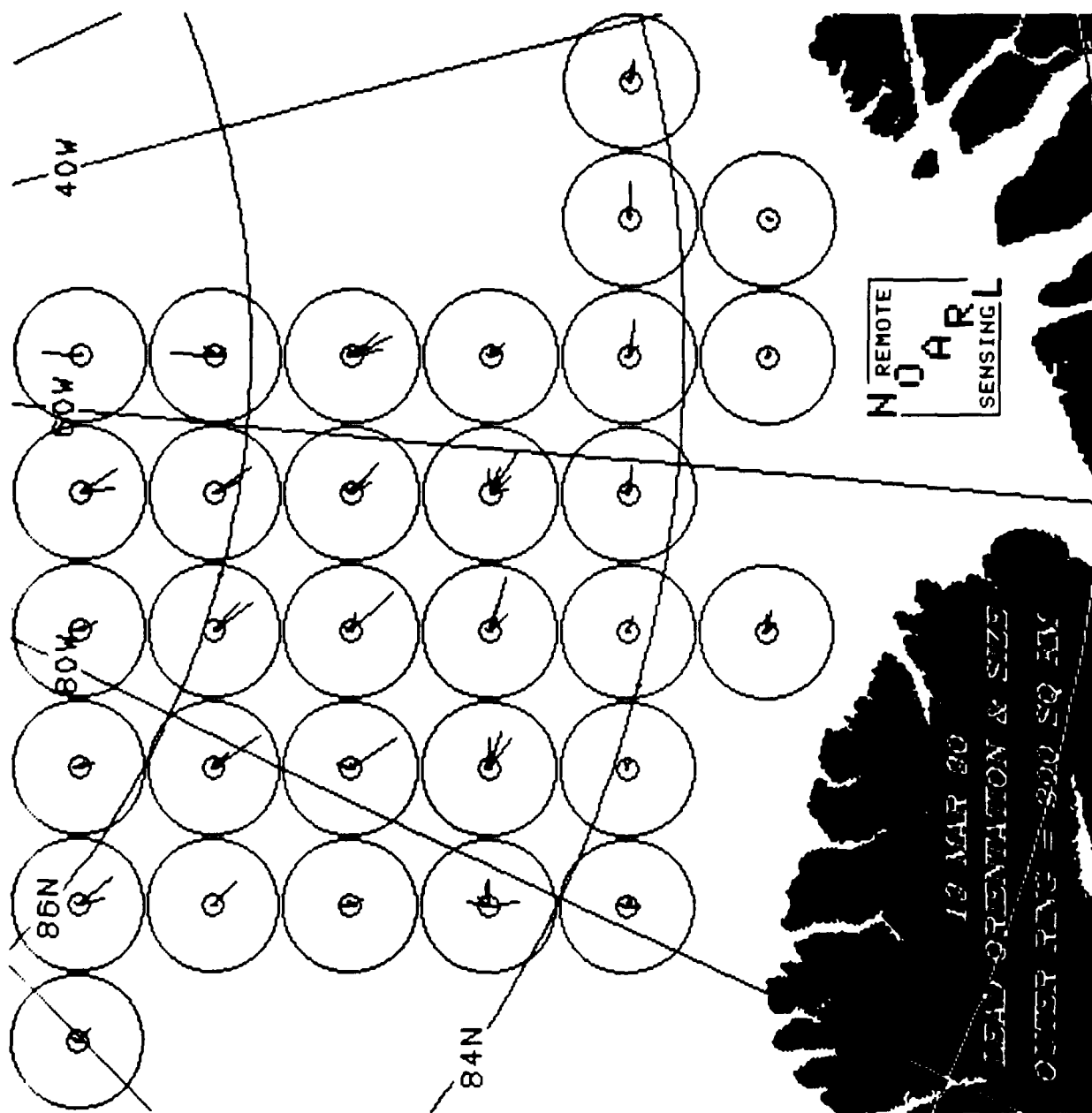| Date	Block Number	Direction (degrees)	km^2
18 March 1990	2	141	121
		166	115
	4	153	51
	5	135	67
		170	97
	6	3	95
	7	151	129
	8	145	86
		168	70
	10	135	71
	11	134	68
		146	93
	13	141	50
		149	105
	14	177	157
	15	147	94
	16	164	82
	19	140	74
		154	57
		159	55
	22	135	50
		136	99
		152	181
		168	90
	23	142	52
	24	0	52
		130	61
		135	82
	26	87	52
		88	107
		91	104
	27	99	108
		106	92
		110	80
	28	106	130
		108	145
	29	112	74
		134	91
		140	66
	31	123	128
		129	93
		133	127
		142	174
	32	11	133
		134	91
		143	51
	37	98	67
	38	99	82
	44	90	52
		109	86
	45	85	180
		106	88

Table 4. 18 March 90 lead spacing and width with orientation.

```
File: cf_bi_18mar90_lsub.dat
Image size (km in one dimension):  512
Percent covered by leads:     4.9
```

| orientation (deg)	# of lead crossings	mean spacing (km)	std spacing (km)	mn width (km)	std wdth (km)
0.	736	20.0	23.6	2.2	2.1
15.	784	19.7	21.3	2.0	1.3
30.	761	20.8	22.3	1.8	1.0
45.	681	23.5	24.1	1.6	0.8
60.	753	21.7	24.8	1.8	1.1
75.	772	20.5	22.7	1.9	1.2
90.	736	22.5	27.2	2.3	1.6
105.	701	22.4	28.1	2.1	1.7
120.	647	22.9	31.4	2.1	1.7
135.	553	25.5	32.4	1.9	1.6
150.	657	20.7	30.5	2.1	2.1
165.	750	19.6	28.9	2.1	1.8
180.	736	20.0	23.6	2.2	2.1
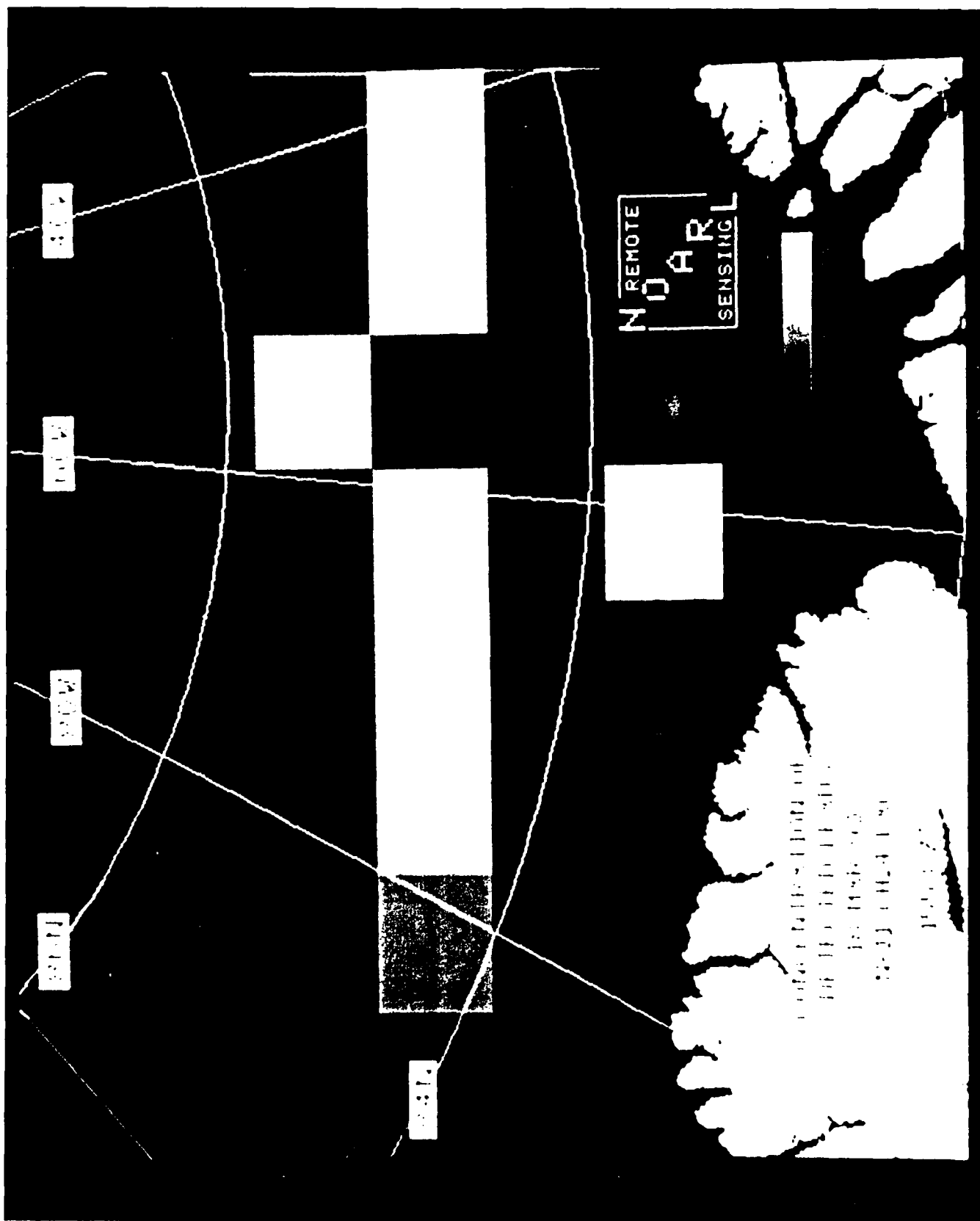
Figure 8. 18 March 90 grey level image (brightness represents lead coverage).
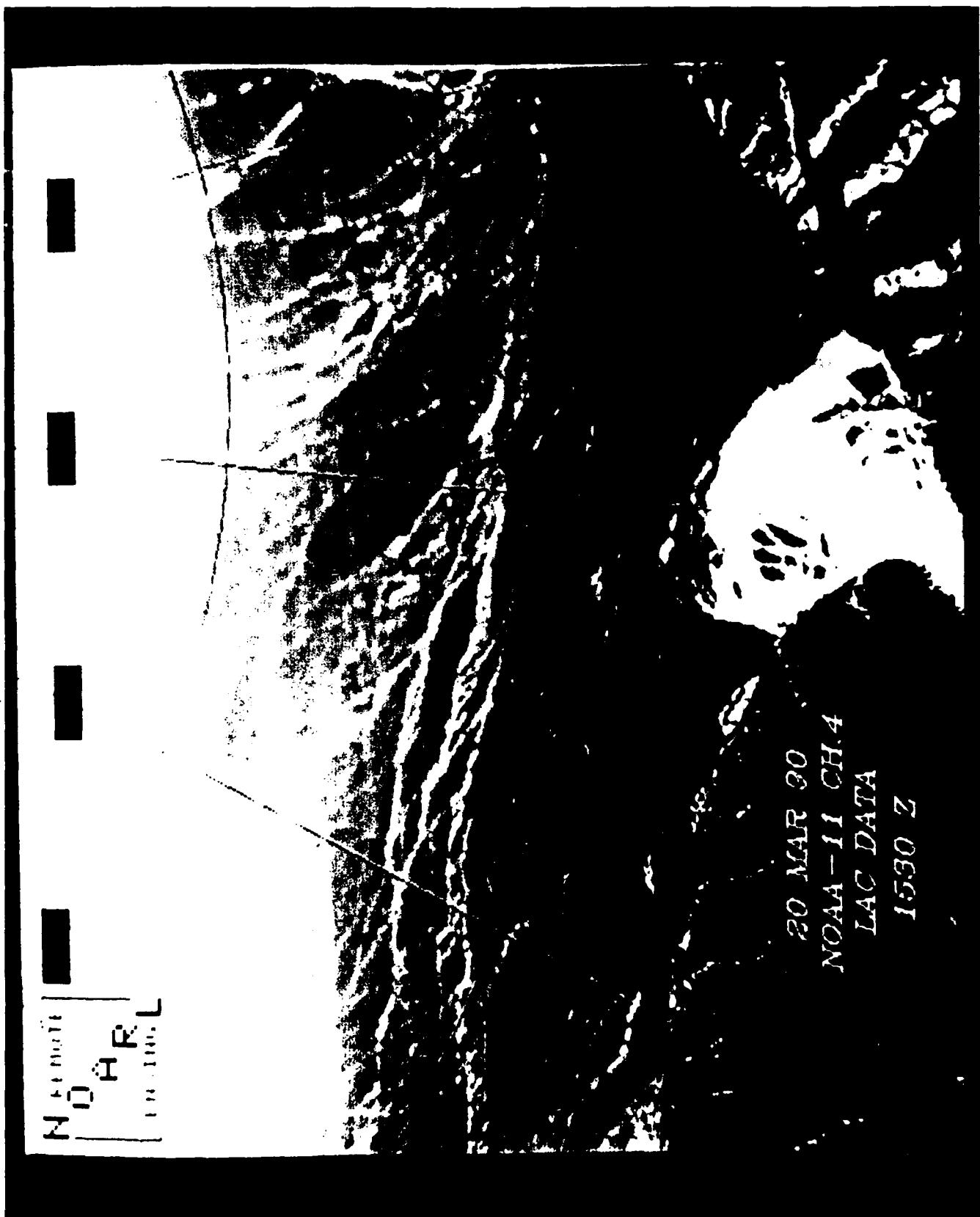
Figure 9. 19 March 90 enhanced image with grid and land mask.
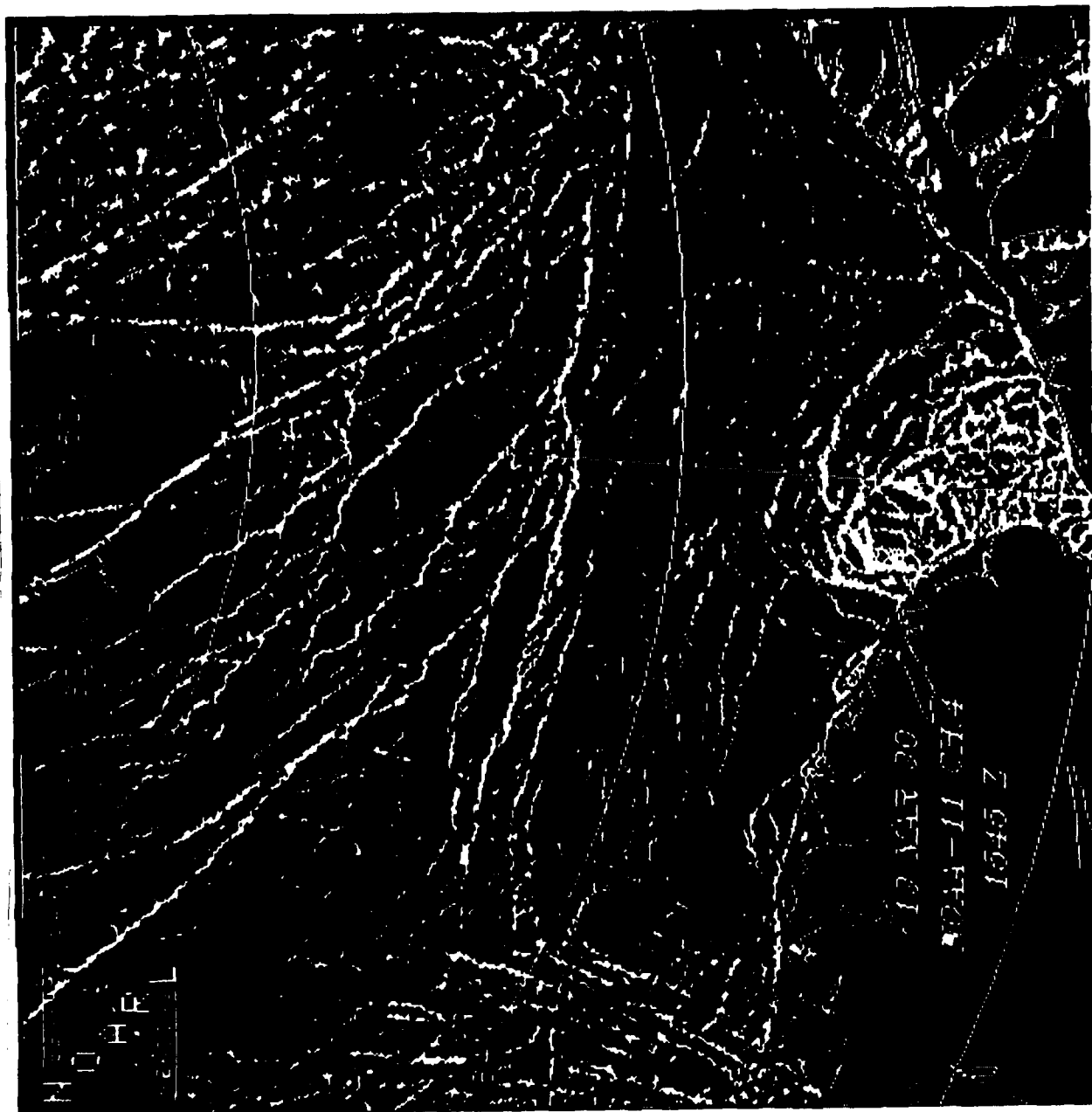
Figure 10. 19 March 90 binary image of leads.

Figure 11a. 19 March 90 binary image of leads with land and cloud blocks removed.

Figure 11b. 19 March 90 rose plots of lead size vs. orientation.

Table 5. 19 March 90 lead size and orientation.

Date	Block Number	Direction (degress)	km^2
19 Mar 1990 LSUB	1	135	61
	2	141	133
		165	78
	3	163	50
	4	153	58
	5	145	131
		172	107
	6	5	108
	10	135	100
	11	135	69
		145	169
	12	132	114
		143	143
	13	144	133
		155	77
	14	3	131
	19	146	162
	20	109	54
		137	170
	21	130	121
		135	55
		151	66
	22	136	106
		151	54
		153	133
		168	92
	26	15	60
		87	63
		93	81
		171	94
	27	90	91
		107	114
		126	110
	28	105	97
		106	165
		134	72
	29	87	73
		109	86
		123	147
		139	78
		162	53
	30	134	54
	37	97	88
	38	99	112
	39	91	107
	40	96	69
	44	90	55
		106	67

Table 6. 19 March 90 lead spacing and width with orientation.

```
File: cf_bi_19mar90_lsub.dat
Image size (km in one dimension):   512
Percent covered by leads:          4.8
```

| orientation (deg)	# of lead crossings	mean spacing (km)	std spacing (km)	mn width (km)	std wdth (km)
0.	736	16.6	17.3	2.1	1.4
15.	779	16.0	16.1	2.0	1.3
30.	746	16.4	17.2	1.9	1.2
45.	671	18.9	19.2	1.7	0.9
60.	754	16.7	19.0	1.8	1.0
75.	733	17.9	20.9	2.1	1.3
90.	738	18.4	23.8	2.2	1.6
105.	651	20.9	28.1	2.2	1.6
120.	643	21.2	28.6	2.2	1.9
135.	514	25.3	31.8	2.0	1.5
150.	641	22.1	33.2	2.1	1.9
165.	661	20.8	30.0	2.2	1.7
180.	736	16.6	17.3	2.1	1.4
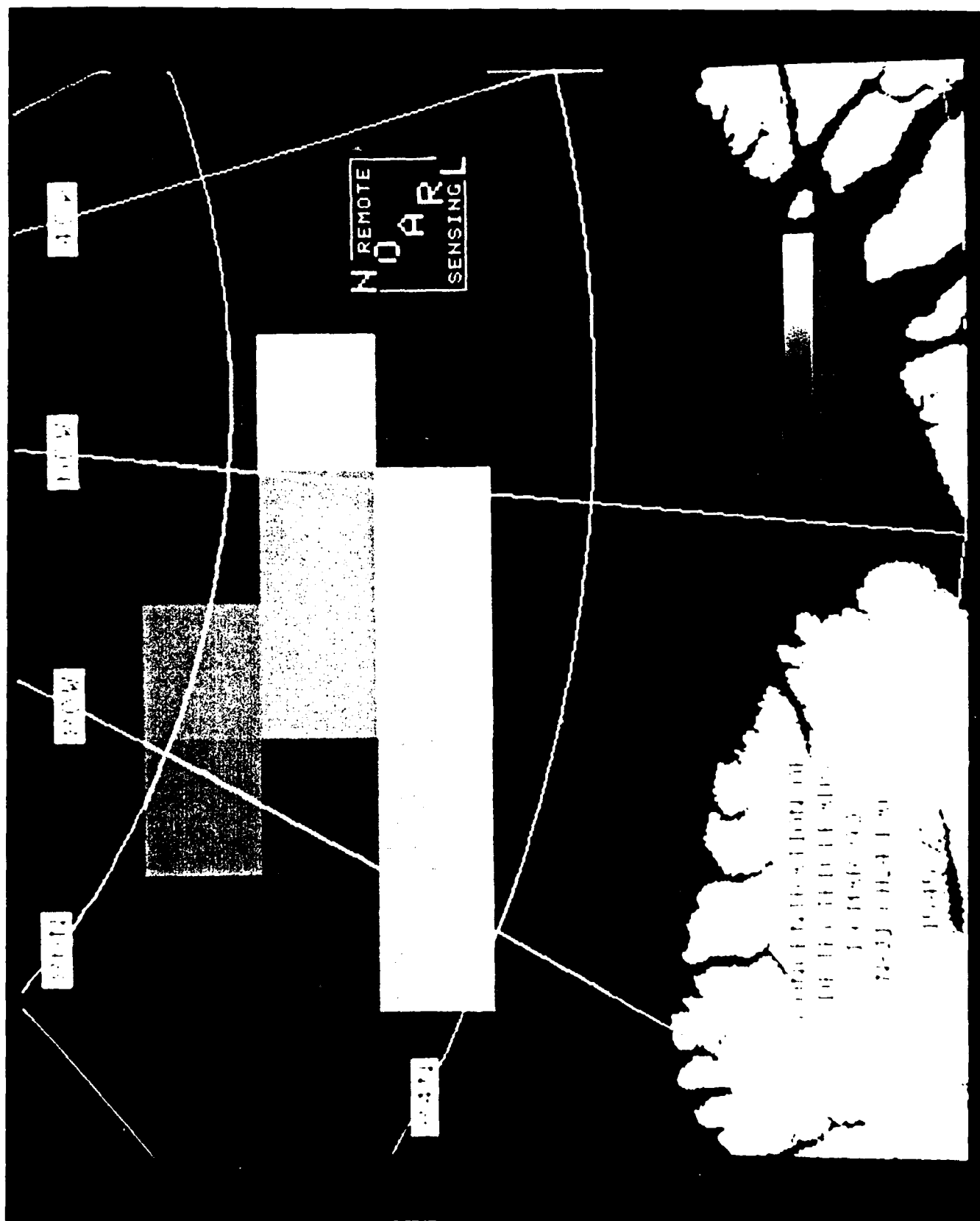
Figure 12. 19 March 90 grey level image (brightness represents lead coverage).
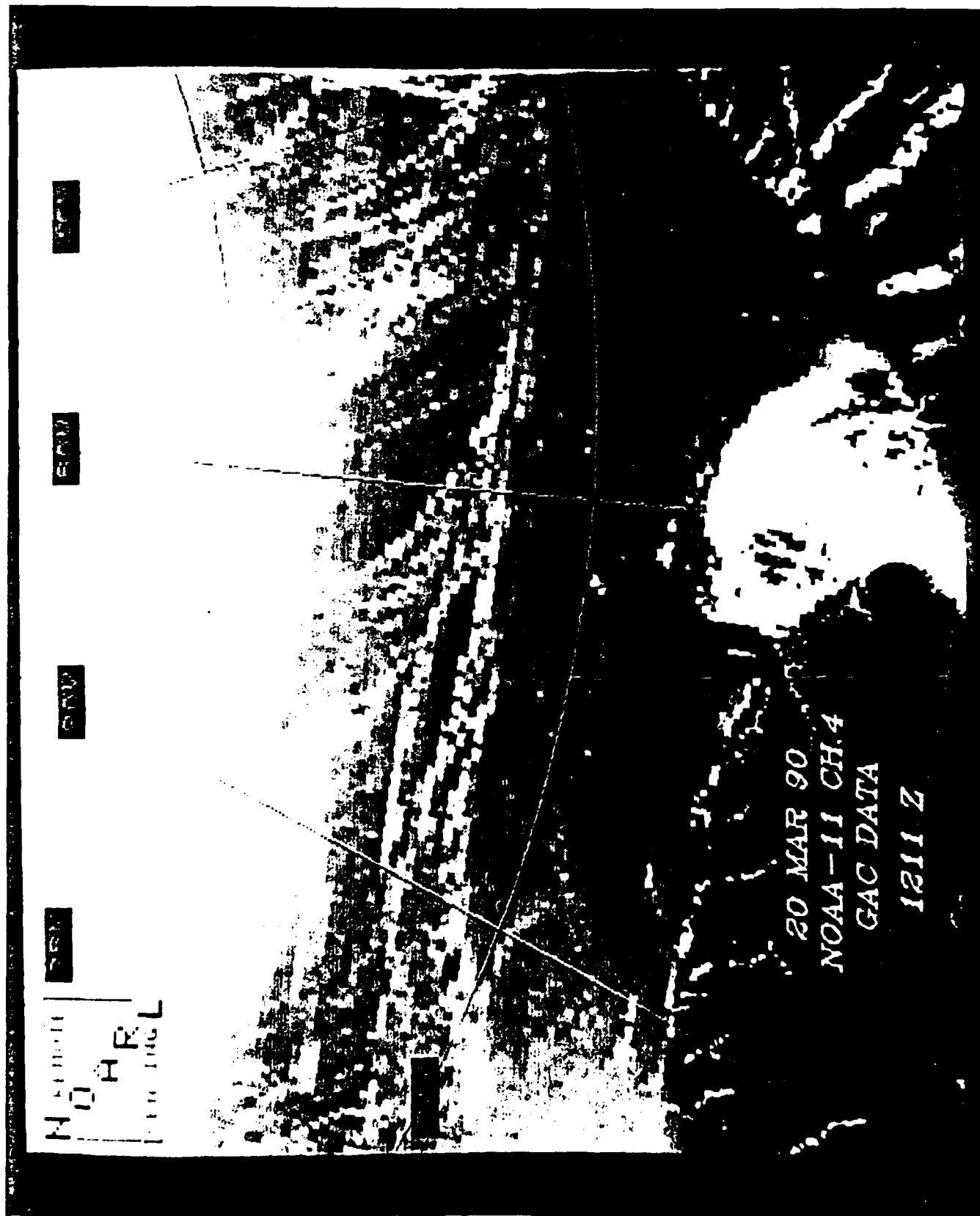
Figure 13. 20 March 90 LAC enhanced image with grid and land mask.

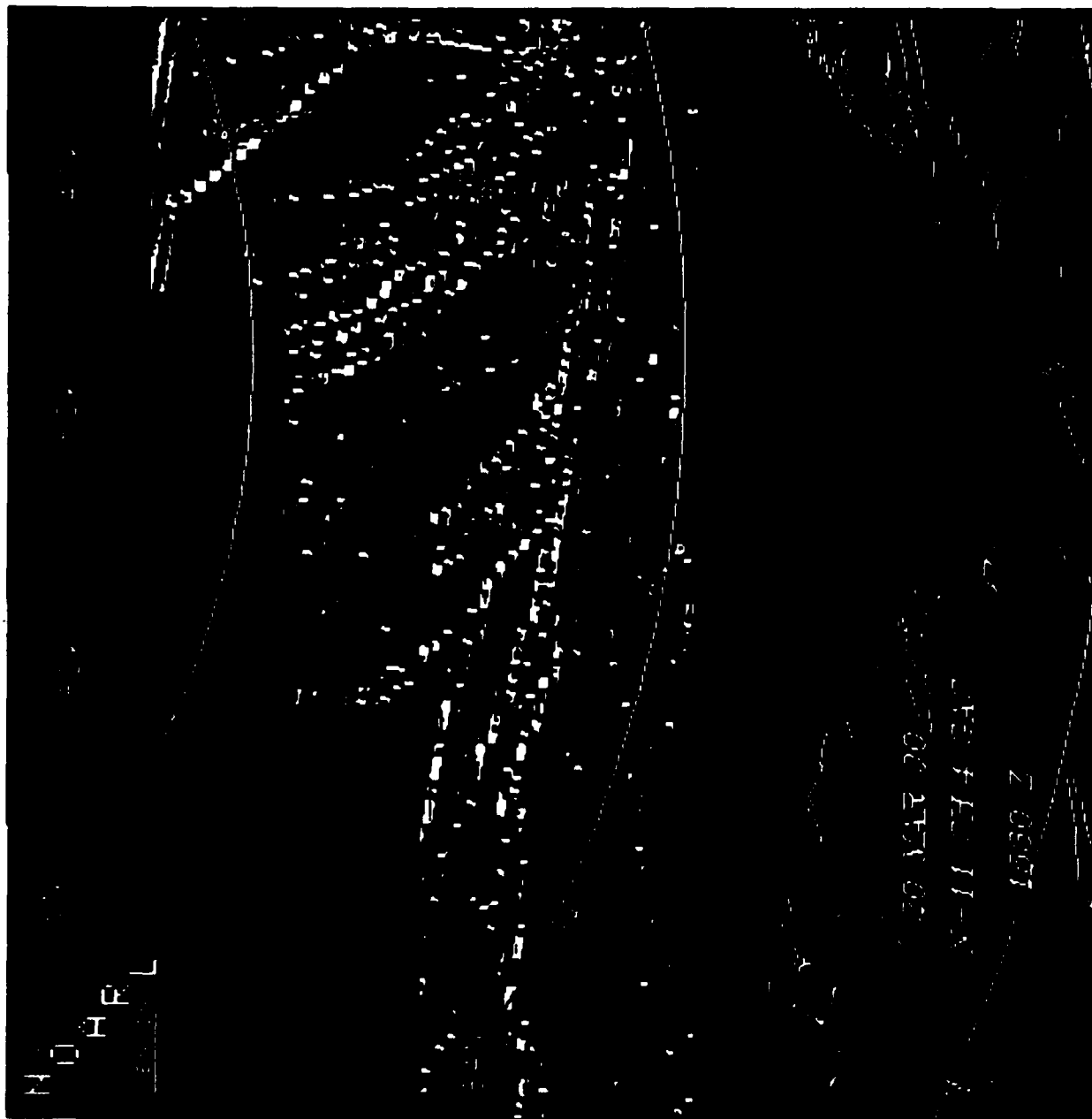Figure 14. 20 March 90 LAC binary image of leads.

Figure 15a. 20 March 90 LAC binary image of leads with land and cloud blocks removed.
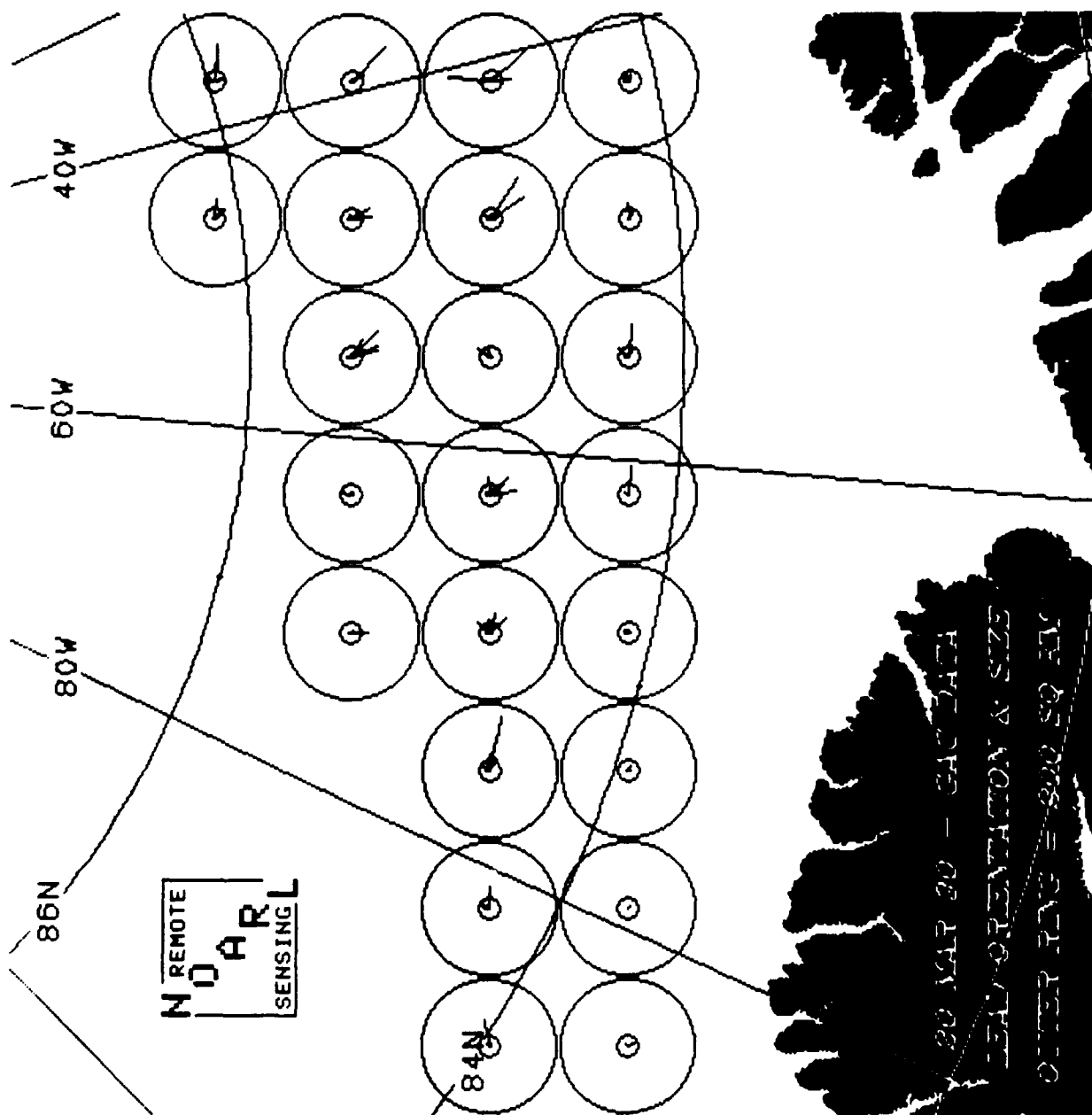
Table 7. 20 March 90 LAC lead size and orientation.

Date	Block Number	Direction (degrees)	km²
20 Mar 1990 LSUB	13	86	58
		140	94
		150	55
	14	45	79
		176	103
	15	147	122
	22	132	57
		152	104
		153	82
		167	92
	23	144	62
	24	135	173
	26	89	81
		94	55
		134	50
	27	98	121
		107	72
		110	81
		127	51
	28	107	96
		109	123
		135	88
	29	110	68
		135	73
		141	50
	31	125	58
		135	53
		142	60
		151	59
	32	8	80
		138	113
	37	98	53
	38	99	61
		103	61
	44	90	57
		107	62
	45	85	119
	48	79	62
	53	107	76
		135	187
		137	60
	53	154	60
		173	208
	54	136	75

Figure 15b. 20 March 90 LAC rose plots of lead size vs. orientation.

Table 8. 20 March 90 LAC lead spacing and width with orientation.

File: cf_bi_20mar90_lsub.dat
Image size (km in one dimension): 512
Percent covered by leads: 4.4

| orientation (deg)	# of lead crossings	mean spacing (km)	std spacing (km)	mn width (km)	std wdth (km)
0.	697	18.9	22.2	2.0	1.5
15.	706	19.0	21.7	2.0	1.3
30.	677	20.1	22.6	1.8	1.1
45.	595	23.8	27.1	1.7	1.0
60.	661	22.2	30.8	1.9	1.3
75.	666	20.5	25.8	2.0	1.4
90.	623	21.7	28.7	2.3	1.7
105.	656	21.9	34.8	2.1	1.8
120.	600	23.1	36.6	2.1	1.8
135.	505	26.1	32.5	1.9	1.4
150.	608	20.6	26.9	2.0	1.7
165.	696	19.0	23.7	2.0	1.5
180.	697	18.9	22.2	2.0	1.5
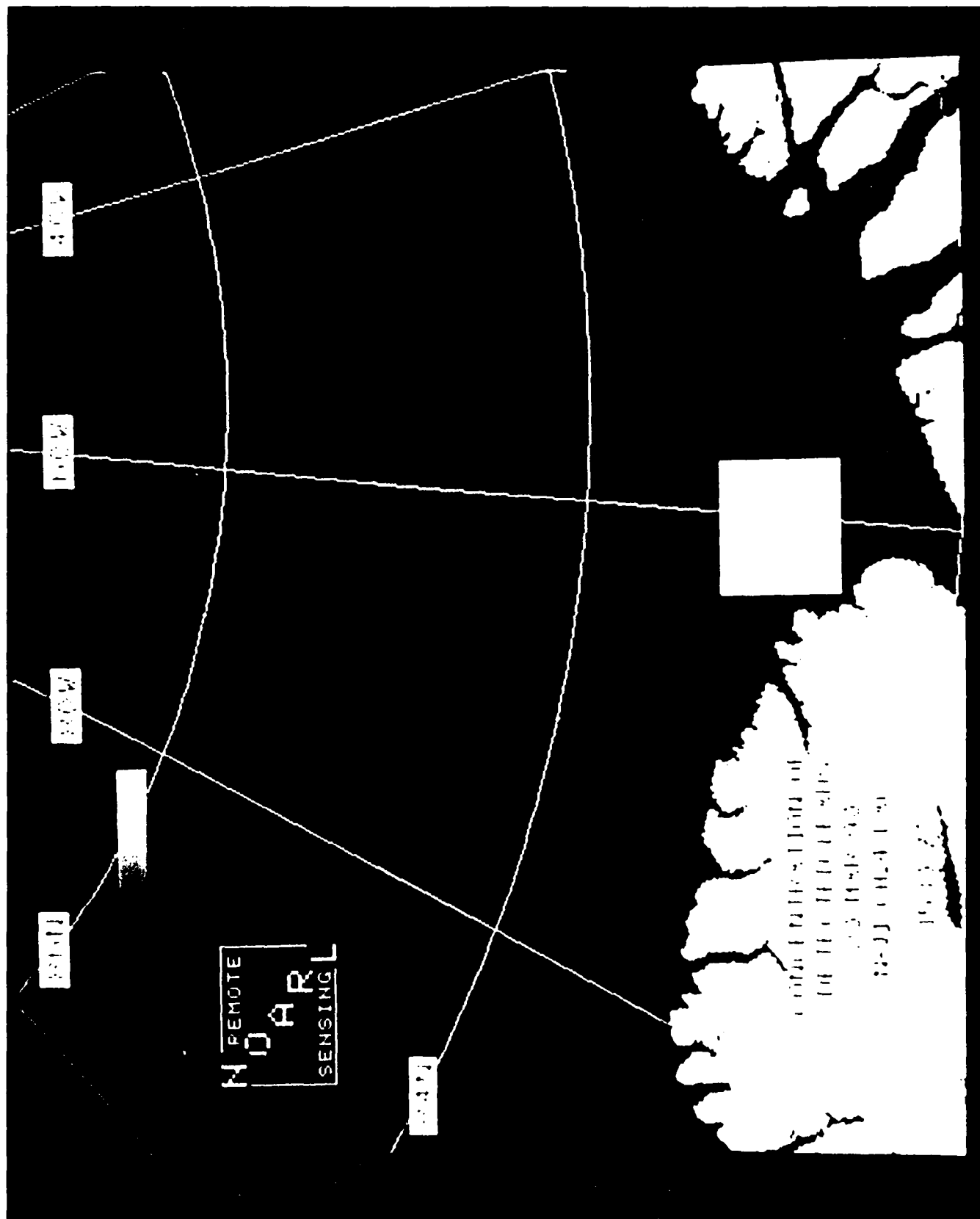
Figure 16. 20 March 90 LAC grey level image (brightness represents lead coverage).
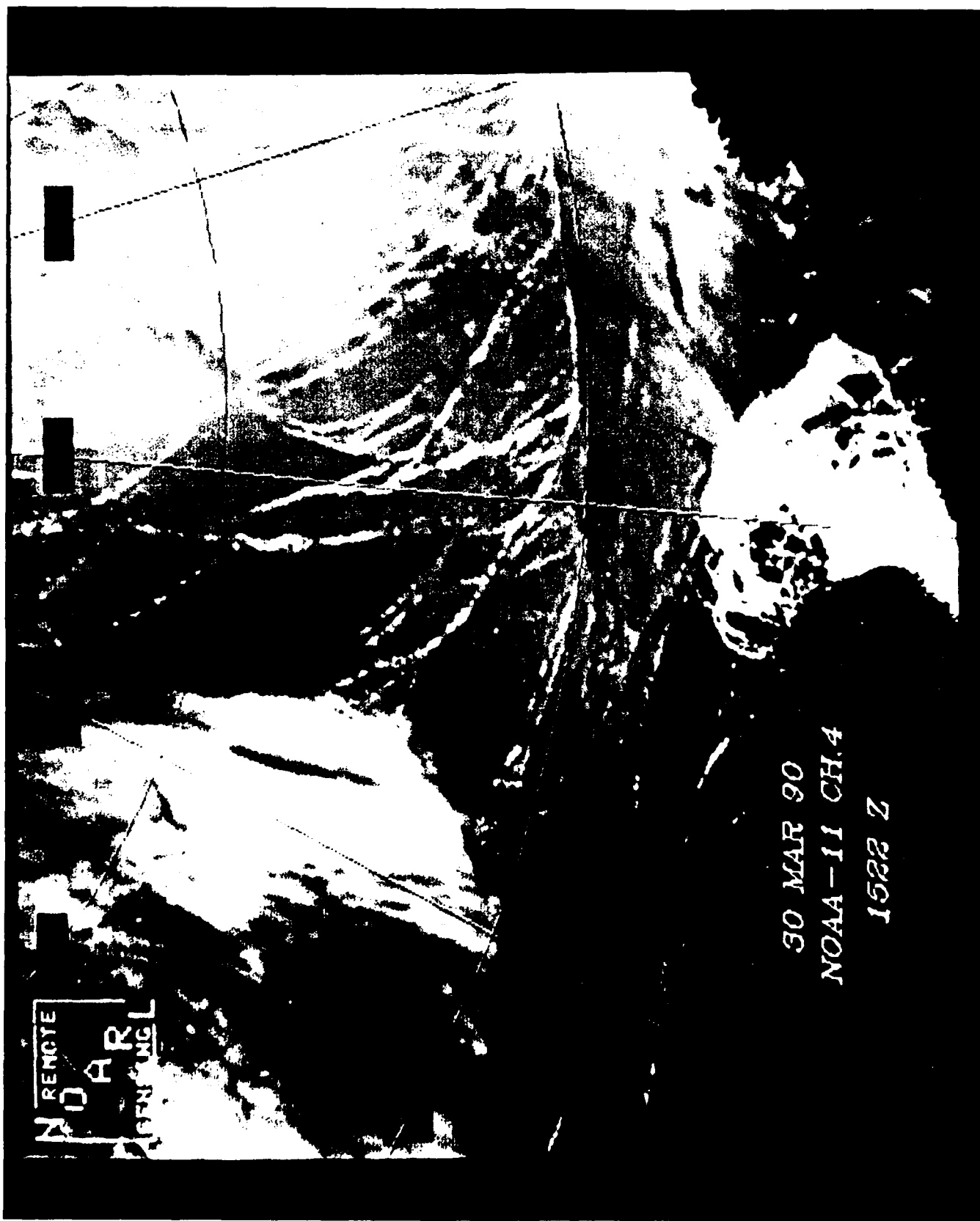
Figure 17. 20 March 90 GAC enhanced image with grid and land mask.
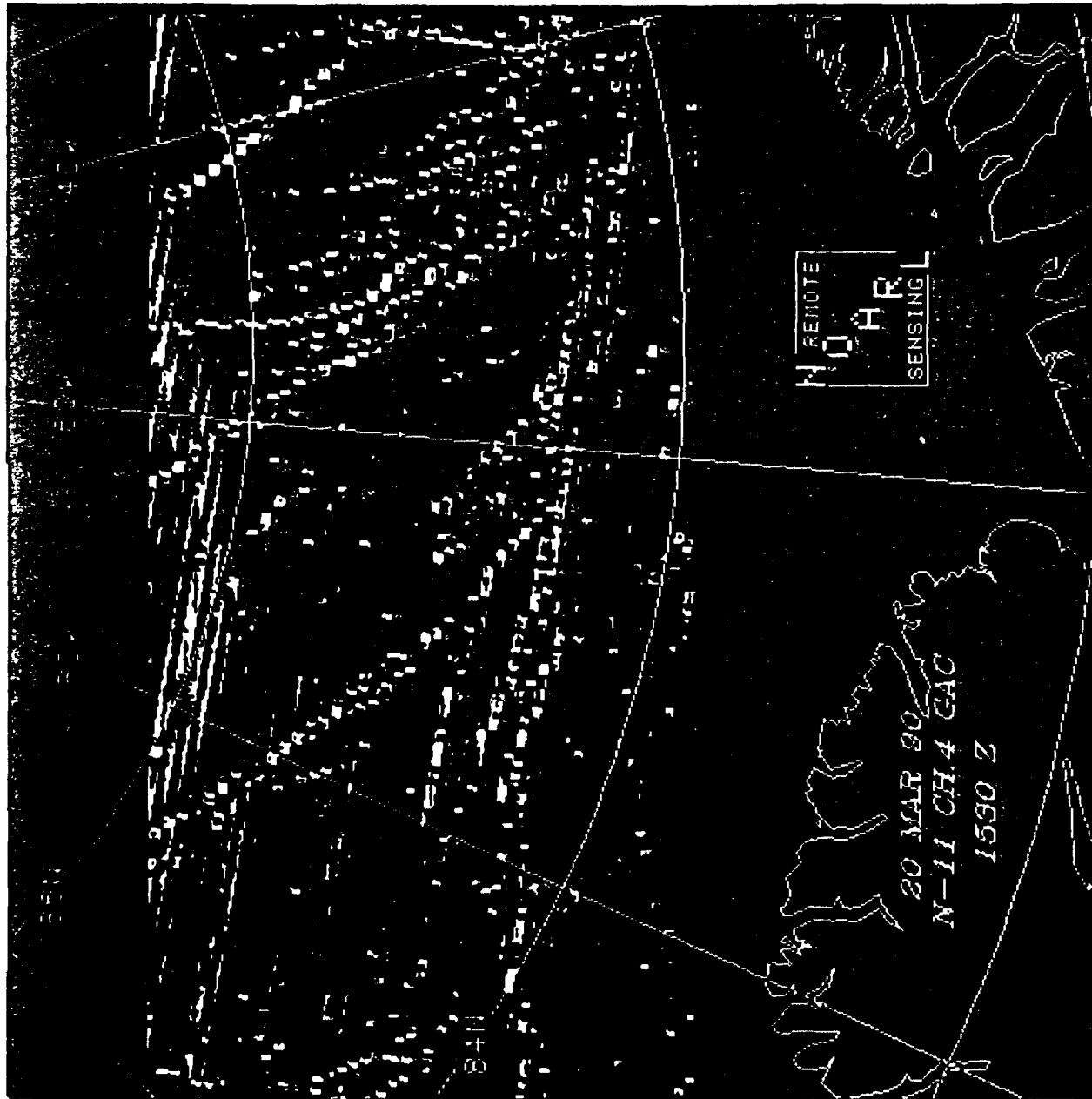
Figure 18. 20 March 90 GAC binary image of leads.

Figure 19a. 20 March 90 GAC binary image of leads with land and cloud blocks removed.

Figure 19b. 20 March 90 GAC rose plots of lead size vs. orientation.

Table 9. 20 March 90 GAC lead size and orientation.

Date	Block Number	Direction (degrees)	km^2
20 Mar 1990 GSUB	15	100	63
	16	95	110
		98	60
	20	176	51
	22	125	62
		134	109
		156	86
		166	80
	23	145	63
		171	60
	24	134	140
	25	83	80
	26	93	67
	27	91	50
		102	161
	28	106	61
		133	66
	29	87	56
		134	76
		135	53
		169	79
	31	122	145
		145	117
	32	6	124
		137	135
		168	58
	37	95	85
	38	96	100

Table 10. 20 March 90 GAC lead spacing and width with orientation.

```
File: cf_bi_20mar90_gsub.dat
Image size (km in one dimension):  512
Percent covered by leads:        2.9
```

| orientation (deg)	# of lead crossings	mean spacing (km)	std spacing (km)	mn width (km)	std wdth (km)
0.	330	22.3	24.4	2.8	1.7
15.	368	20.3	23.0	2.5	1.7
30.	361	21.7	24.4	2.3	1.4
45.	348	25.3	28.6	1.9	1.1
60.	349	26.7	33.5	2.3	1.4
75.	342	27.6	36.9	2.5	1.5
90.	306	26.6	40.8	2.9	2.0
105.	367	21.4	33.3	2.5	1.8
120.	378	19.8	29.3	2.3	1.4
135.	359	20.2	27.4	1.8	1.1
150.	363	17.8	24.6	2.3	1.3
165.	355	20.0	25.5	2.6	1.8
180.	330	22.3	24.4	2.8	1.7
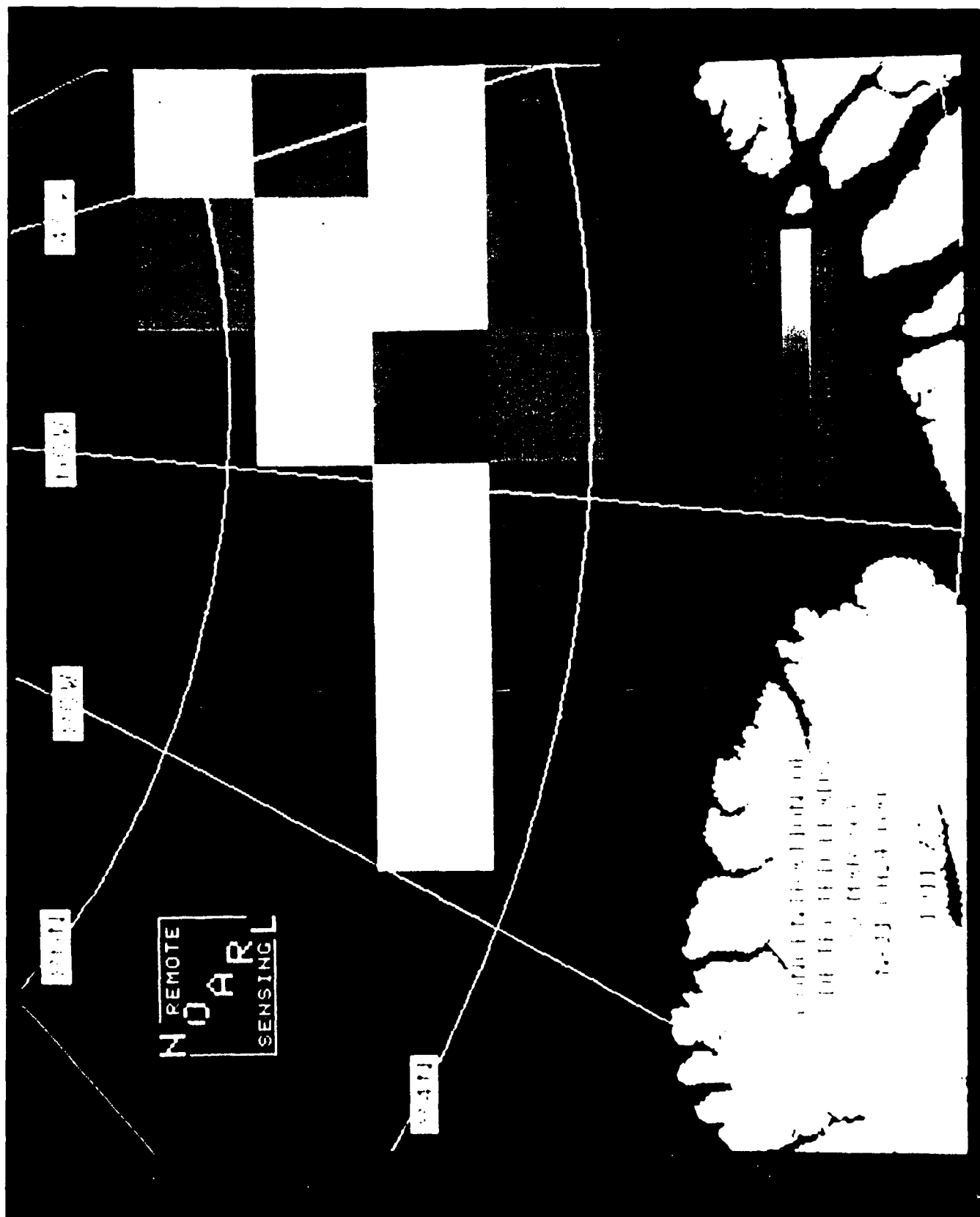
Figure 20. 20 March 90 GAC grey level image (brightness represents lead coverage).
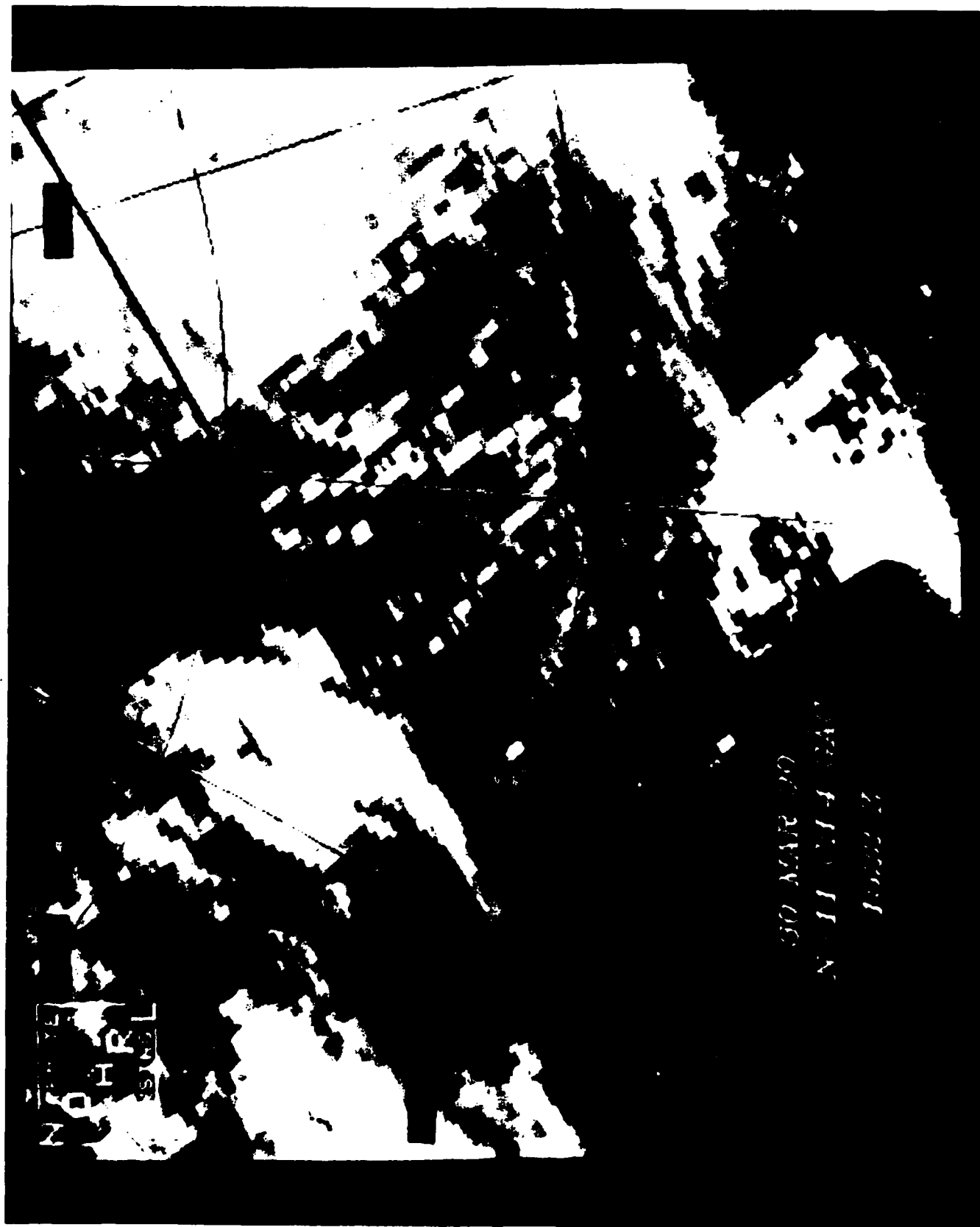
Figure 21. 30 March 90 LAC enhanced image with grid and land mask.
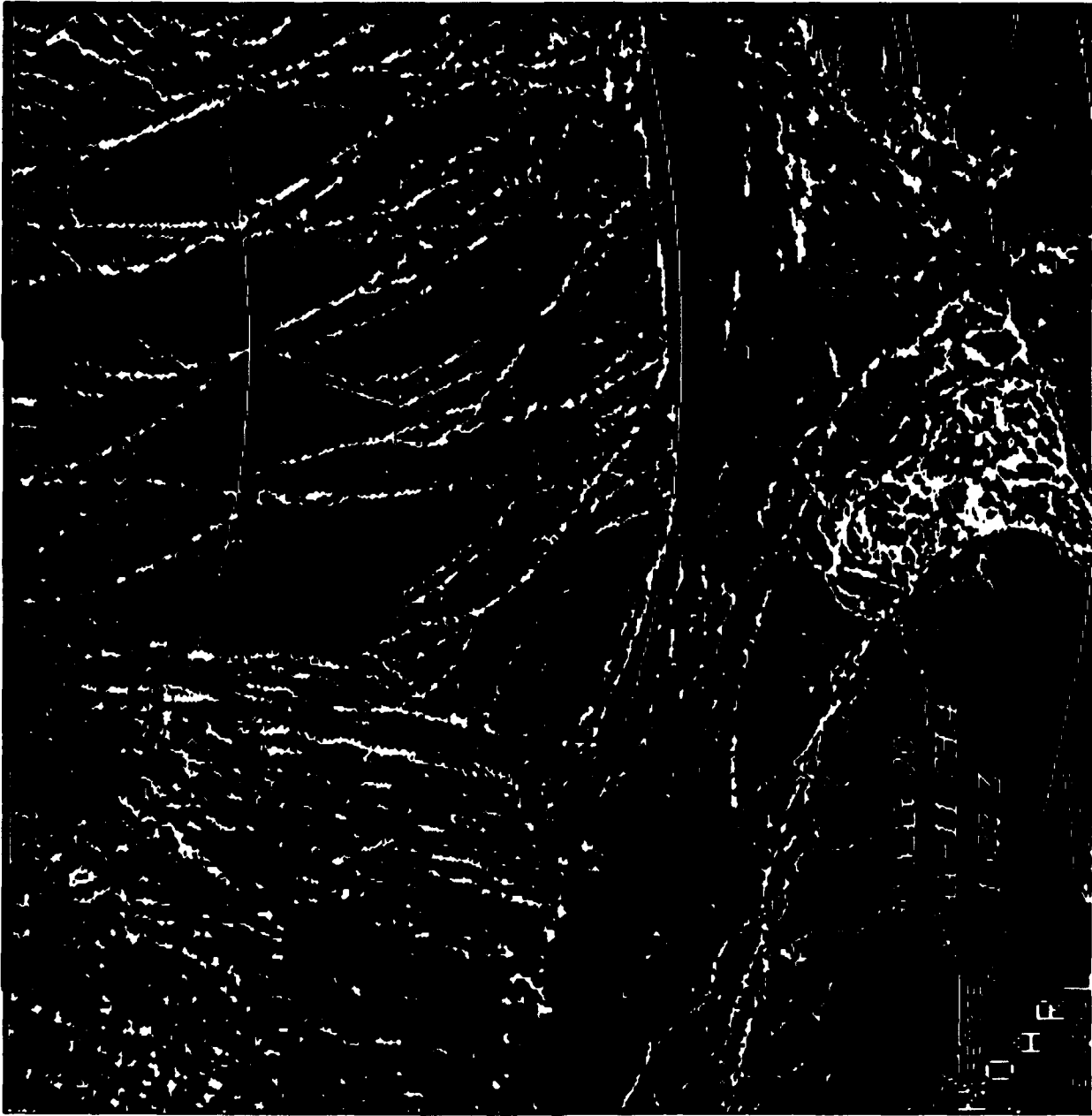
Figure 22. 30 March 90 LAC binary image of leads.

Figure 23a. 30 March 90 LAC binary image of leads with land and cloud blocks removed.
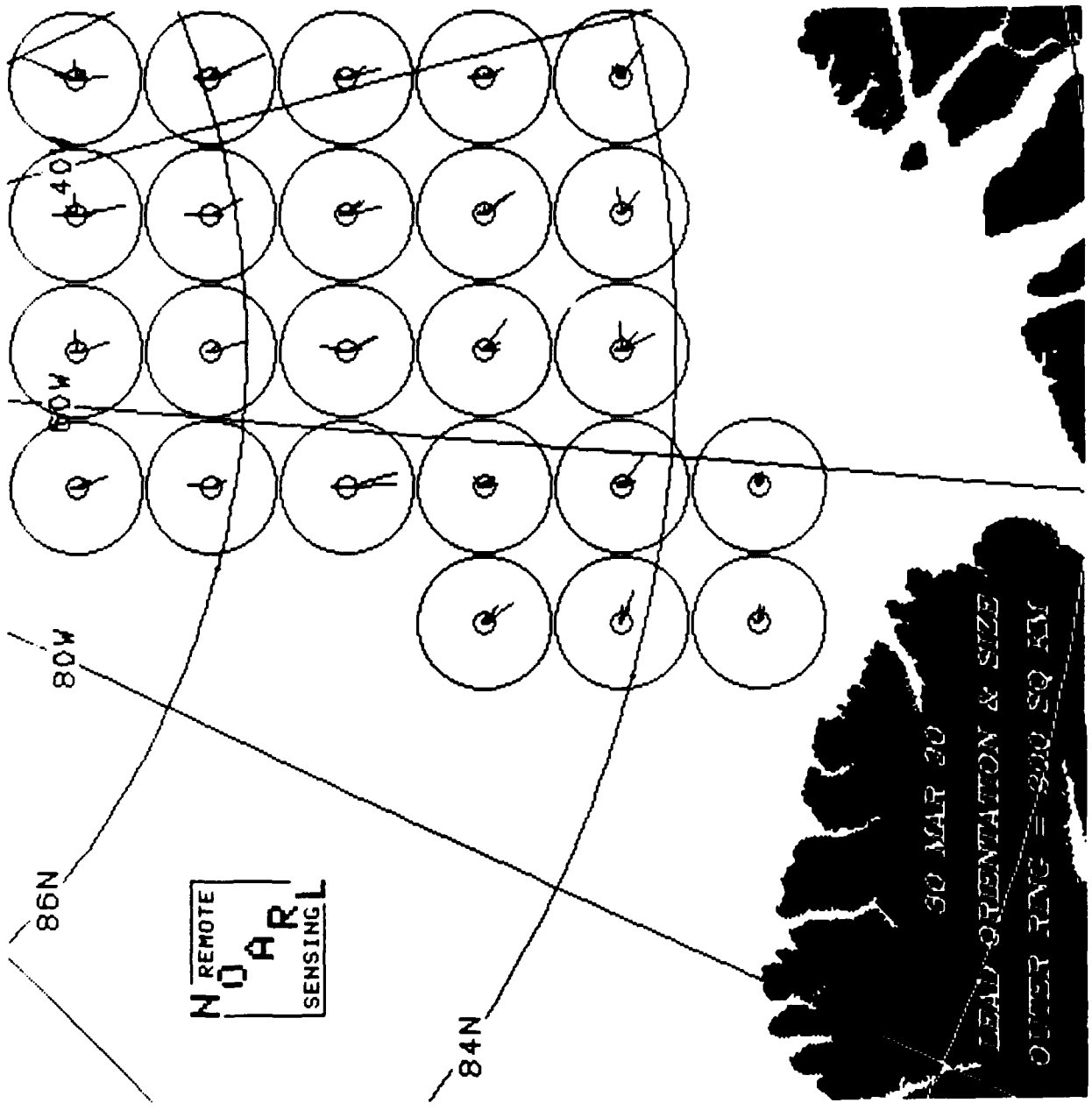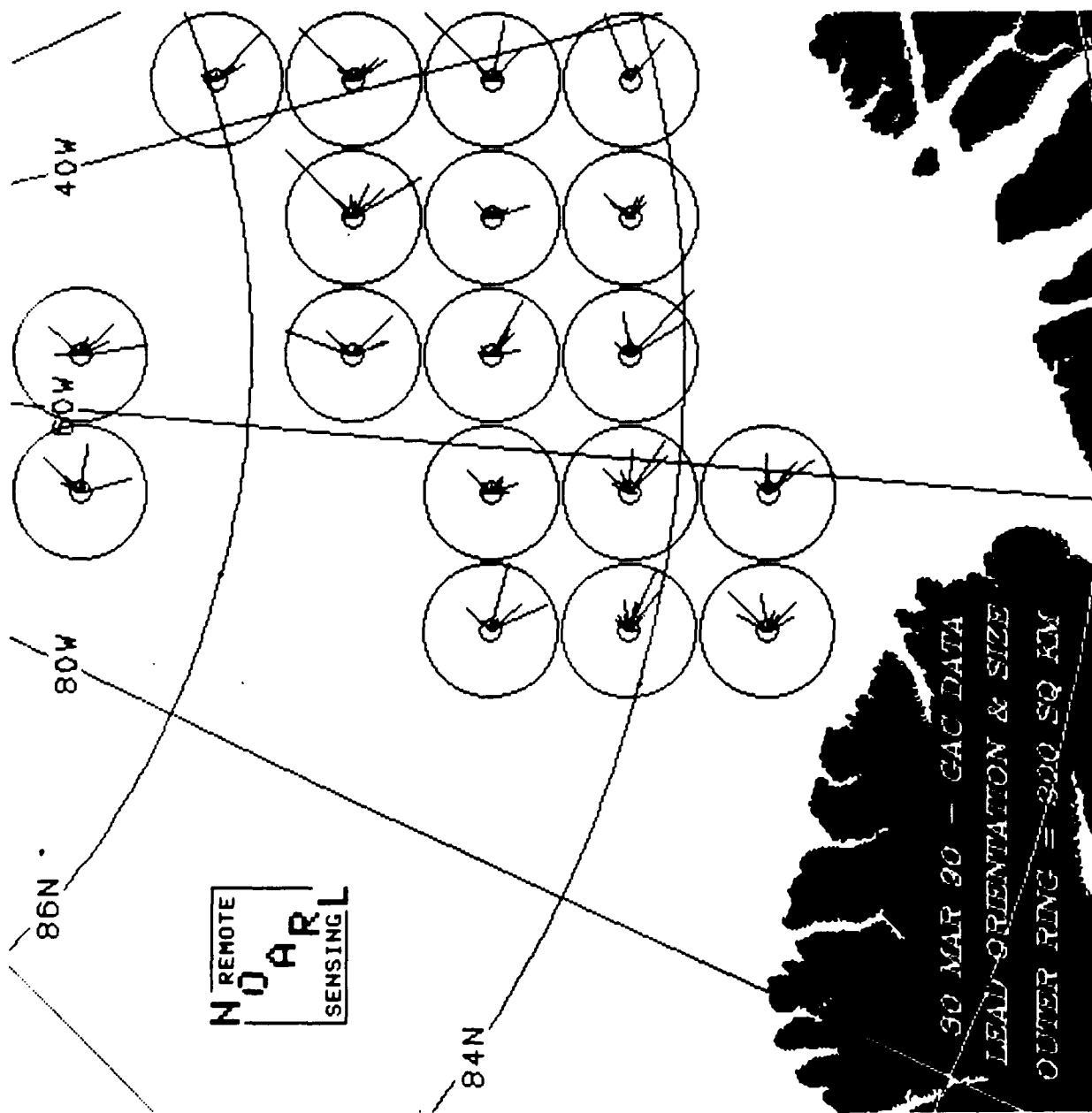
Figure 23b. 30 March 90 LAC rose plots of lead size vs. orientation.

Table 11. 30 March 90 LAC lead size and orientation.

Date	Block Number	Direction (degrees)	km^2
30 Mar 1990 LSUB	5	159	97
	6	89	65
		165	103
	7	0	66
		89	63
		167	74
		169	147
	8	16	64
		24	167
		89	61
		175	100
	13	6	65
		153	52
	14	164	108
	15	2	73
		154	108
	16	156	183
		164	67
	21	165	155
		176	150
	22	14	75
		155	96
		156	102
	23	134	56
		144	68
		166	104
	24	151	65
		165	108
	28	129	66
		143	104
	30	126	114
		156	53
	31	141	81
		143	110
	32	155	68
	36	96	54
		108	105
		114	54
	37	126	114
	38	86	85
		133	69
		154	107
	39	81	79
		128	81
	40	124	120
	44	90	54

Table 12. 30 March 90 LAC lead spacing and width with orientation.

File: cf_bi_30mar90_lsub.dat
Image size (km in one dimension):   512
Percent covered by leads: 4.3

| orientation (deg)	# of lead crossings	mean spacing (km)	std spacing (km)	mn width (km)	std wdth (km)
0.	573	18.2	25.2	2.4	2.3
15.	647	17.3	23.4	2.1	1.4
30.	620	17.3	20.2	2.0	1.3
45.	553	19.0	20.1	1.8	1.0
60.	593	17.8	20.5	2.0	1.1
75.	600	17.5	24.7	2.1	1.2
90.	622	16.2	17.7	2.2	1.5
105.	608	15.3	16.1	2.1	1.3
120.	569	15.7	18.2	2.1	1.4
135.	457	20.1	22.2	2.1	1.5
150.	576	16.8	26.4	2.2	1.9
165.	596	17.2	26.8	2.2	2.0
180.	573	18.2	25.2	2.4	2.3
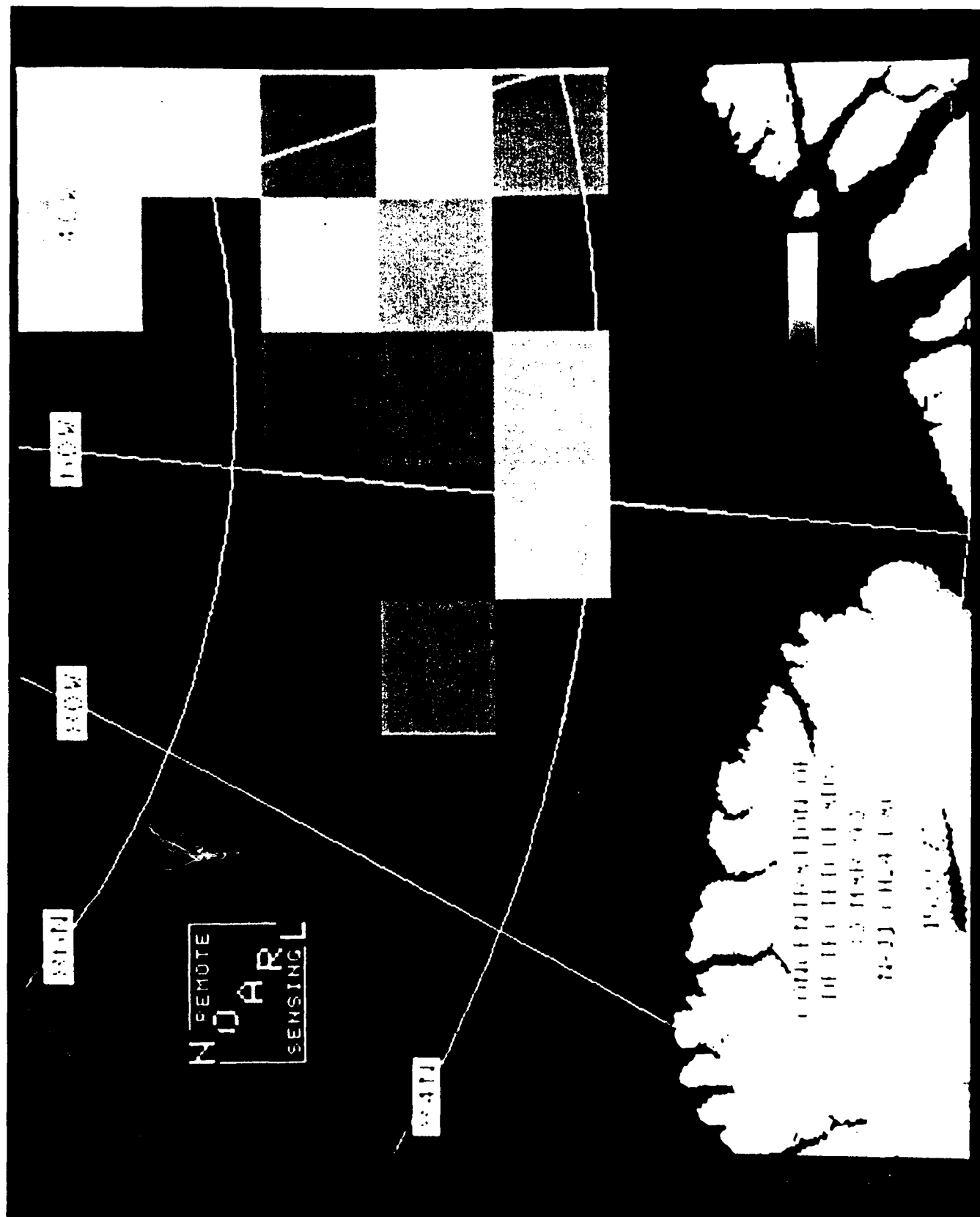
Figure 24. 30 March 90 LAC grey level image (brightness represents lead coverage).

Figure 25. 30 March 90 GAC enhanced image with grid and land mask.

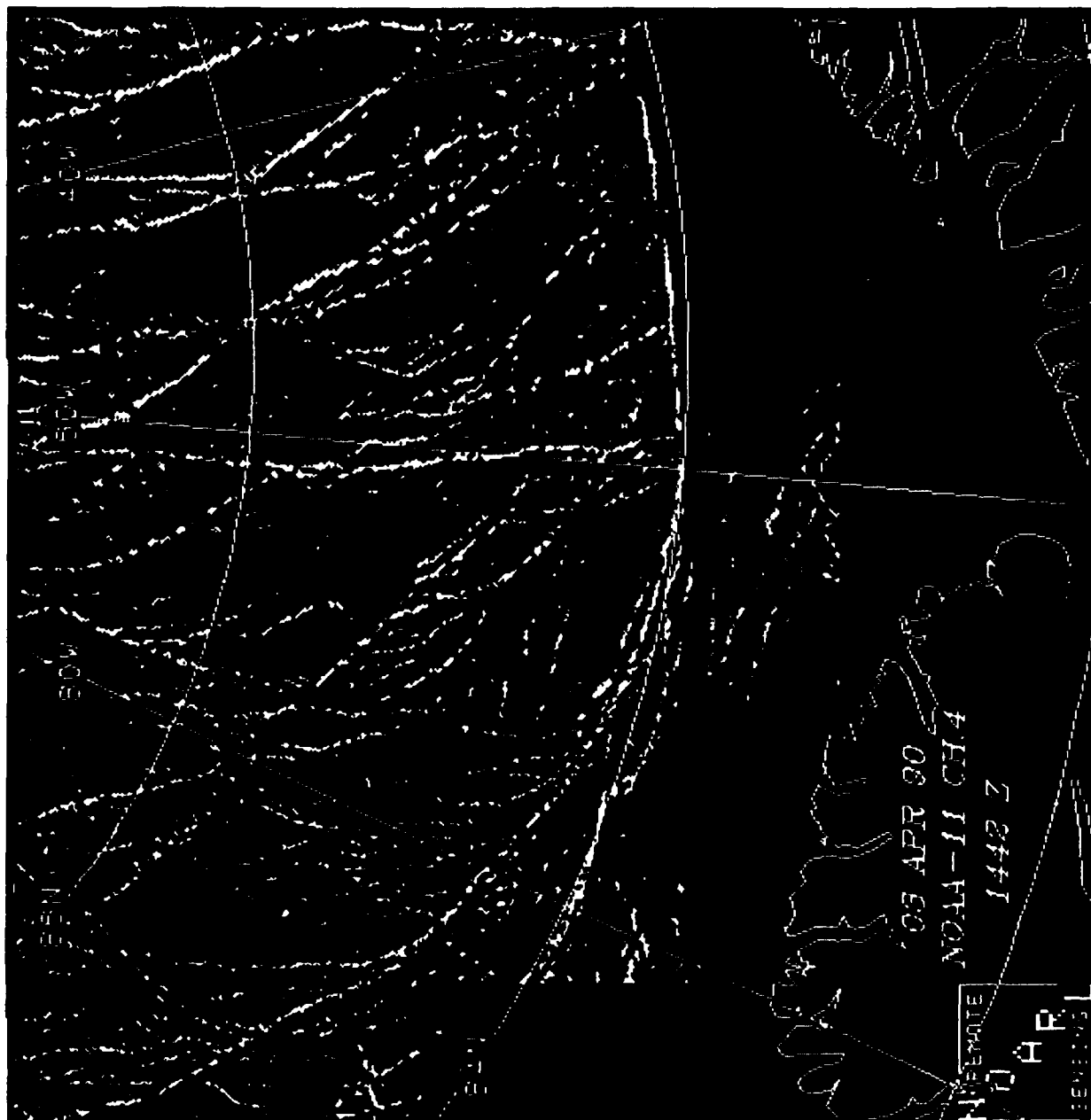Figure 26. 30 March 90 GAC binary image of leads.

Figure 27a. 30 March 90 GAC binary image of leads with land and cloud blocks removed.

Figure 27b. 30 March 90 GAC rose plots of lead size vs. orientation.

Table 13. 30 March 90 GAC lead size and orientation.

Date	Block Number	Direction (degrees)	km²
30 Mar 1990 GSUB	5	28	61
		44	78
		45	142
		99	144
		164	160
	0	0	69
		44	133
		109	59
		136	134
		155	90
		173	217
	16	134	192
		142	67
		152	94
	22	18	228
		44	50
		45	103
		135	163
		156	97
		159	113
	23	45	328
		52	71
		89	63
		117	109
		135	57
		136	125
		149	229
	24	44	53
		45	216
		126	58
		135	97
		148	113
		153	62
	28	46	94
		104	229
		139	118
		154	184
	29	44	91
		125	59
		134	50
		160	86
		176	55
	30	120	186
		122	95
		133	69
		134	90
		171	83
	31	45	66
		146	54
		164	116
	32	44	54
		45	283
		102	177
		134	132
	36	45	50
		63	56
		82	90
		103	87
		108	83
		113	196
		128	170
		135	66

Date	Block Number	Direction (degrees)	km²
30 Mar 1990 GSUB (cont)	37	30	52
		45	105
		69	69
		95	126
		124	186
		135	155
	38	45	58
		82	132
		134	269
		148	185
	39	44	71
		45	105
		110	65
		120	78
		132	66
	40	72	238
		110	50
		129	157
	44	31	96
		46	160
		83	108
		108	65
	44	124	57
		135	123
		152	86
	45	88	115
		89	51
		134	123
		135	93
		145	165

Table 14. 30 March 90 GAC lead spacing and width with orientation.

File: cf_bi_30mar90_gsub.dat
Image size (km in one dimension): 512
Percent covered by leads: 9.0

orientation (deg)	# of lead crossings	mean spacing (km)	std spacing (km)	mn width (km)	std wdth (km)
0.	447	17.2	26.4	6.5	5.3
15.	475	17.6	26.9	5.9	5.0
30.	423	19.6	31.1	6.0	4.7
45.	390	20.0	28.0	5.4	4.0
60.	415	17.0	23.7	5.9	5.1
75.	405	16.9	23.2	6.1	4.9
90.	428	13.1	13.7	6.6	5.6
105.	458	14.2	18.7	6.1	5.7
120.	444	16.5	23.5	5.8	5.2
135.	421	17.5	23.5	4.8	4.8
150.	451	15.8	24.9	5.5	5.9
165.	469	15.8	23.6	6.0	5.6
180.	447	17.2	26.4	6.5	5.3
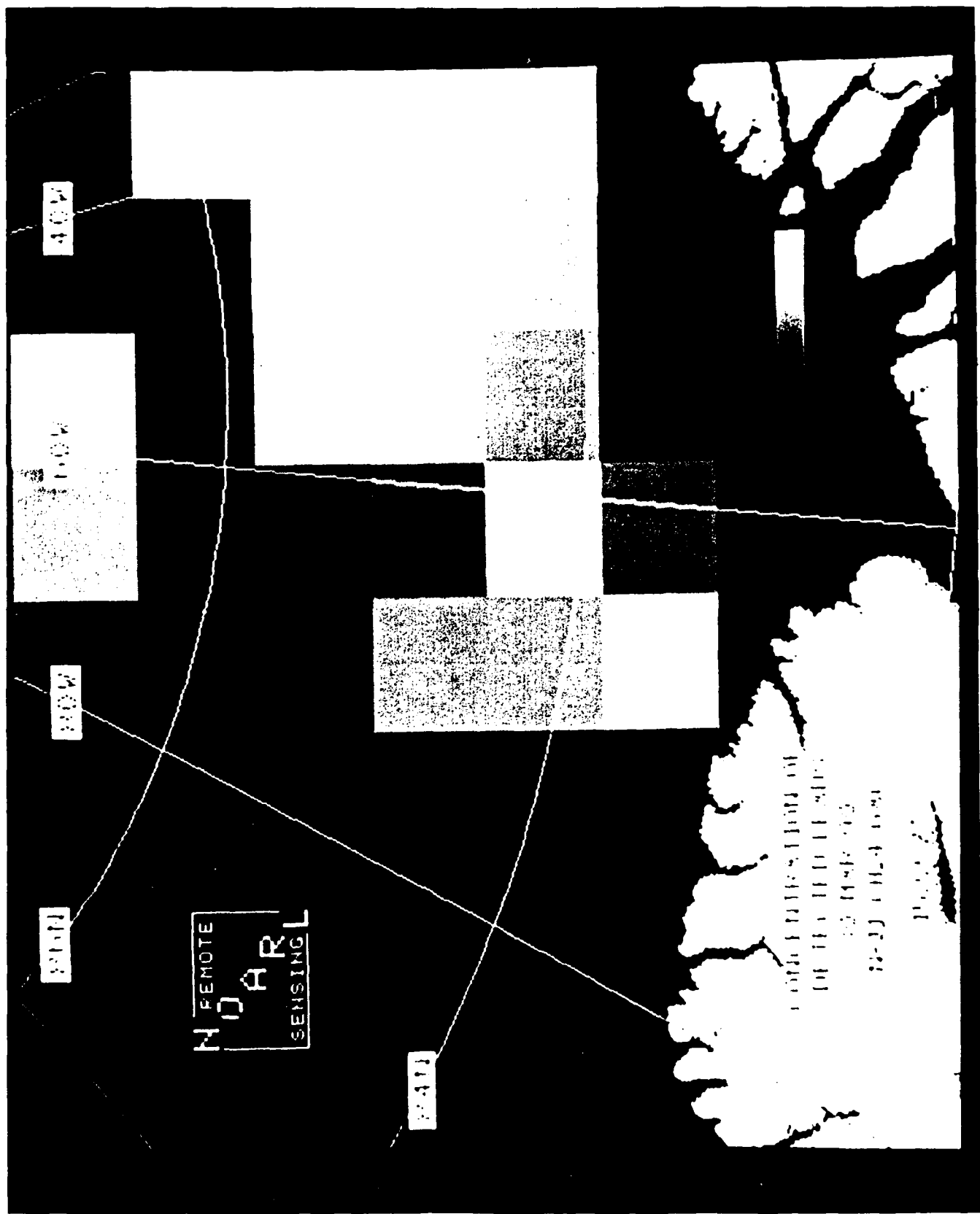
Figure 28. 30 March 90 GAC grey level image (brightness represents lead coverage).

Figure 29. 03 April 90 enhanced Image with grid and land mask.

Figure 30. 03 April 90 binary image of leads.

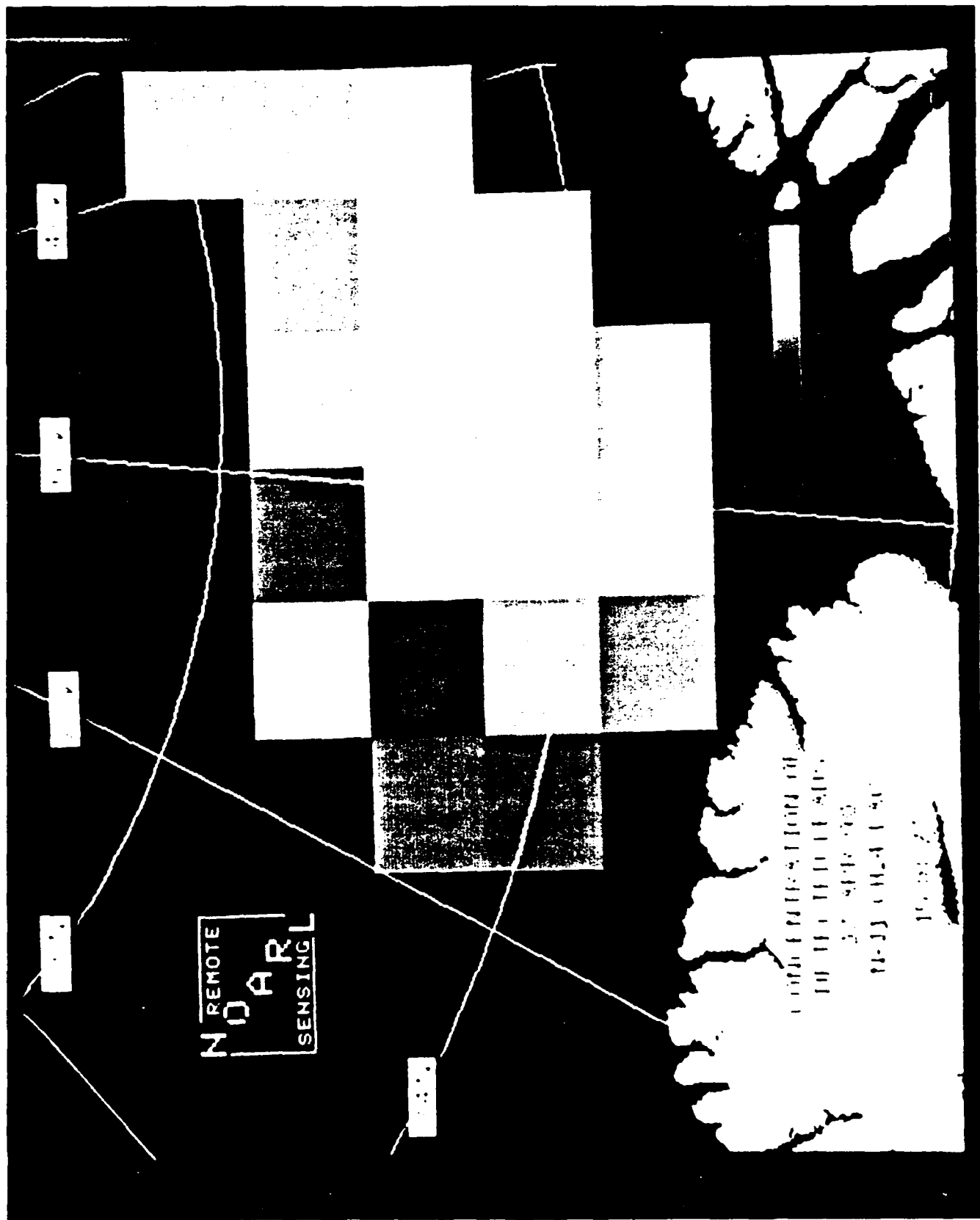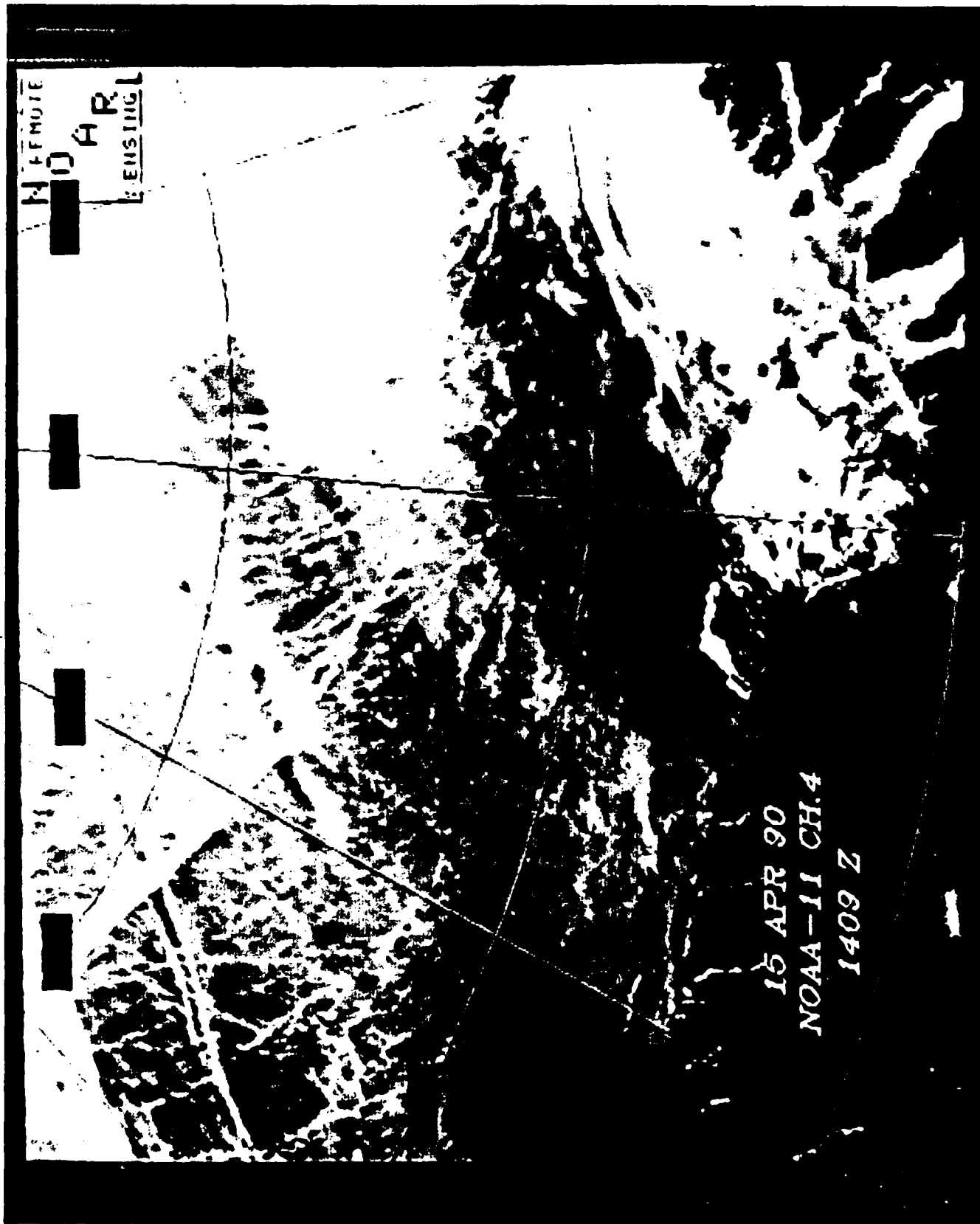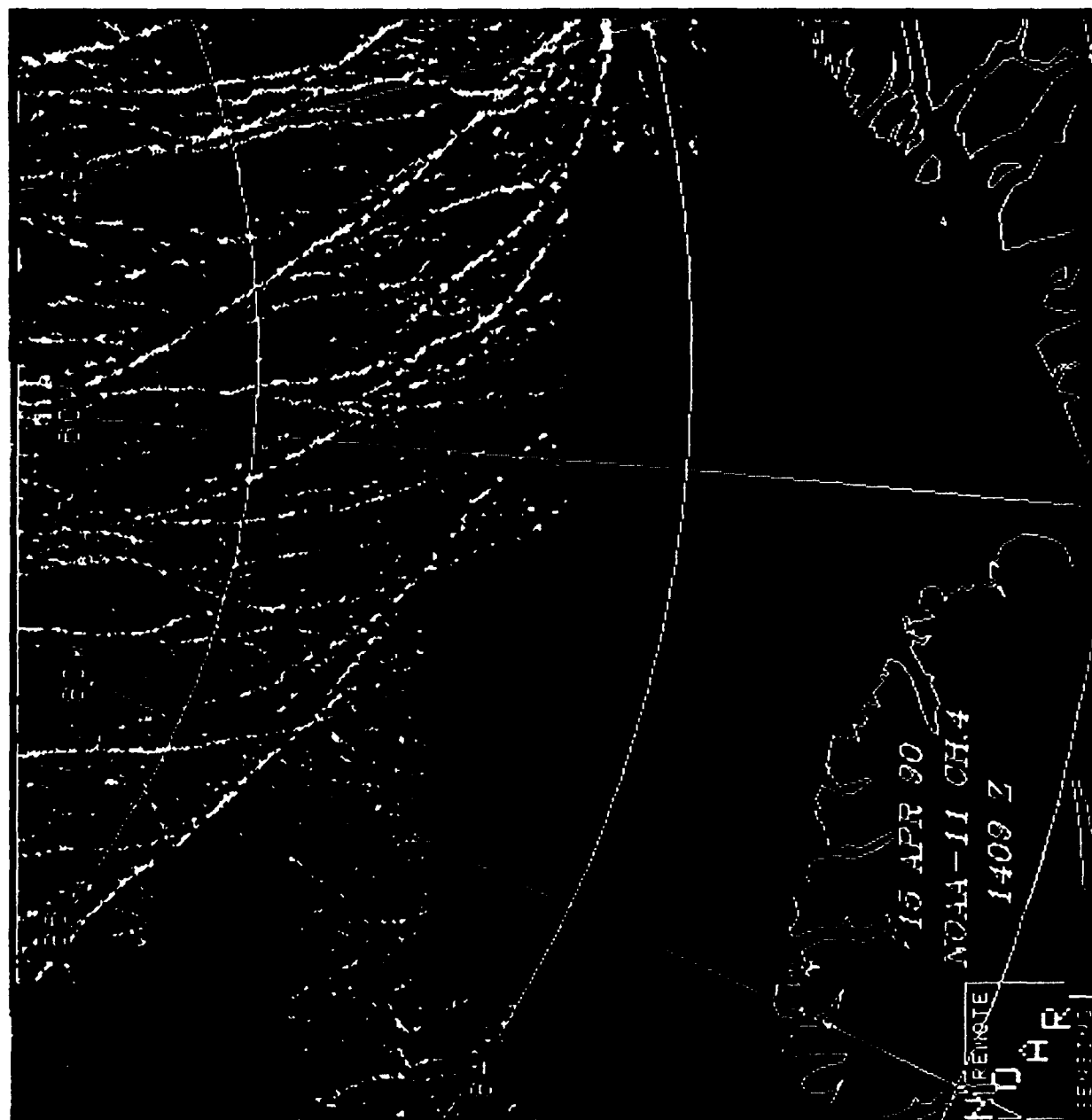Figure 31a. 03 April 90 binary Image of leads with land and cloud blocks removed.
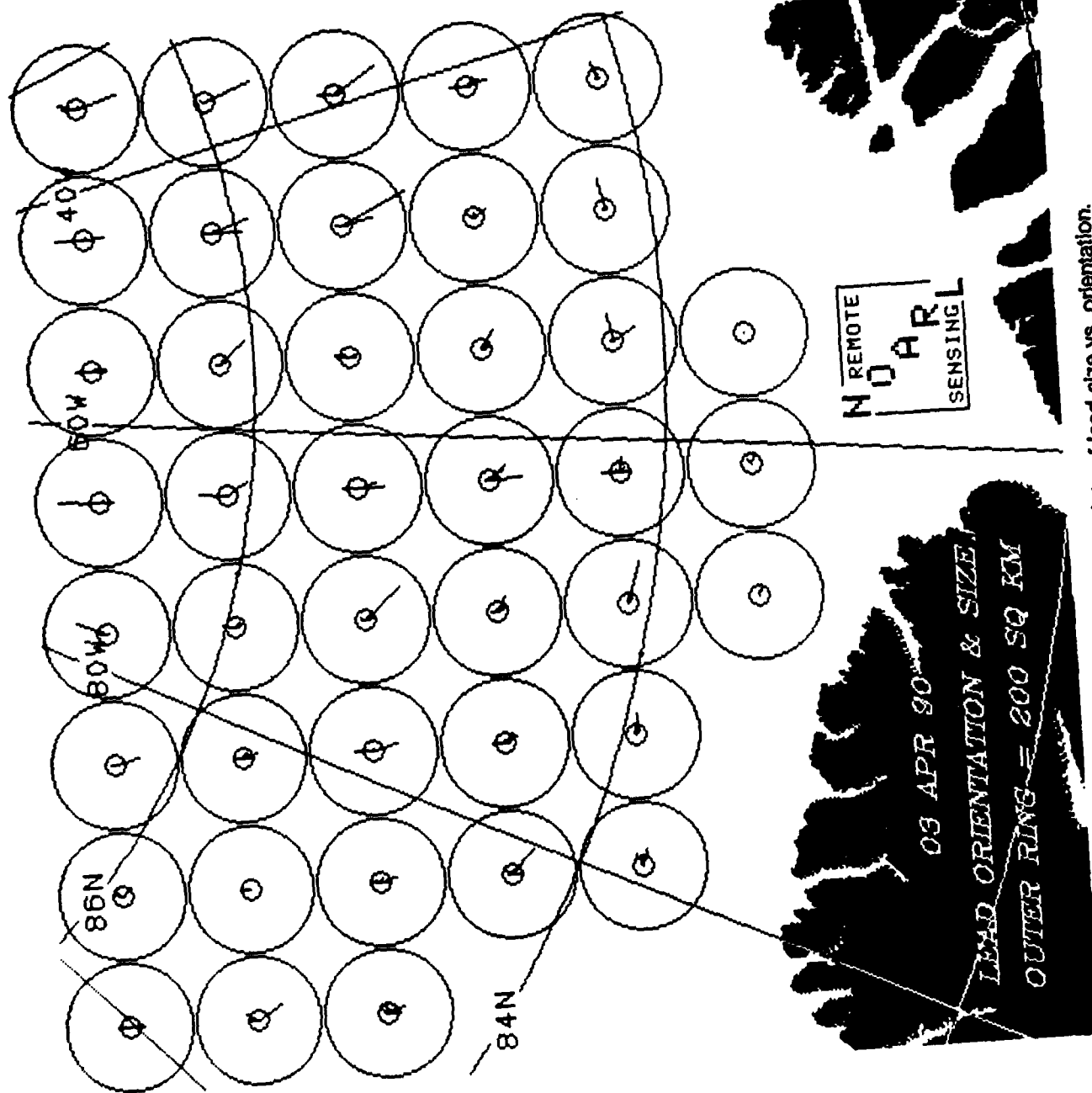
Figure 31b. 03 April 90 rose plots of lead size vs. orientation.

Table 15. 03 April 90 lead size and orientation.

Date	Block Number	Direction (degrees)	km^2
03 Apr 1990	3	166	79
	4	24	100
	5	3	120
	5	176	50
	6	1	50
	6	167	50
	6	174	50
	7	0	82
		172	68
	8	19	54
		163	137
	9	148	90
	11	165	50
	13	6	85
		150	78
	14	140	108
	15	161	121
		177	94
	16	158	159
	17	157	56
	18	165	52
	19	2	51
		164	82
	20	138	144
	21	164	59
		178	84
	23	155	229
		166	101
	24	145	153
	25	95	92
		134	90
		146	62
	26	131	75
	27	134	50
	28	122	54
	29	139	70
		141	57
		173	101
	30	126	71
	32	161	70
	33	65	50
		73	77
	33	89	79
	34	103	56
	35	96	64
	36	108	125
	37	5	54
	38	85	82
		152	84
	39	81	100
	40	76	54
	54	136	58

Table 16. 03 April 90 lead spacing and width with orientation.

```
File: cf_bi_03apr90_lsub.dat
Image size (km in one dimension):   512
Percent covered by leads:        8.2
```

orientation (deg)	# of lead crossings	mean spacing (km)	std spacing (km)	mn width (km)	std wdth (km)
0.	1050	12.7	22.5	2.4	2.4
15.	1168	10.3	12.2	2.2	1.7
30.	1103	11.5	16.1	2.1	1.3
45.	977	12.8	14.5	1.9	1.0
60.	1091	11.0	13.3	2.1	1.3
75.	1178	10.2	11.8	2.1	1.3
90.	1150	10.7	12.6	2.3	1.8
105.	1113	11.1	14.7	2.3	1.6
120.	983	13.0	17.4	2.3	1.7
135.	832	15.6	18.8	2.3	1.7
150.	978	12.9	17.8	2.3	2.3
165.	1074	11.9	18.2	2.4	2.2
180.	1050	12.7	22.5	2.4	2.4

Figure 32. 03 April 90 grey level image (brightness represents lead coverage).

07 APR 90
NOAA-11 CH.4
1538 Z
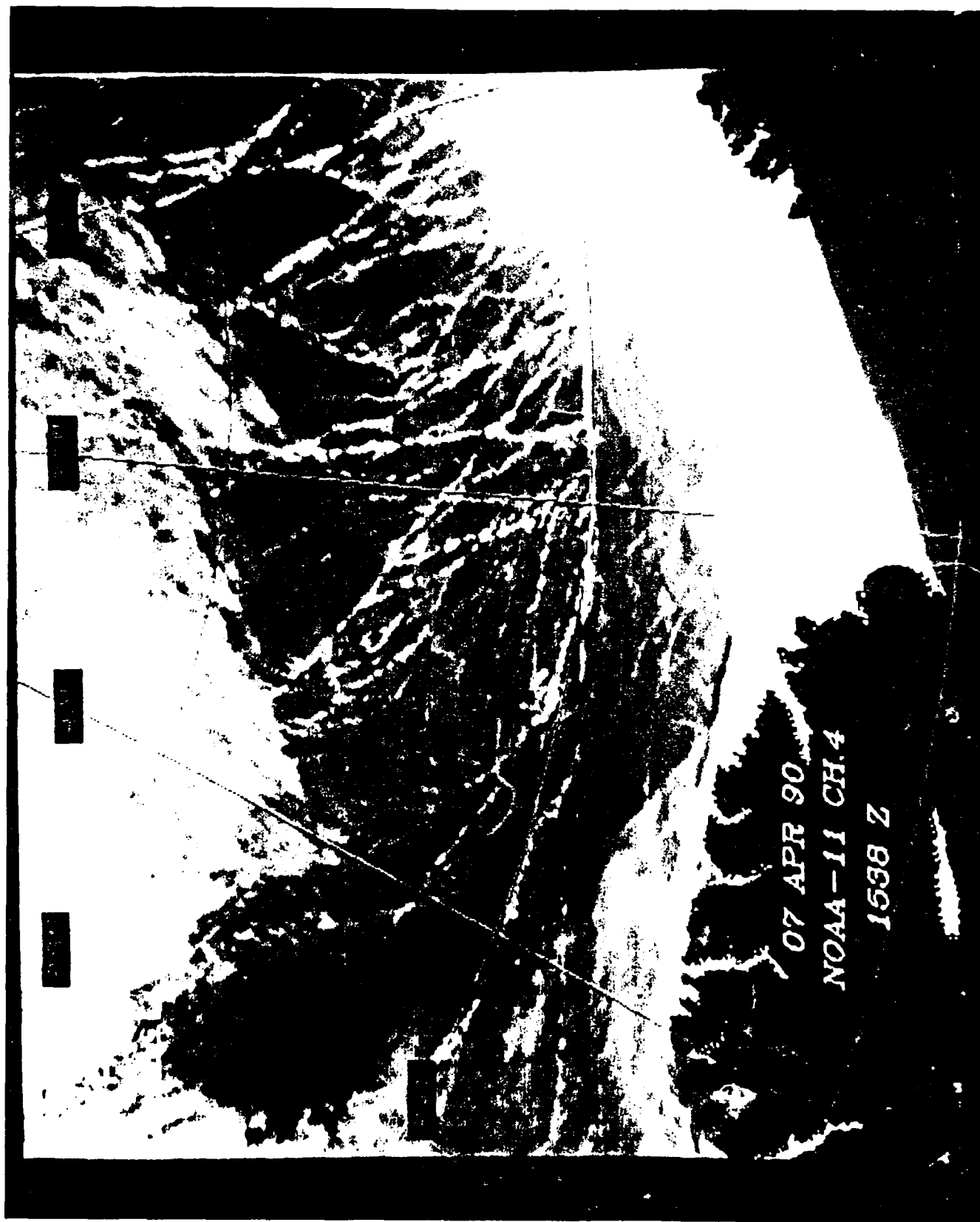
Figure 33. 07 April 90 enhanced image with grid and land mask.

Figure 34. 07 April 90 binary image of leads.
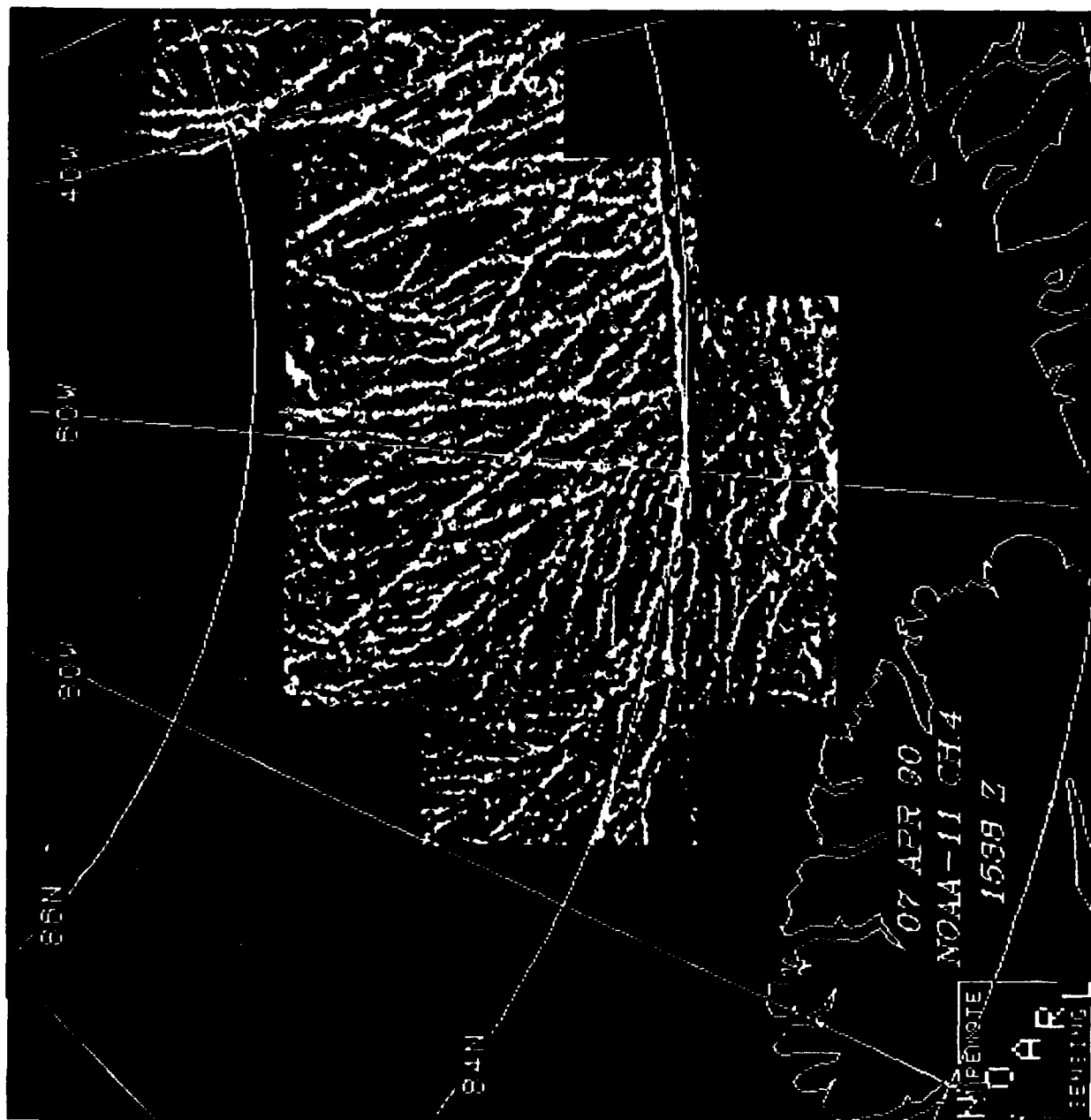
Figure 35a. 07 April 90 binary image of leads with land and cloud blocks removed.
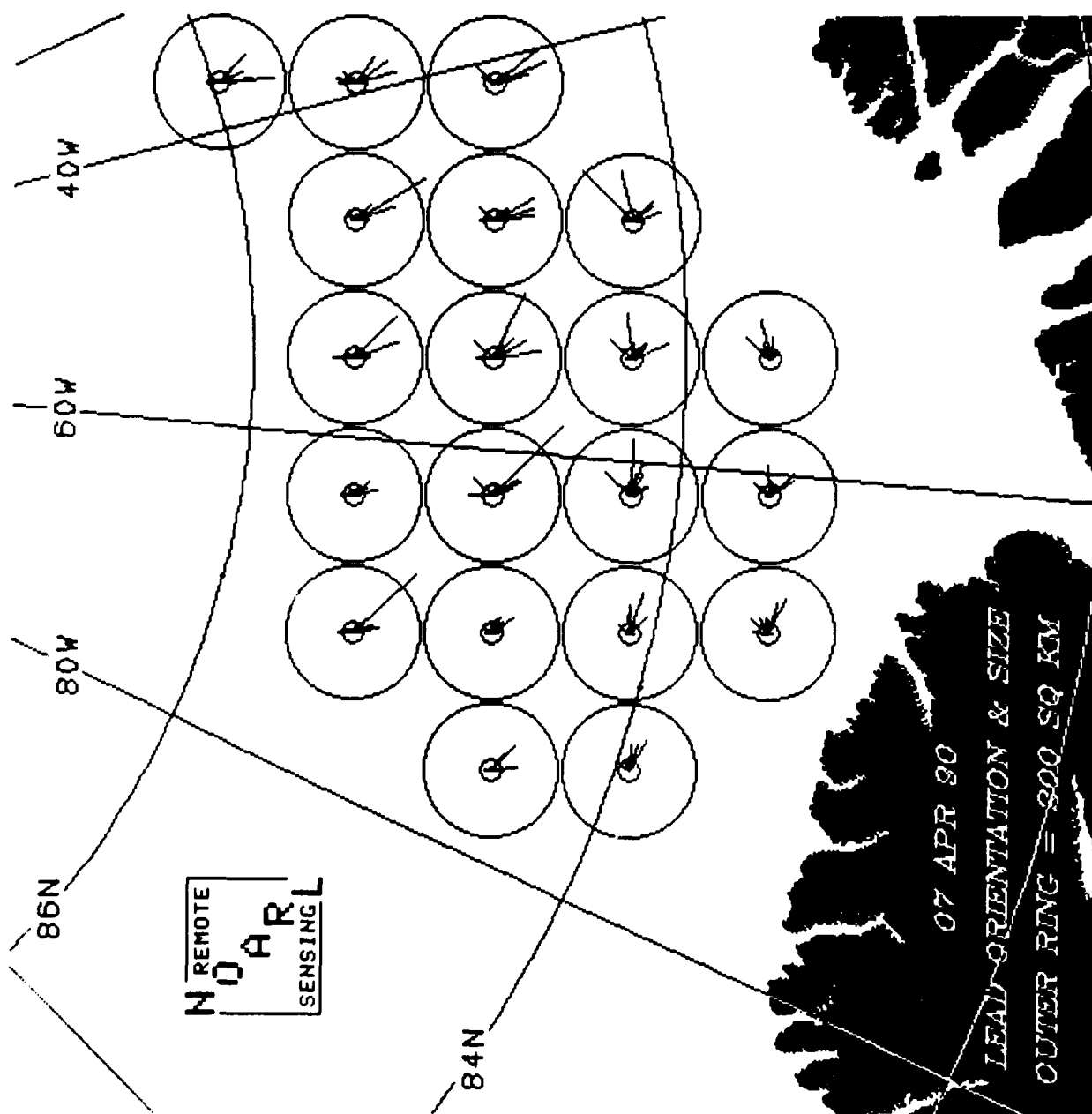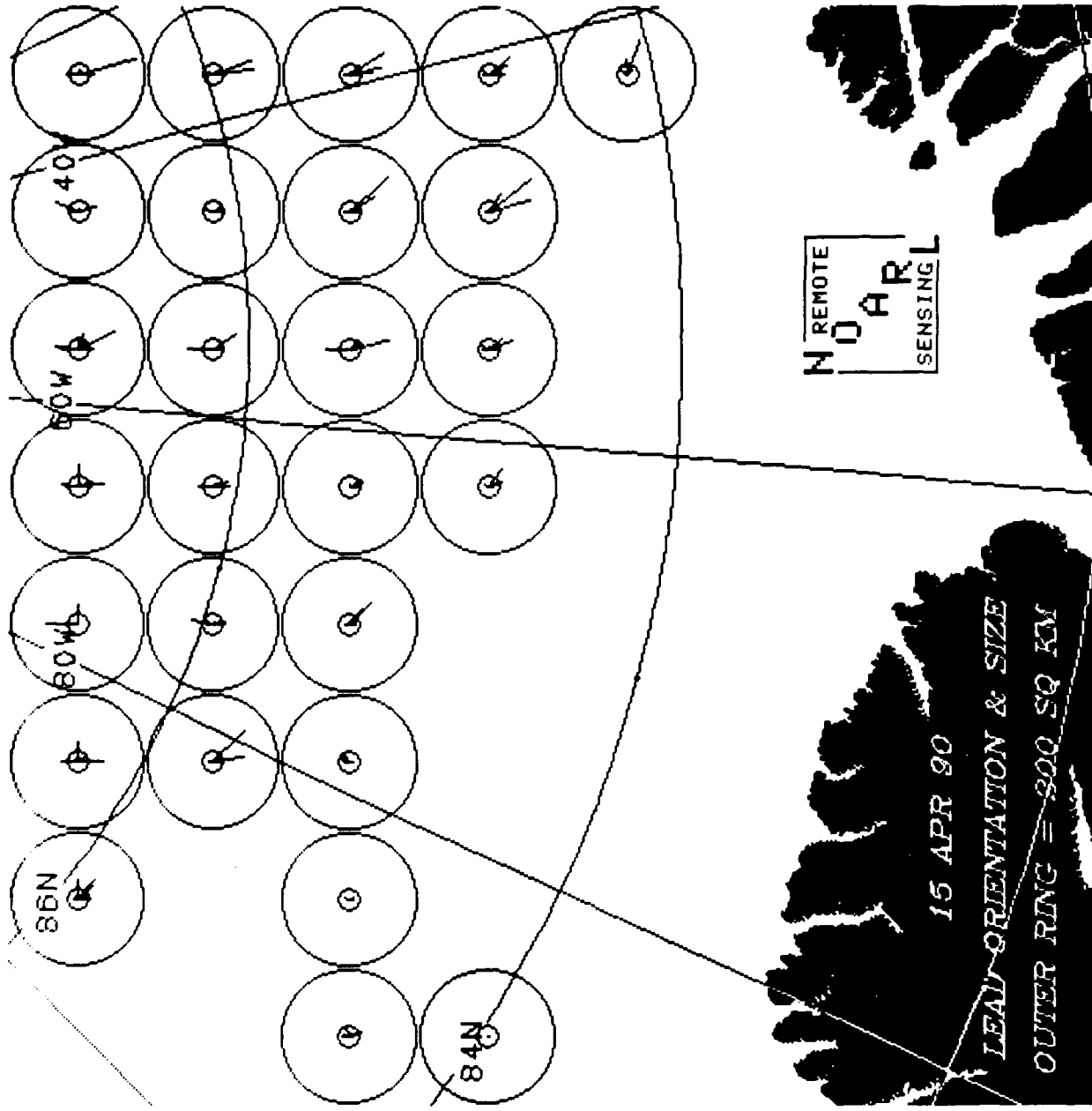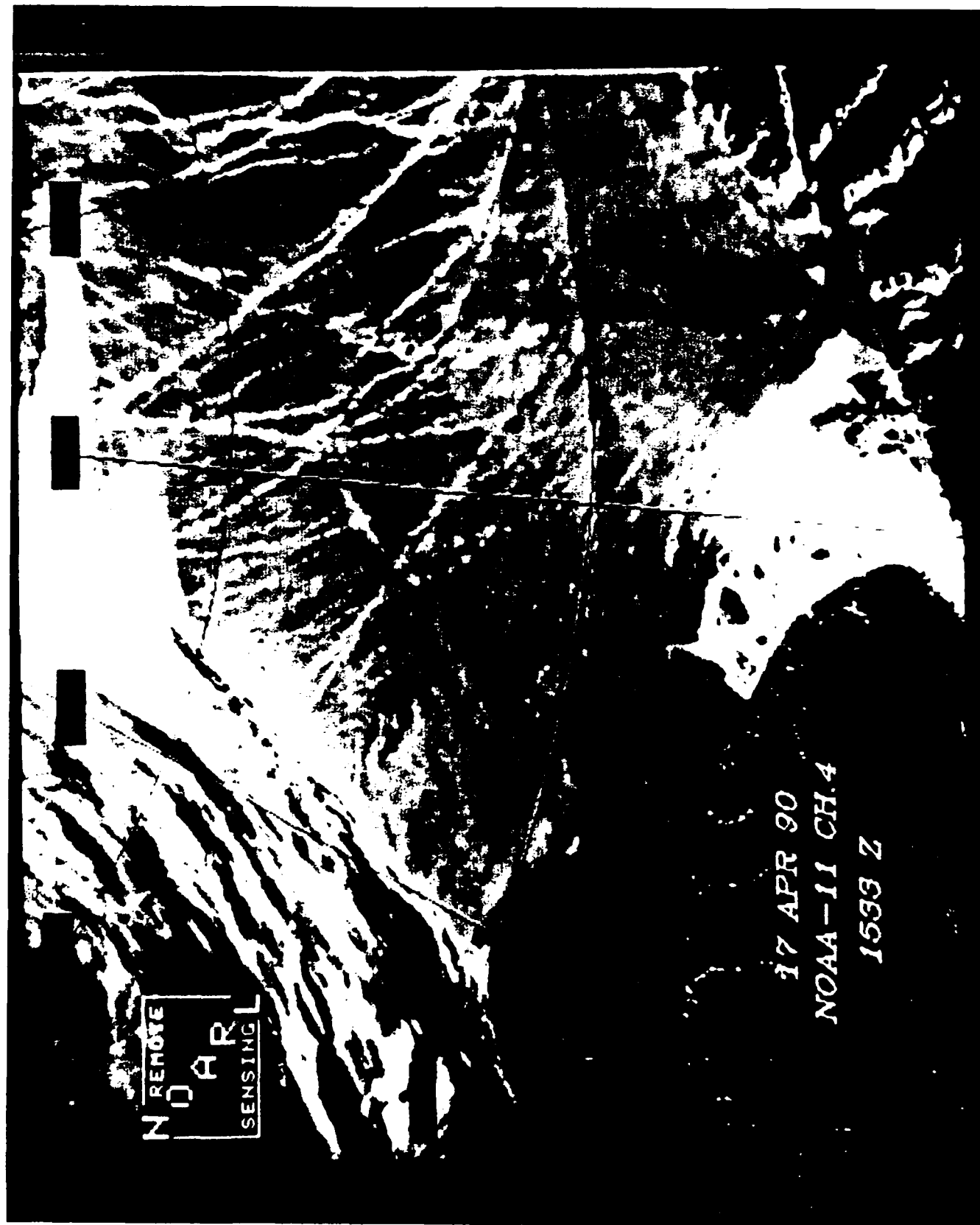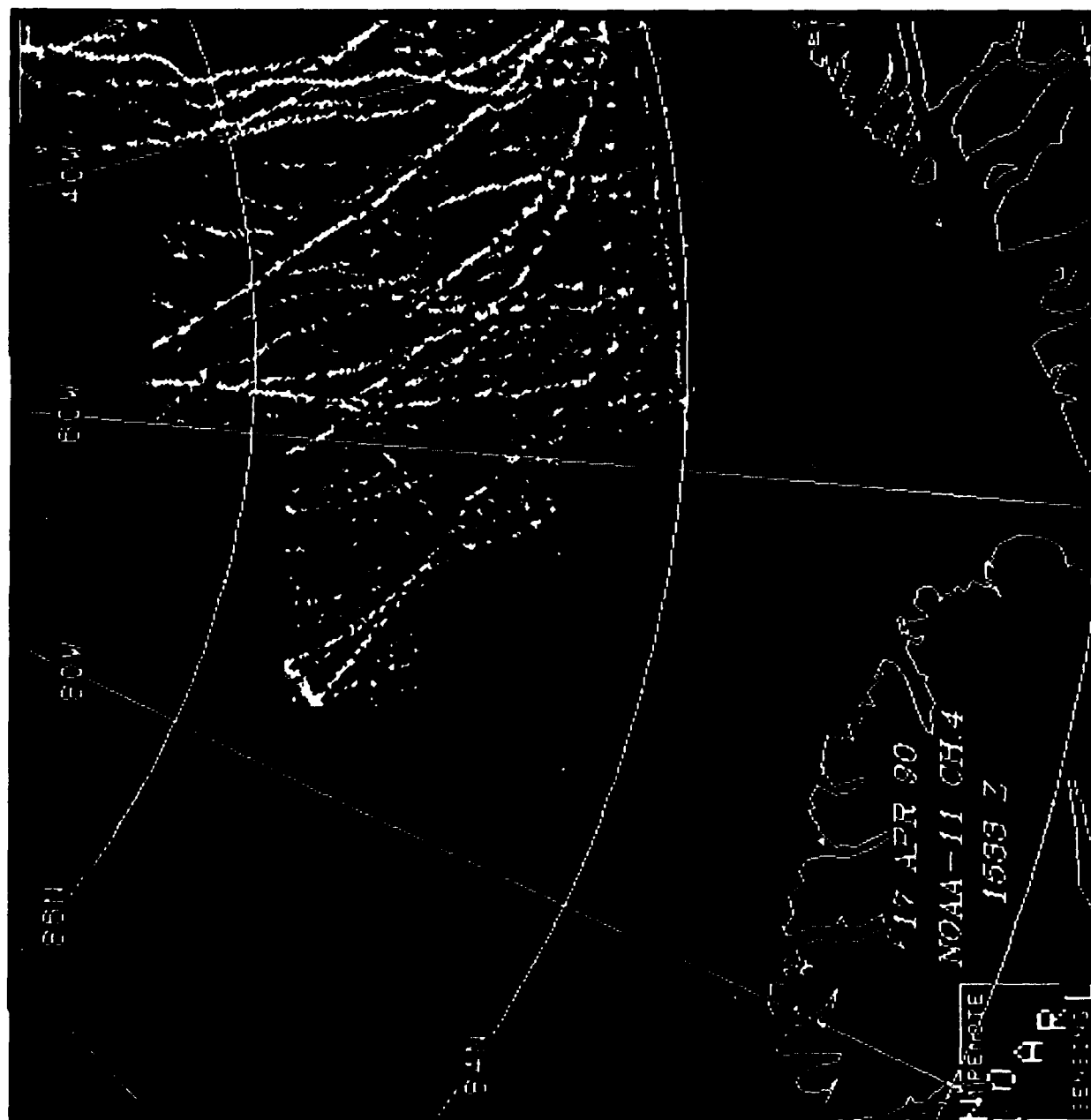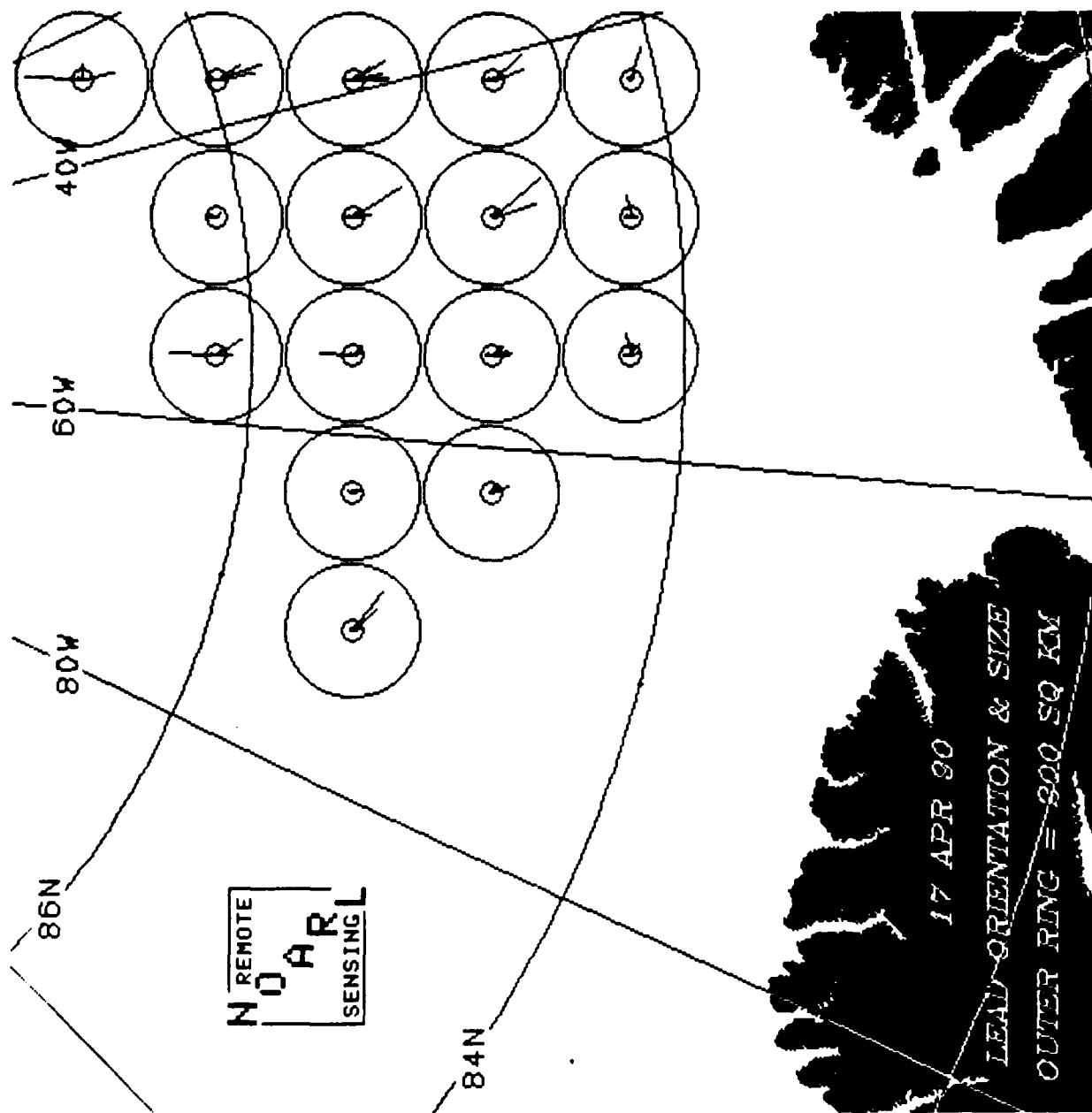
Figure 35b. 07 April 90 rose plots of lead size vs. orientation.

Table 17. 07 April 90 lead size and orientation.

Date	BLK	Deg	km²
07 April 1990	16	133	113
		156	78
		172	106
		174	168
	20	137	250
		155	59
		161	61
		169	80
	21	139	62
		167	75
	22	1	62
		135	175
		159	139
		168	51
	23	134	67
		149	235
		161	123
	24	19	54
		45	51
		124	91
		143	111
		163	118
	27	133	63
		134	104
		175	81
	28	121	55
		135	52
		145	78
	29	1	64
		45	79
		135	287
		146	87
		156	95
		162	64
	30	45	78
		115	210
		136	83
		152	110
		154	54
		172	143
	31	45	60
		141	52
		150	130
		163	124
		172	119
	32	45	75
		135	51
		140	175
		157	162
		162	101

Date	BLK	Deg	km^2
07 April 1990	35	97	80
		112	81
		120	104
	36	87	52
		91	82
		95	66
		108	130
		133	74
		135	51
	37	45	100
		94	165
		102	66
		108	110
		116	74
		151	60
	38	45	80
		85	135
		128	62
		135	68
		140	53
		156	118
	39	45	203
		79	150
		135	88
		141	78
		161	87
	44	45	64
		63	50
		107	98
		117	115
	45	45	51
		88	92
		136	96
		141	60
		146	87
	46	45	90
		69	51
		80	117
		101	64

Table 18. 07 April 90 lead spacing and width with orientation.

```
File: cf_bi_07apr90_lsub.dat
Image size (km in one dimension):   512
Percent covered by leads:        7.4
```

orientation (deg)	# of lead crossings	mean spacing (km)	std spacing (km)	mn width (km)	std wdth (km)
0.	931	7.8	7.8	2.6	2.1
15.	1025	7.3	7.4	2.4	1.7
30.	966	7.9	8.5	2.2	1.5
45.	893	9.2	11.2	1.9	1.1
60.	1001	7.9	10.3	2.1	1.4
75.	1004	8.4	14.2	2.4	1.8
90.	1005	7.5	7.2	2.4	1.9
105.	1009	7.3	7.7	2.3	1.8
120.	888	8.2	9.7	2.3	1.5
135.	716	10.2	11.6	2.4	1.9
150.	872	8.4	9.8	2.4	2.1
165.	950	7.6	8.3	2.4	2.2
180.	931	7.8	7.8	2.6	2.1

Figure 36. 07 April 90 grey level Image (brightness represents lead coverage).

Figure 37. 15 April 90 enhanced image with grid and land mask.

Figure 38. 15 April 90 binary image of leads.

Figure 39a. 15 April 90 binary image of leads with land and cloud blocks removed.

-15 APR 90
NOAA-11 CH.4
1409 Z

Figure 39b. 15 April 90 rose plots of lead size vs. orientation.

Table 19. 15 April 90 lead size and orientation.

Date	Block Number	Direction (degrees)	km^2
15 April 1990	2	90	61
		132	81
		137	61
		141	56
	3	90	60
		17	77
	4	2	90
		90	61
	5	90	64
		172	81
	6	155	122
	7	25	73
		163	57
	8	165	175
	11	136	133
		170	96
	12	17	60
	13	174	56
	14	4	70
		147	84
	16	161	121
		169	60
		171	121
	20	130	59
		136	91
	22	2	65
		165	117
	23	136	151
		146	86
	24	147	117
		166	92
		174	69
	29	126	66
	30	141	53
		158	78
	31	121	64
	31	142	157
		163	128
	32	139	78
		151	59
	40	107	107

Table 20. 15 April 90 lead spacing and width with orientation.

```
File: cf_bi_15apr90_lsub.dat
Image size (km in one dimension):  512
Percent covered by leads:        4.3
```

orientation (deg)	# of lead crossings	mean spacing (km)	std spacing (km)	mn width (km)	std wdth (km)
0.	568	20.0	25.9	2.3	2.4
15.	658	18.8	25.0	1.9	1.4
30.	672	17.8	21.5	1.8	1.1
45.	585	20.6	21.9	1.6	0.9
60.	665	17.3	19.3	1.7	0.8
75.	761	15.4	18.3	1.7	0.9
90.	736	17.0	22.8	1.9	1.1
105.	722	18.7	32.8	1.8	1.1
120.	648	18.0	19.7	1.9	1.2
135.	518	19.7	20.5	1.8	1.4
150.	622	17.8	22.5	1.9	1.6
165.	677	16.2	24.2	2.1	2.0
180.	568	20.0	25.9	2.3	2.4
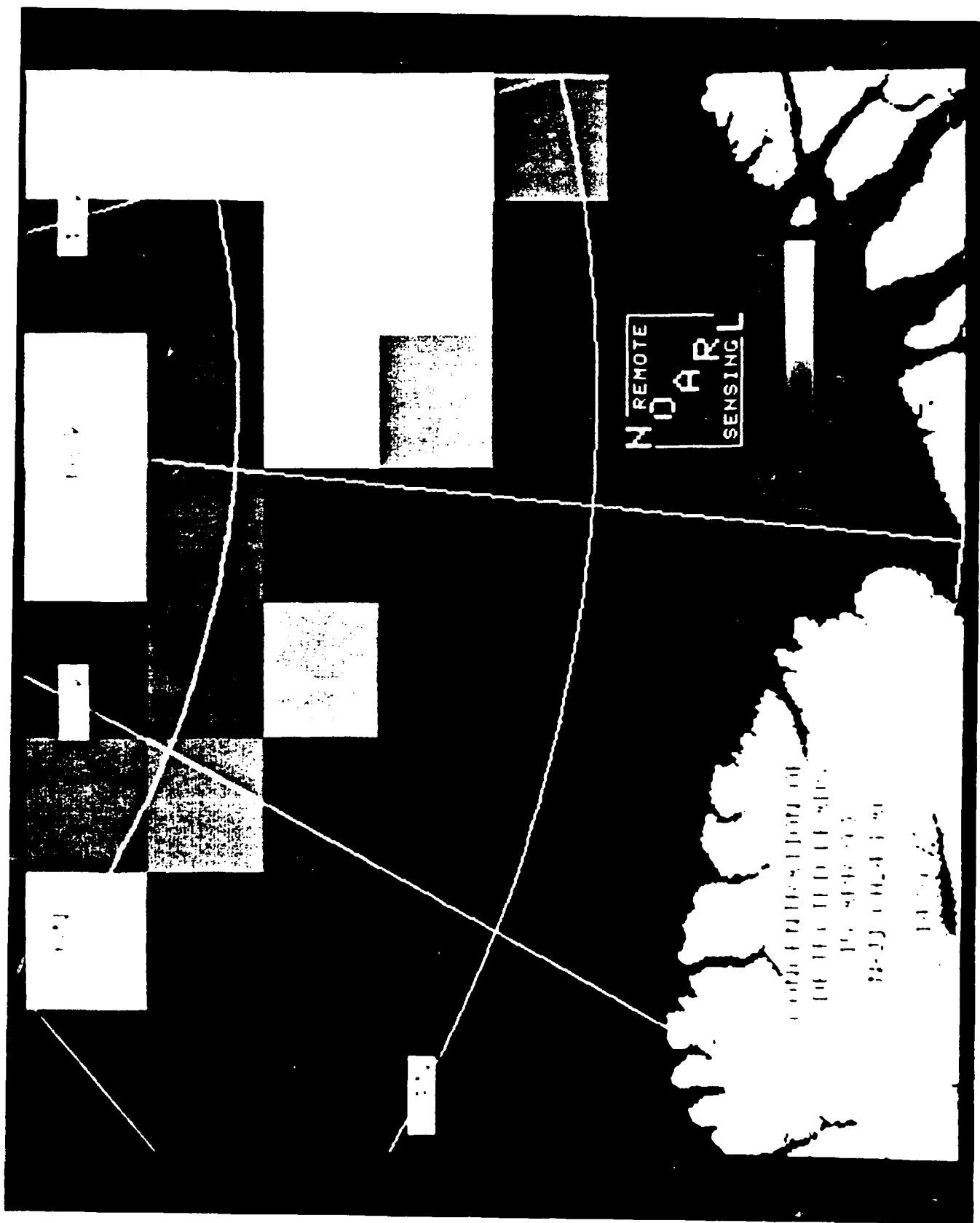
Figure 40. 15 April 90 grey level image (brightness represents lead coverage).

Figure 41. 17 April 90 enhanced image with grid and land mask.

Figure 42. 17 April 90 binary image of leads.

Figure 43a. 17 April 90 binary image of leads with land and cloud blocks removed.

Figure 43b. 17 April 90 rose plots of lead size vs. orientation.

Table 21. 17 April 90 lead size and orientation.

Date	Block Number	Direction (degrees)	km^2
17 April 1990	8	4	169
		168	101
	14	5	137
		148	94
		177	52
	16	145	87
		161	140
		170	117
	20	129	146
		135	97
		141	54
	22	4	94
	23	146	167
		173	56
	24	135	62
		146	107
		165	87
		175	106
		177	96
	29	156	55
	30	173	59
		177	51
	31	140	184
		163	135
	32	139	115
		159	94
	38	84	67
	39	80	66
	40	105	101

Table 22. 17 April 90 lead spacing and width with orientation.

```
File: cf_bi_17apr90_lsub.dat
Image size (km in one dimension):   512
Percent covered by leads:        2.8
```

orientation (deg)	# of lead crossings	mean spacing (km)	std spacing (km)	mn width (km)	std wdth (km)
0.	385	15.3	19.9	2.3	2.2
15.	402	14.9	17.2	2.3	1.8
30.	404	15.7	17.6	1.9	1.3
45.	366	18.3	20.4	1.7	1.0
60.	404	16.2	17.6	1.8	1.1
75.	421	15.8	18.0	1.9	1.1
90.	434	14.4	13.7	2.0	1.2
105.	414	15.6	14.2	2.0	1.2
120.	409	15.2	17.5	2.0	1.4
135.	289	20.1	25.2	2.1	1.8
150.	369	15.0	20.8	2.3	2.2
165.	375	14.8	19.2	2.3	2.1
180.	385	15.3	19.9	2.3	2.2
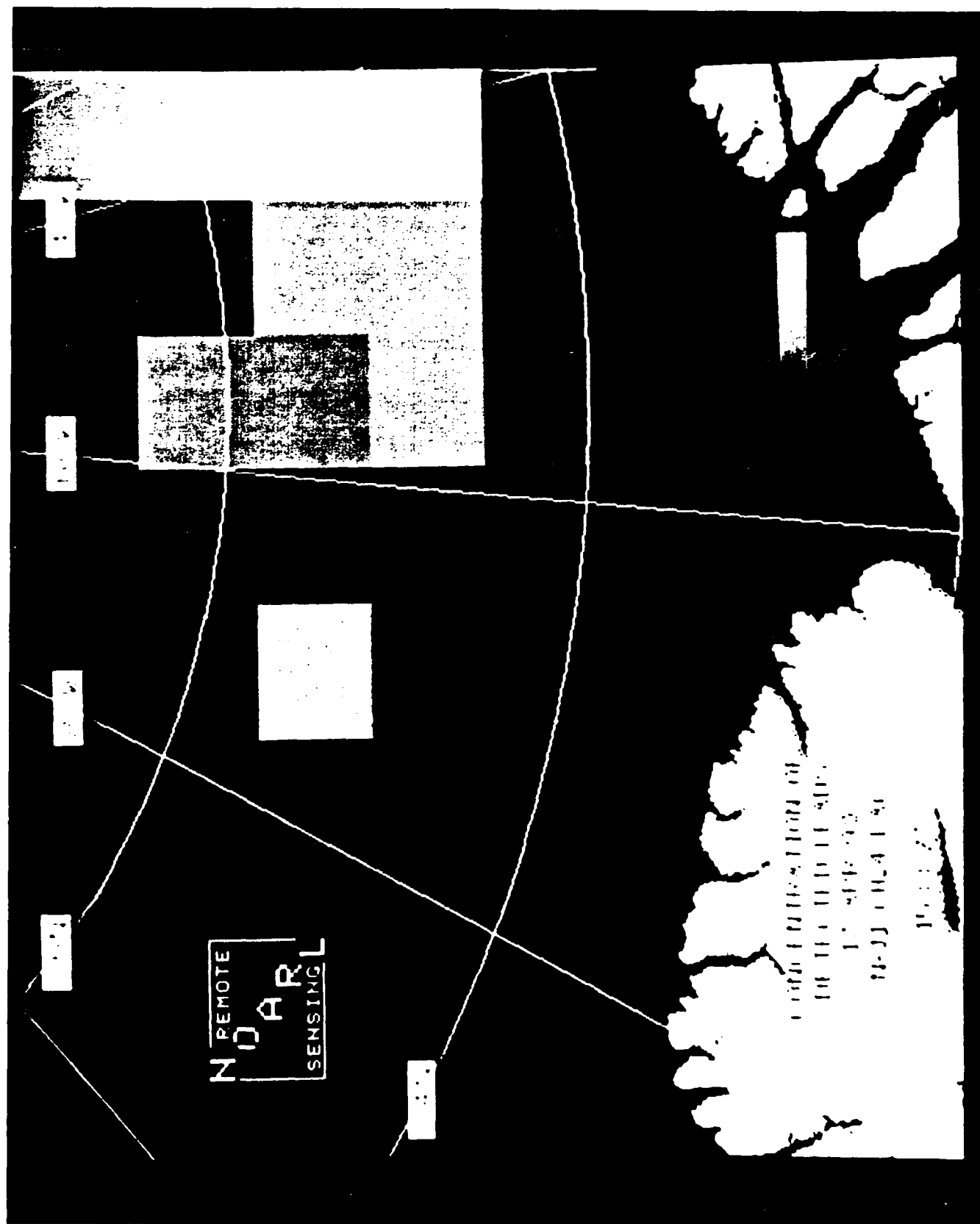
Figure 44. 17 April 90 grey level image (brightness represents lead coverage).

Figure 45. 19 March 90 binary Image with two areas selected for analysis.

Table 23. 19 March 90 lead spacing and width with orientation for areas 1 and 2.

File: 19MAR90_AREA1.dat
Image size (km in one dimension): 128
Percent covered by leads: 15.3

orientation (deg)	# of lead crossings	mean spacing (km)	std spacing (km)	mn width (km)	std wdth (km)
0.	131	12.5	12.6	2.5	1.5
15.	136	12.1	10.8	2.2	1.2
30.	142	11.2	10.1	1.9	1.0
45.	127	12.3	11.3	1.8	1.0
60.	139	11.4	11.4	1.9	1.0
75.	138	11.5	12.2	2.3	1.6
90.	126	12.5	13.6	2.2	1.5
105.	121	10.5	14.2	2.4	1.6
120.	117	12.2	17.2	2.4	2.0
135.	91	13.3	19.0	2.2	1.7
150.	92	16.4	21.2	2.6	2.2
165.	121	12.4	14.7	2.5	1.9
180.	131	12.5	12.6	2.5	1.5

File: 19MAR90_AREA2.dat
Image size (km in one dimension): 128
Percent covered by leads: 10.7

orientation (deg)	# of lead crossings	mean spacing (km)	std spacing (km)	mn width (km)	std wdth (km)
0.	77	22.4	23.3	2.6	1.9
15.	100	15.0	14.3	2.0	1.4
30.	95	14.9	12.4	2.1	1.2
45.	86	18.8	12.5	1.7	0.7
60.	109	14.6	11.2	1.8	0.9
75.	106	14.9	11.7	2.0	1.0
90.	107	15.4	12.1	2.2	1.2
105.	92	17.1	15.9	2.2	1.4
120.	90	16.9	18.5	2.2	1.5
135.	71	18.9	27.5	2.4	1.6
150.	89	10.7	20.1	2.1	2.3
165.	75	16.3	22.3	2.5	2.2
180.	77	22.4	23.3	2.6	1.9
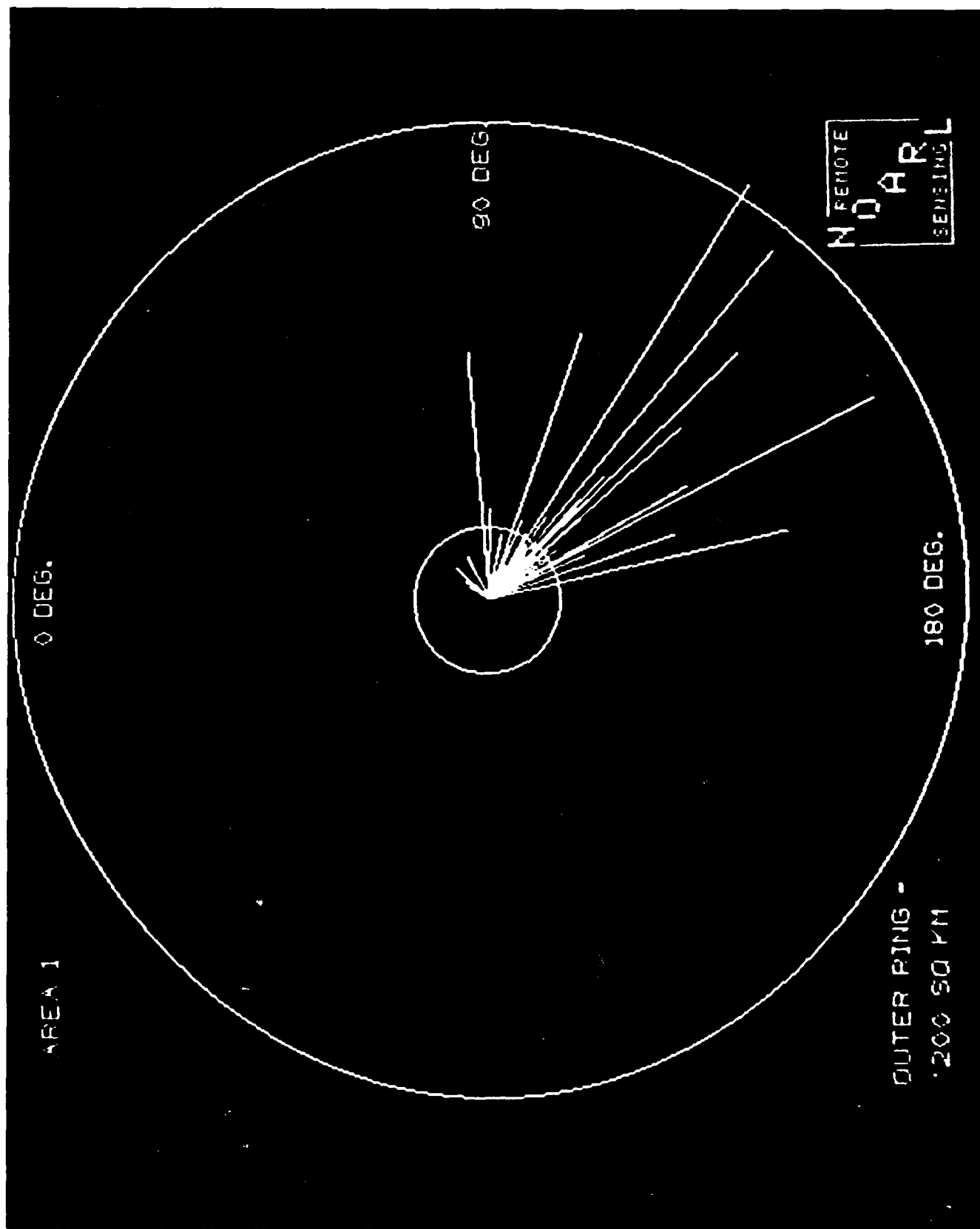
Figure 46a. 19 March 90 rose plot of lead vs. orientation for area 1.
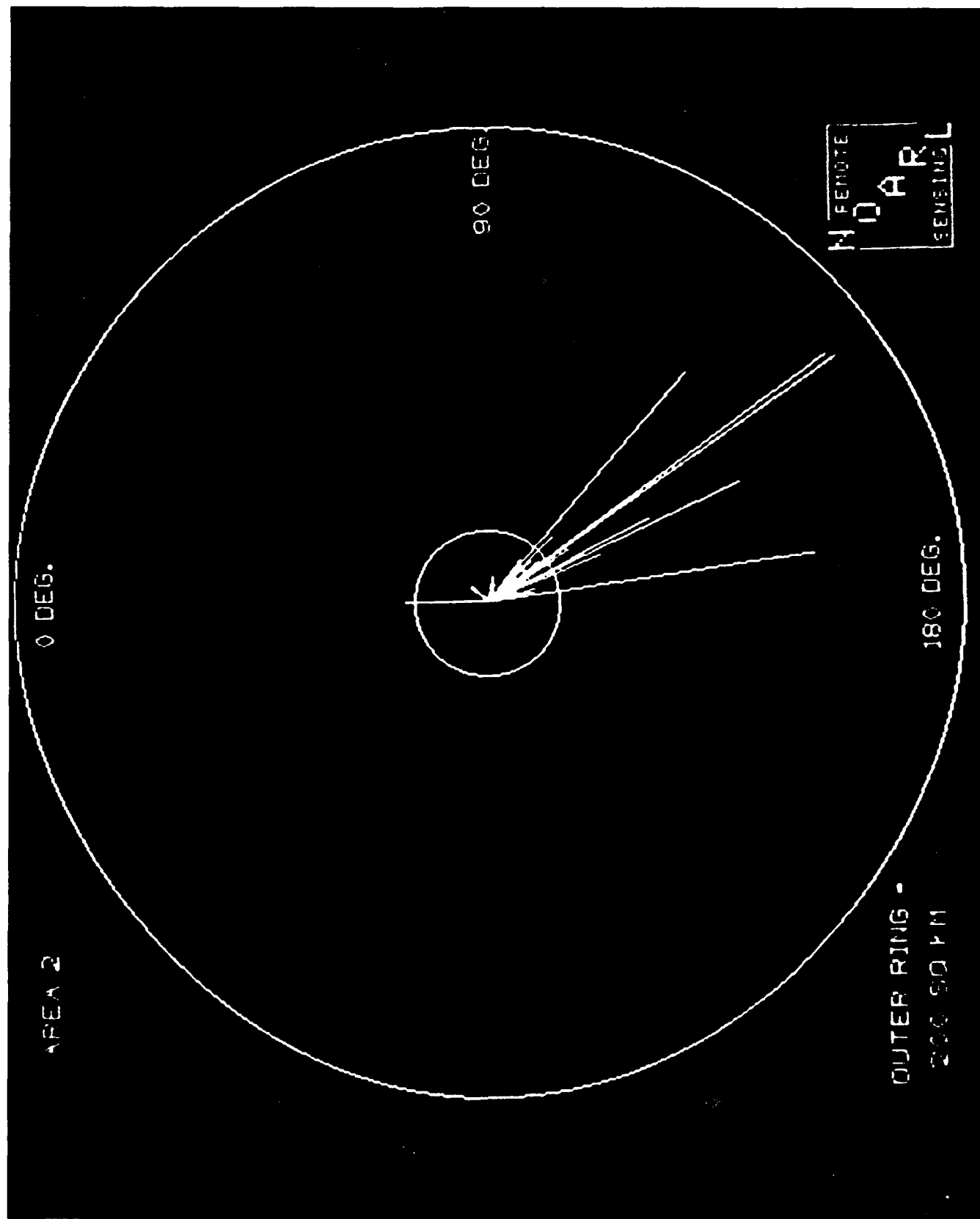
Figure 46b. 19. March 90 rose plot of lead size vs. orientation for area 2.

Figure 47. Ice motion vectors for 30 March-03 April 1990.

Table 2. Summary of ICESHELF '90 processing.

	BI	CF	DAT	ACCS	ROSE	STATS	OR	GREY
18Mar90_LSUB	x	x	x	x	x	x	x	x
19Mar90_LSUB	x	x	x	x	x	x	x	x
20Mar90_LSUB	x	x	x	x	x	x	x	x
20Mar90_GSUB	x	x	x	x	x	x	x	x
30Mar90_LSUB	x	x	x	x	x	x	x	x
03Apr90_LSUB	x	x	x	x	x	x	x	x
07Apr90_LSUB	x	x	x	x	x	x	x	x
15Apr90_LSUB	x	x	x	x	x	x	x	x
17Apr90_LSUB	x	x	x	x	x	x	x	x

BI	Binary Image
CF	Cloud Free Image
DAT	Cloud Free Binary Data File
ACCS	Accumulator File
ROSE	Lead Orientation Image
STATS	Lead Statistics Data File
OR	Orientation Rose Image
GREY	Lead Concentration Image
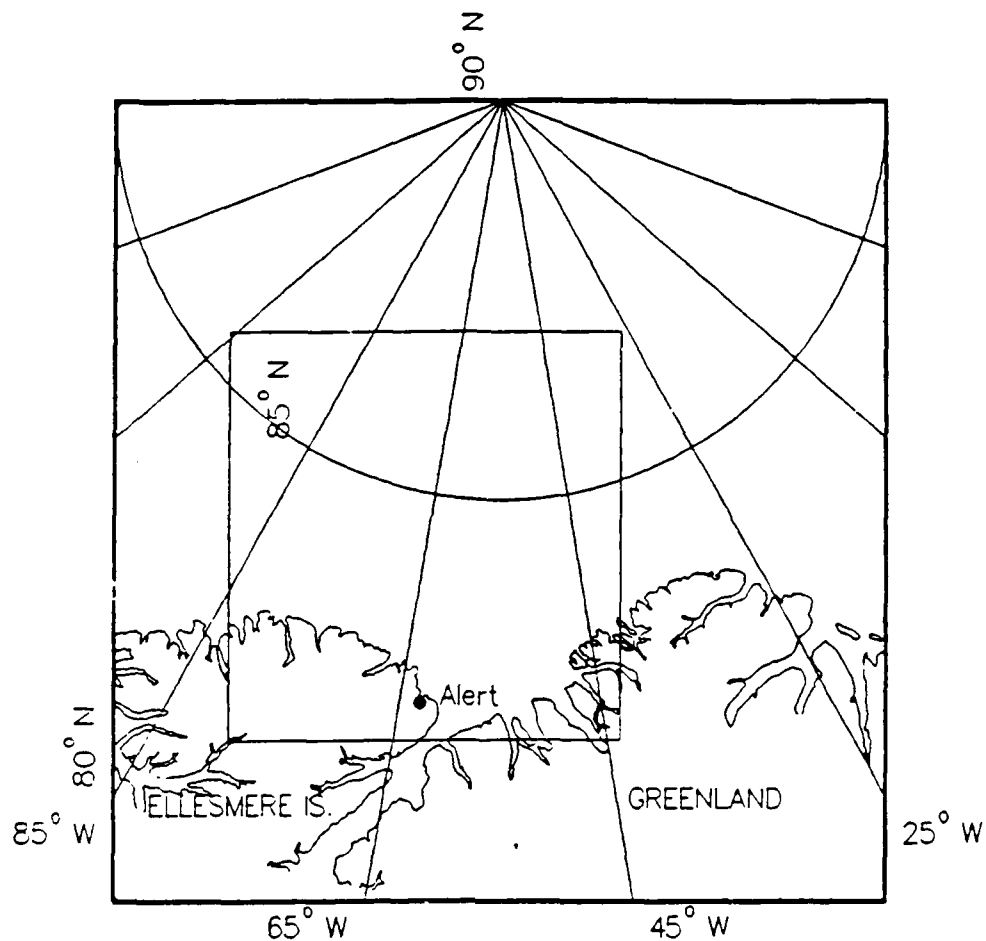
Figure 1. Area over which satellite imagery was acquired by NOARL for the ICESHELF exercise. Square encompasses the 512 km² subsection for which lead statistics were obtained.
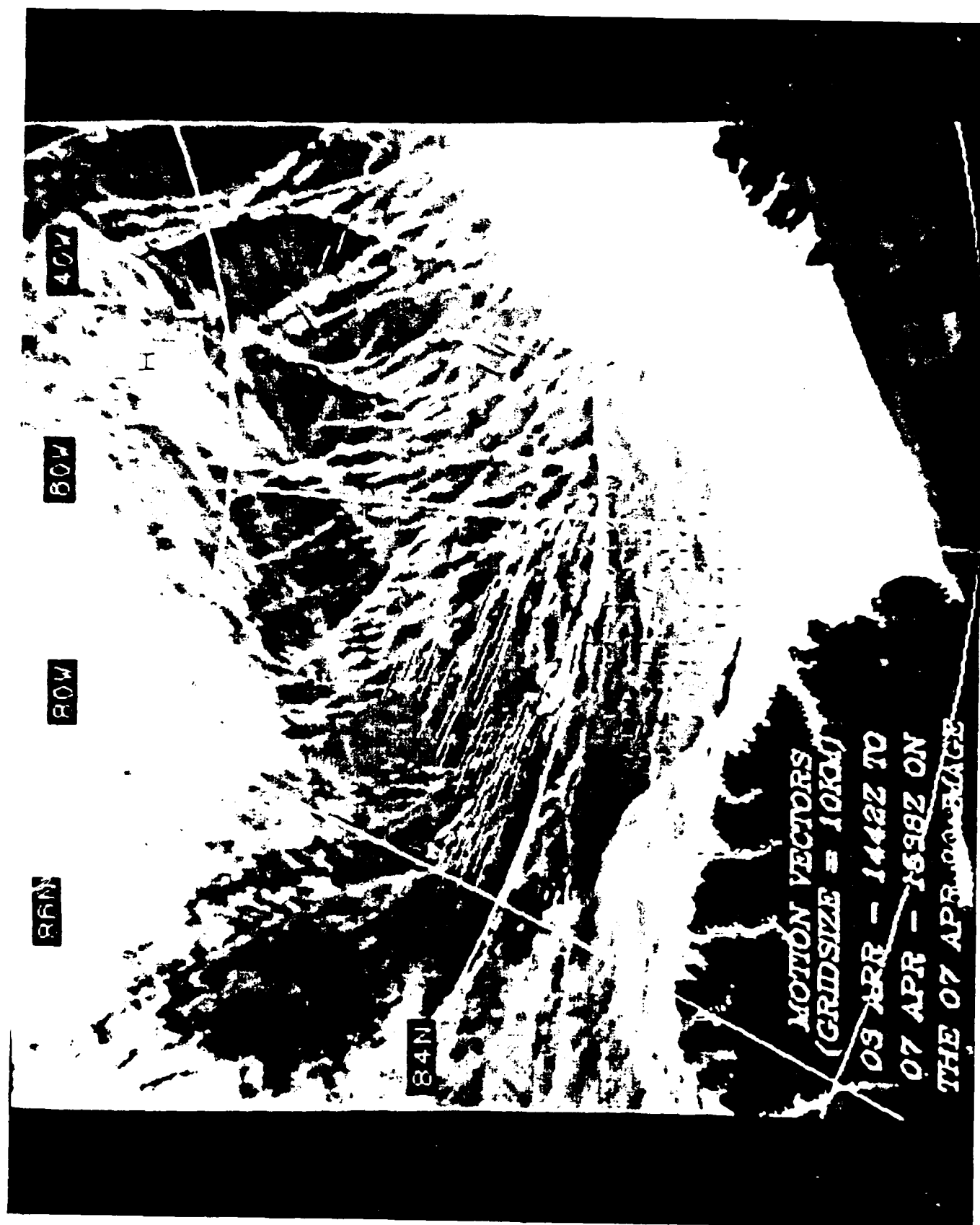
Figure 48. Ice motion vectors for 03-07 April 1990.
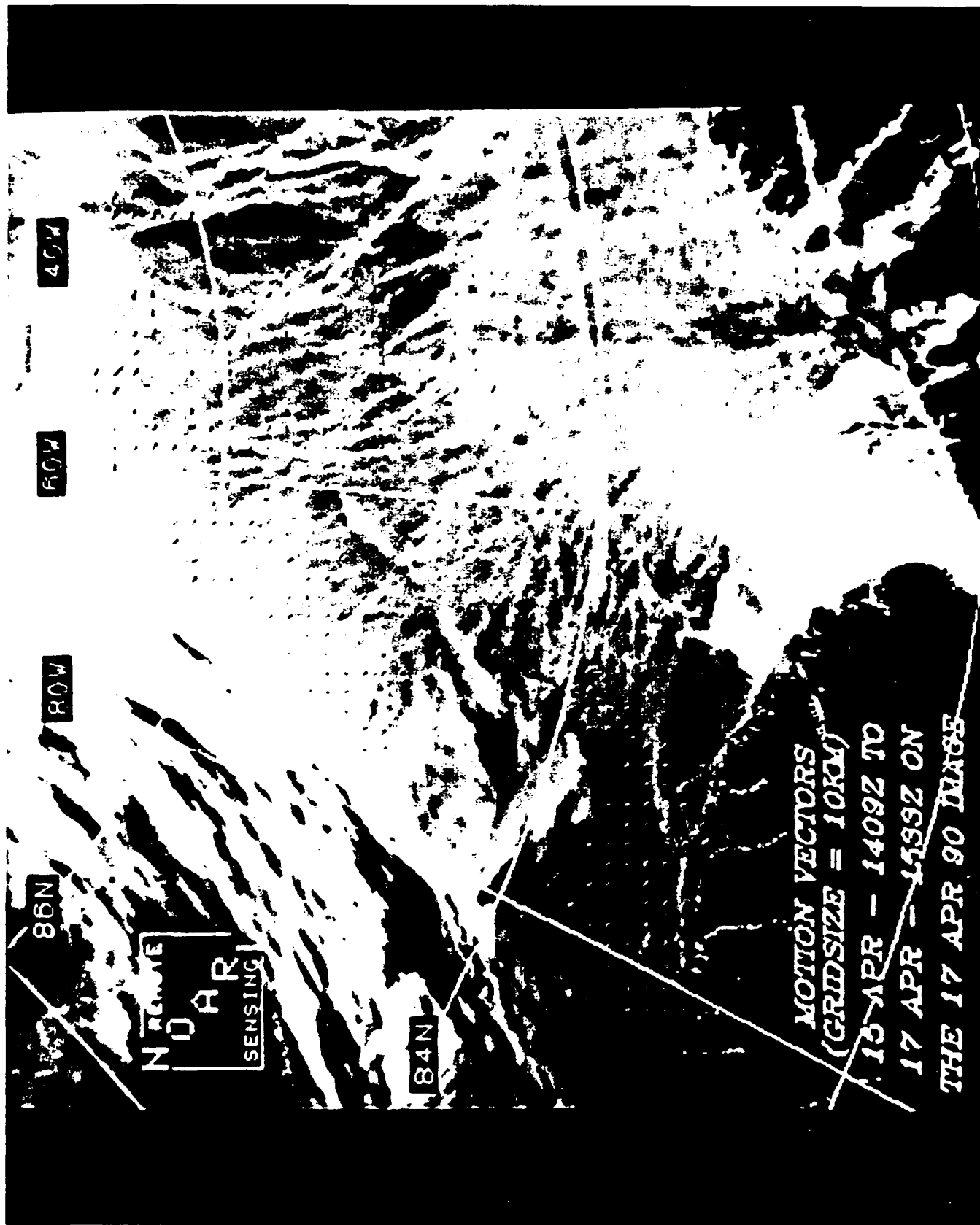
Figure 49. Ice motion vectors for 15-17 April 1990.
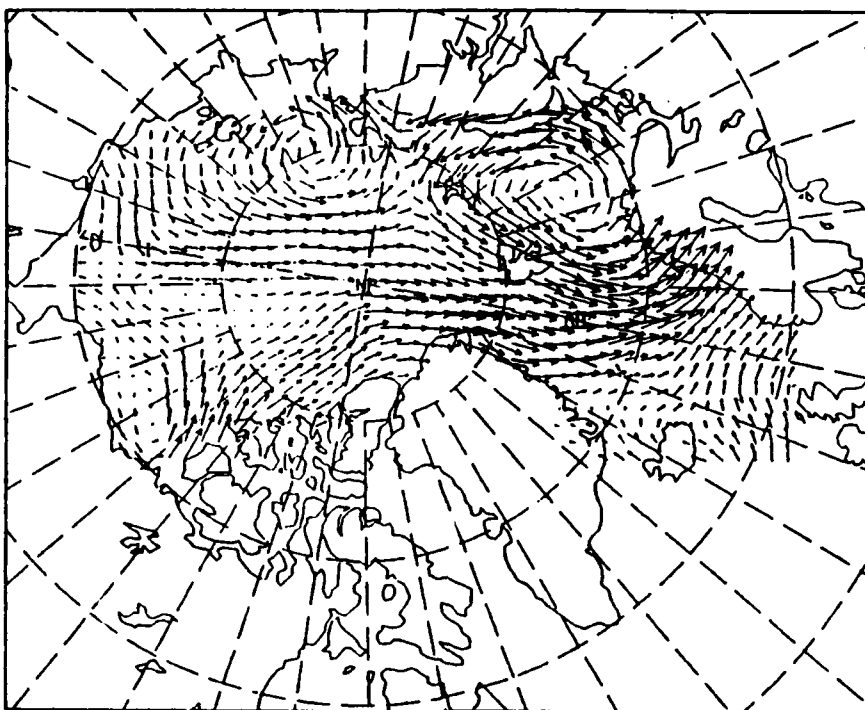
Figure 50a. PIPS 30 March 90 wind velocities (maximum vector is 50 meters per second).

ICE VELOCITIES

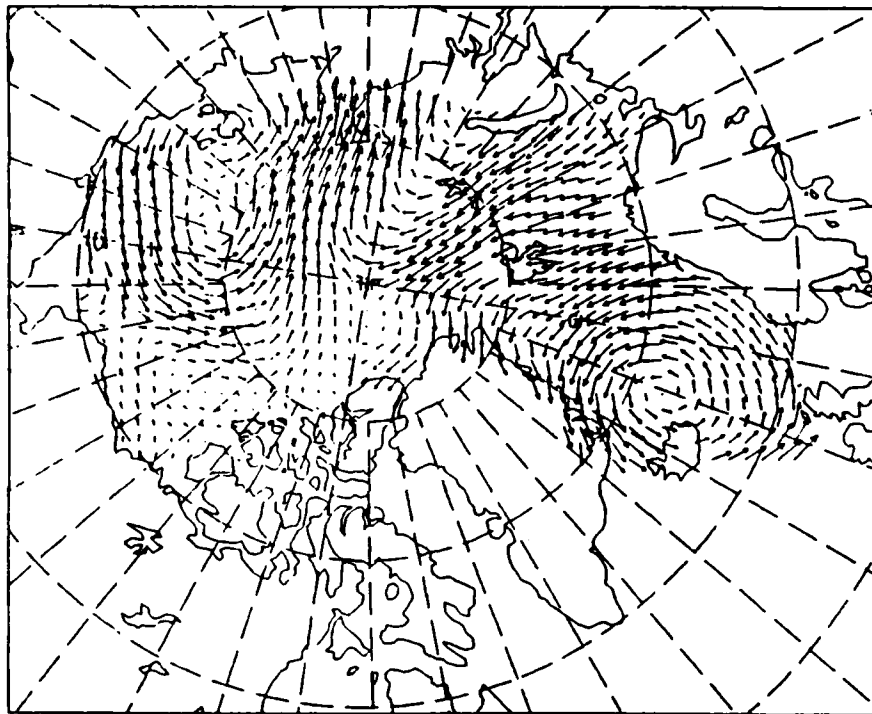Figure 50b. PIPS 30 March 90 Ice velocities (maximum vector is 50 centimeters per second).
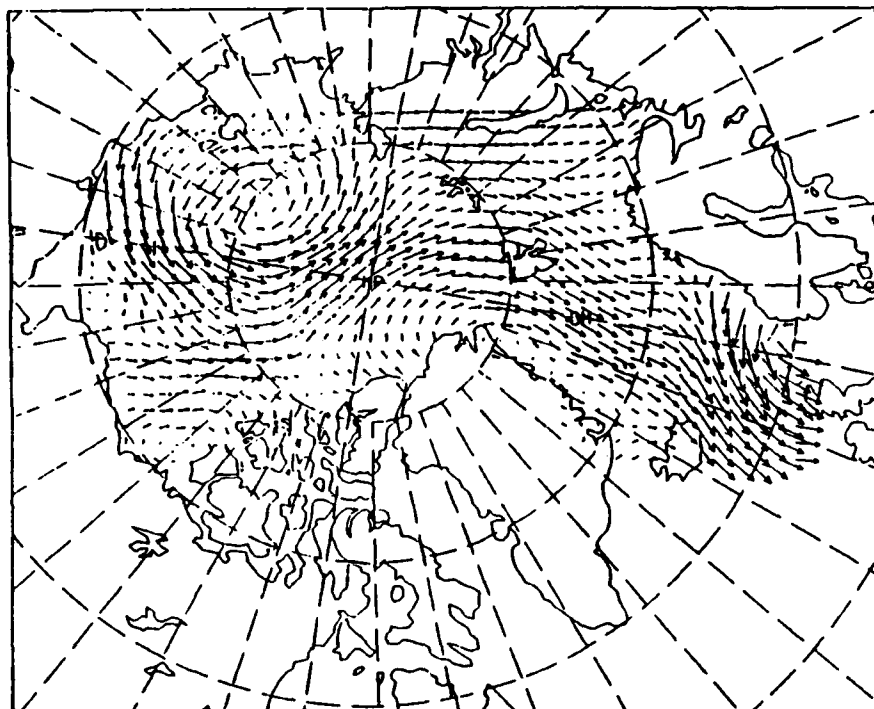
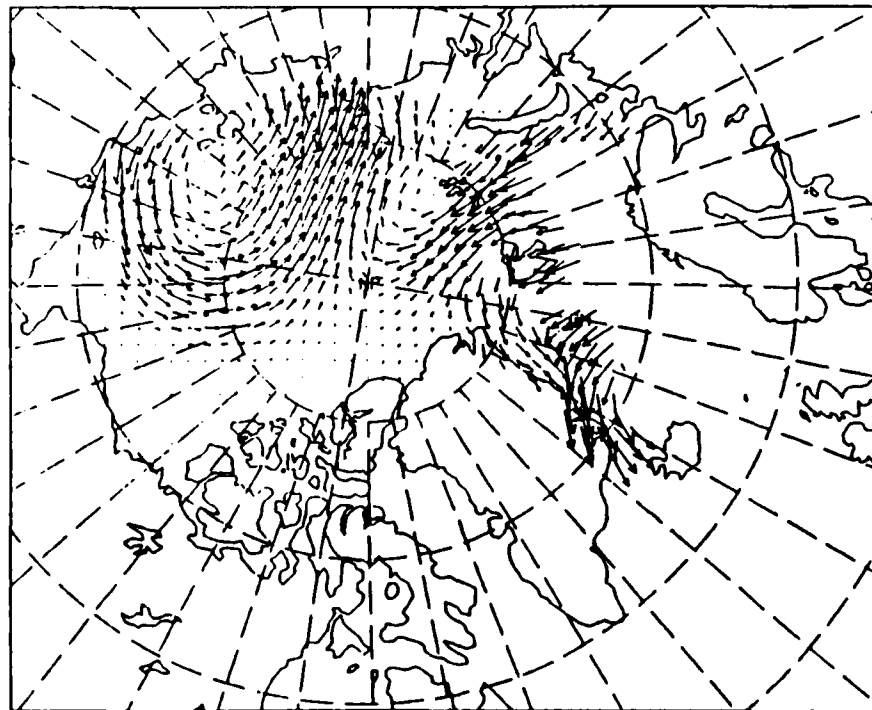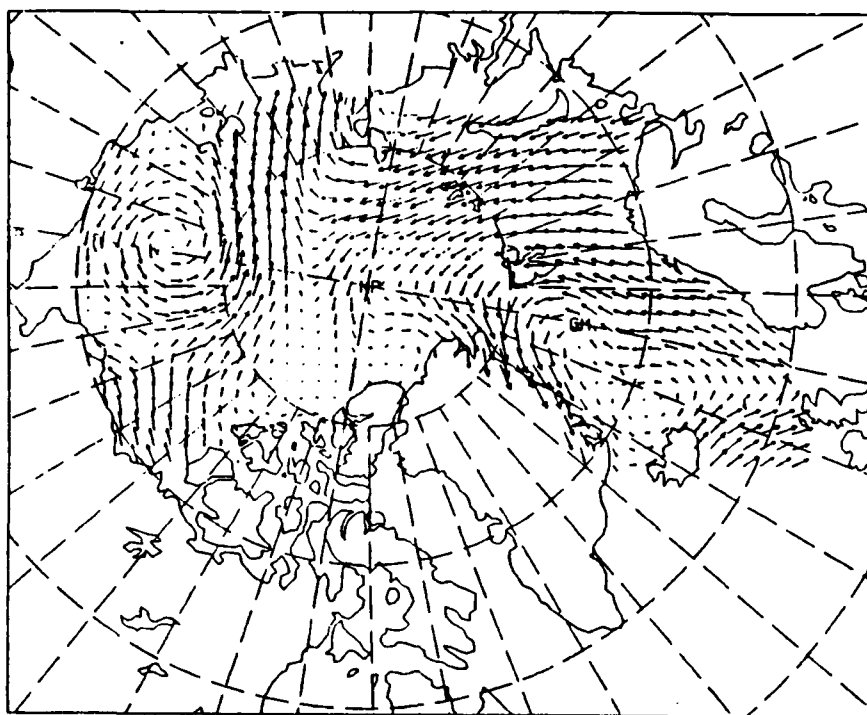Figure 50c. PIPS 02 April 90 wind velocities (maximum vector is 50 meters per second).

ICE VELØCITIES

Figure 50d. PIPS 02 April 90 ice velocities (maximum vector is 50 centimeters per second).
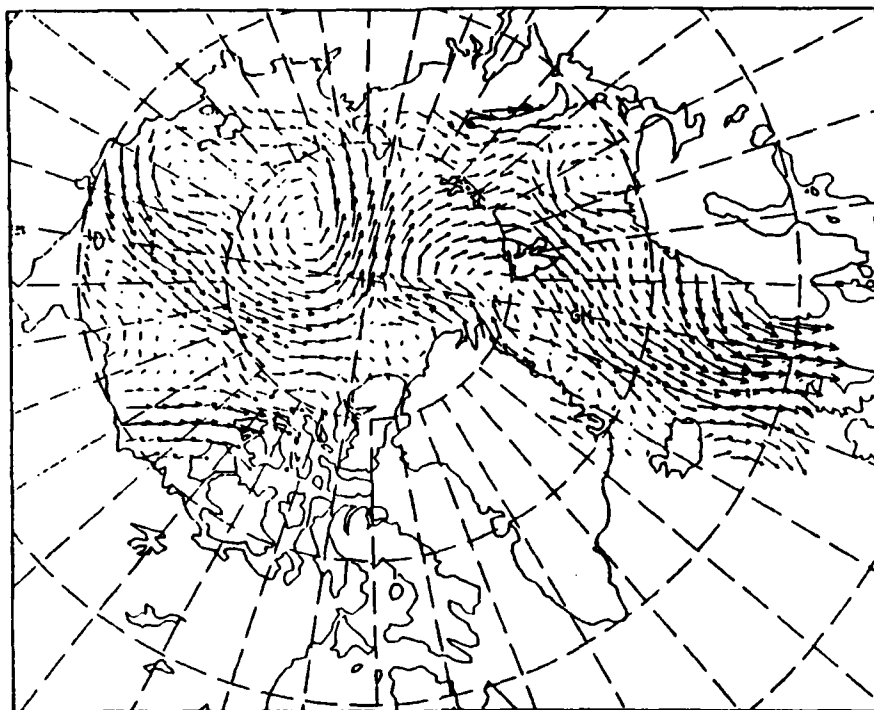
Figure 50e. PIPS 03 April 90 wind velocities (maximum vector is 50 meters per second).
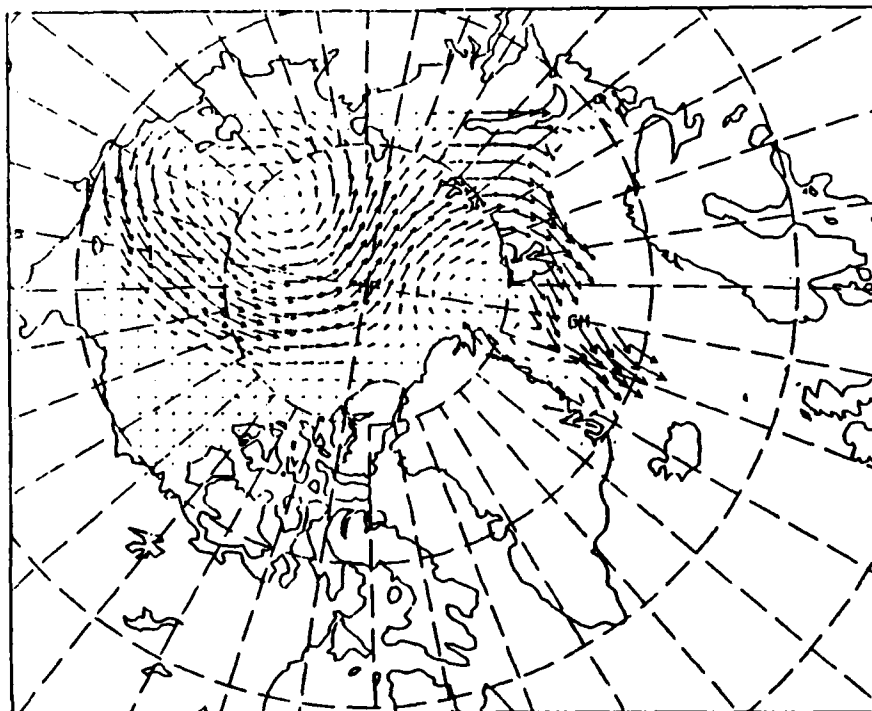
ICE VELOCITIES

Figure 50f. PIPS 03 April 90 ice velocities (maximum vector is 50 centimeters per second).
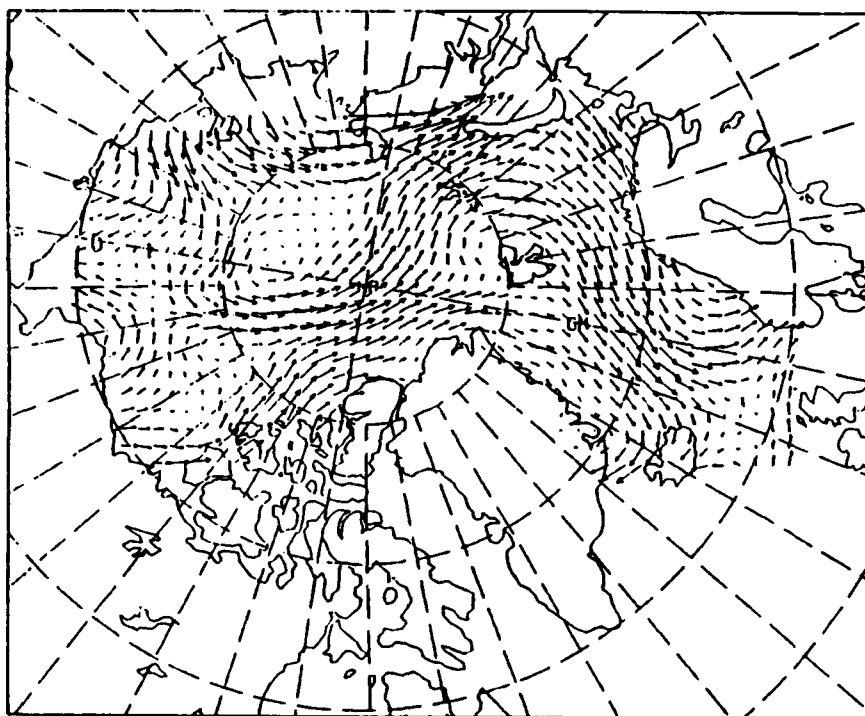
Figure 51a. PIPS 04 April 90 wind velocities (maximum vector is 50 meters per second).
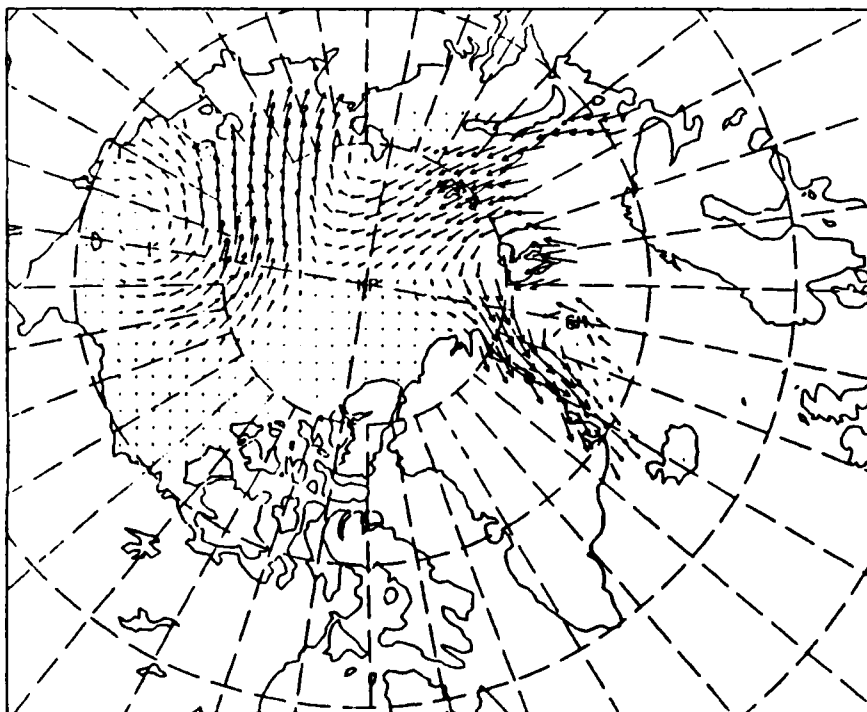
ICE VELOCITIES

Figure 51b. PIPS 04 April 90 ice velocities (maximum vector is 50 centimeters per second).
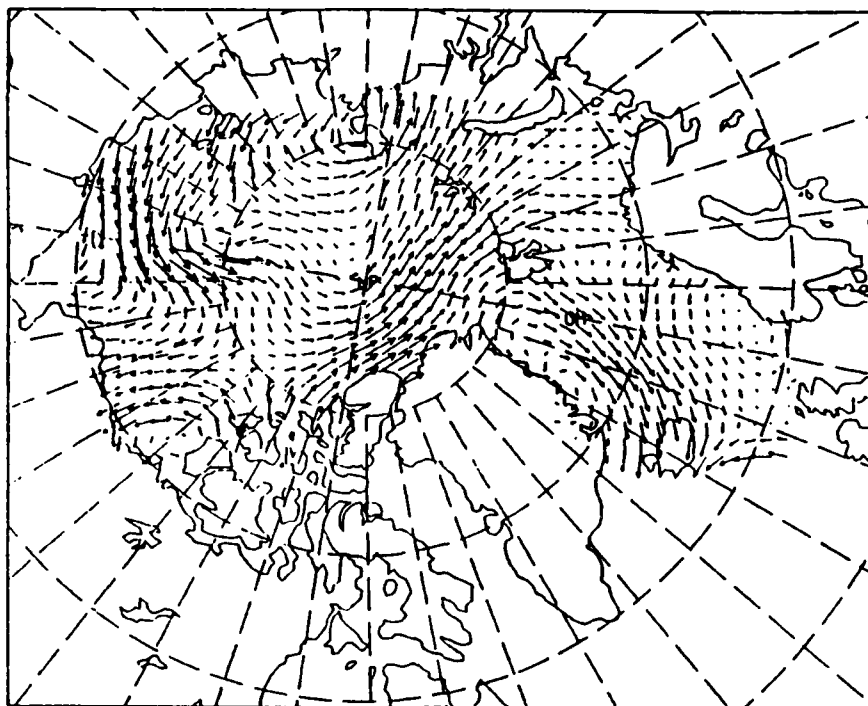
Figure 51c. PIPS 05 April 90 wind velocities (maximum vector is 50 meters per second).

ICE VELOCITIES

Figure 51d. PIPS 05 April 90 ice velocities (maximum vector is 50 centimeters per second).
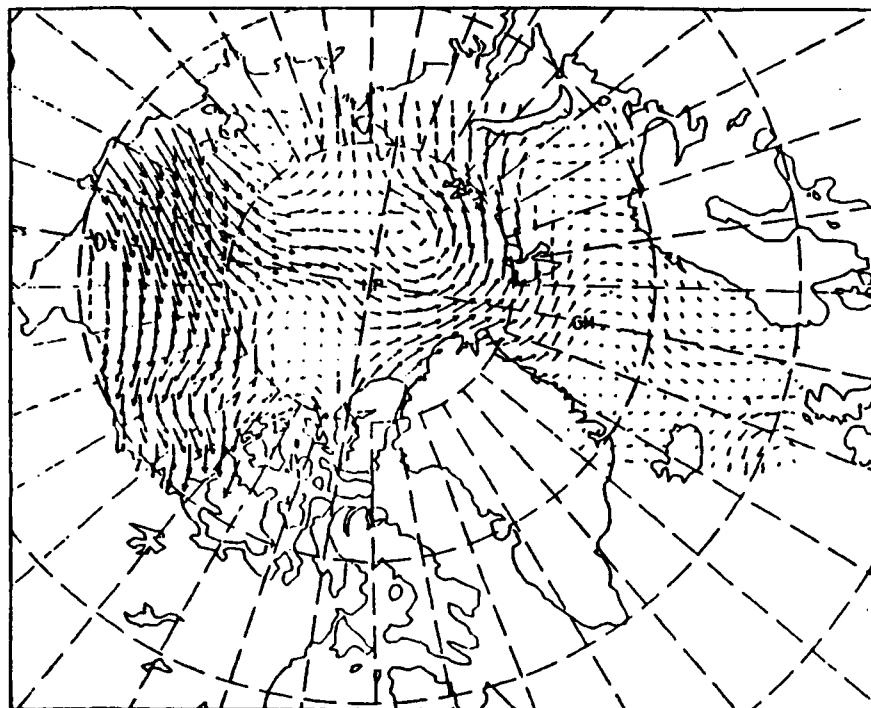
Figure 51e. PIPS 06 April 90 wind velocities (maximum vector is 50 meters per second).

0.500·02
MAXIMUM VECTOR

ICE VELOCITIES
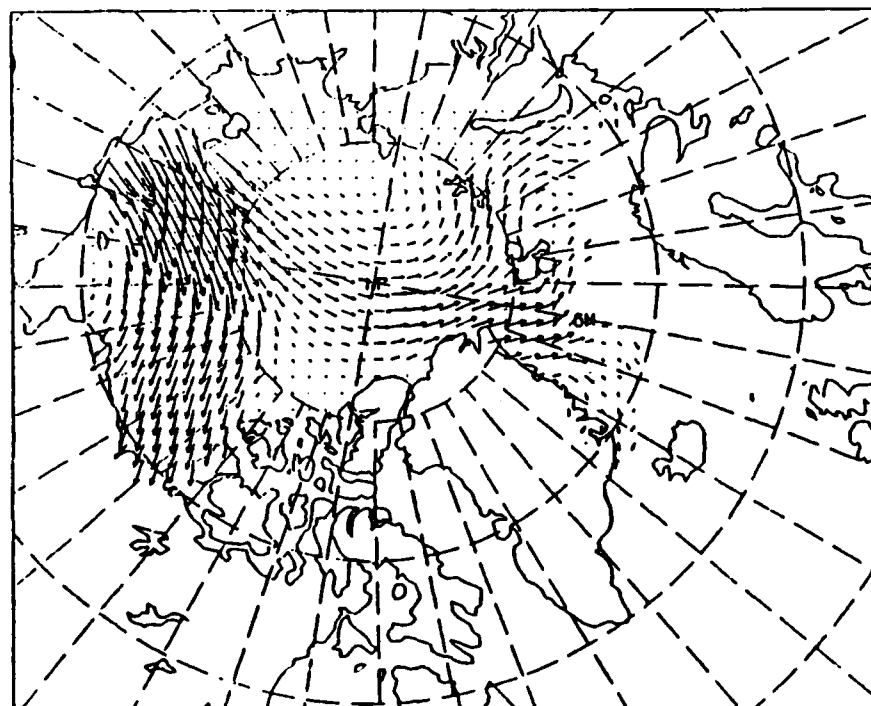
Figure 51f. PIPS 06 April 90 ice velocities (maximum vector is 50 centimeters per second).

0.500·00
MAXIMUM VECTOR
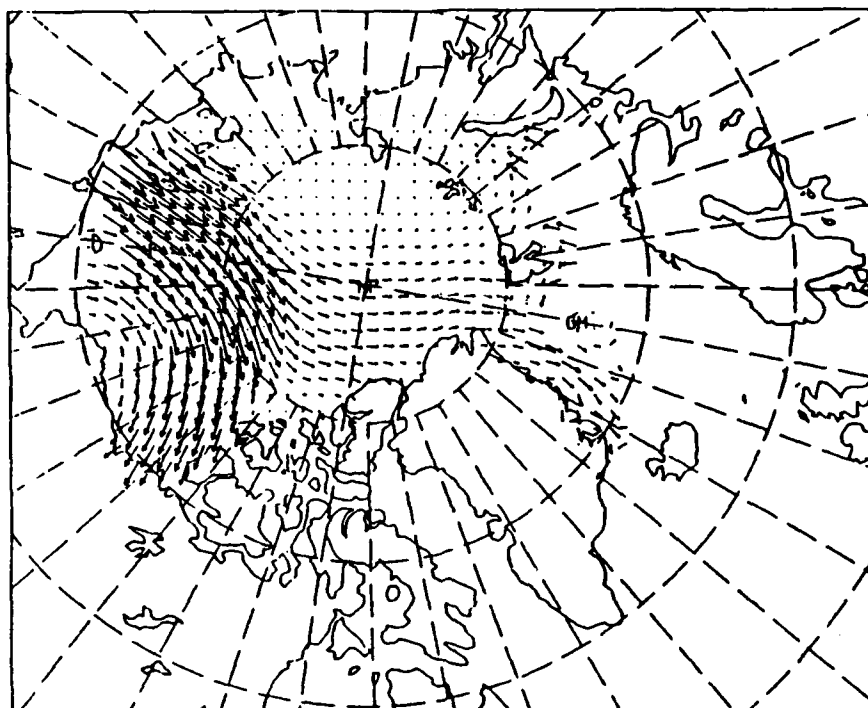
Figure 51g. PIPS 07 April 90 wind velocities (maximum vector is 50 meters per second).

WIND VELØCITIES   DTG - 90040703
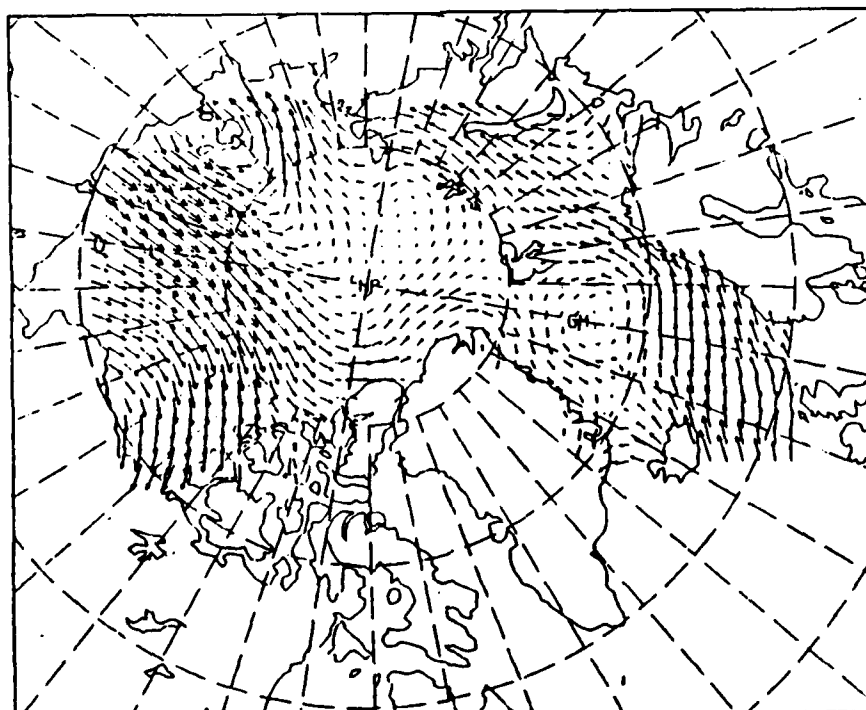
Figure 51h. PIPS 07 April 90 ice velocities (maximum vector is 50 centimeters per second).
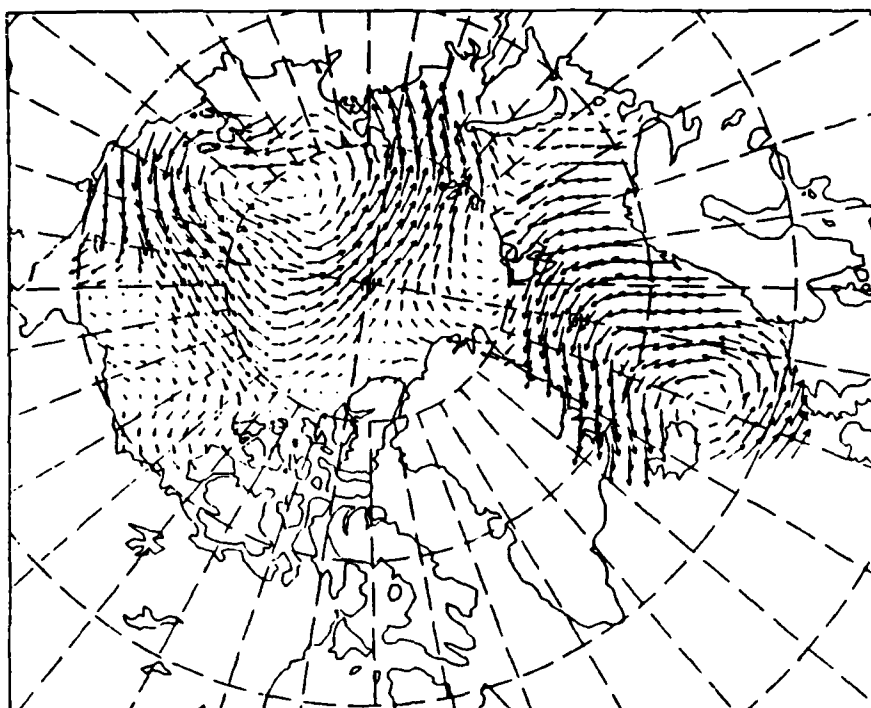
Figure 52a. PIPS 15 April 90 wind velocities (maximum vector is 50 meters per second).
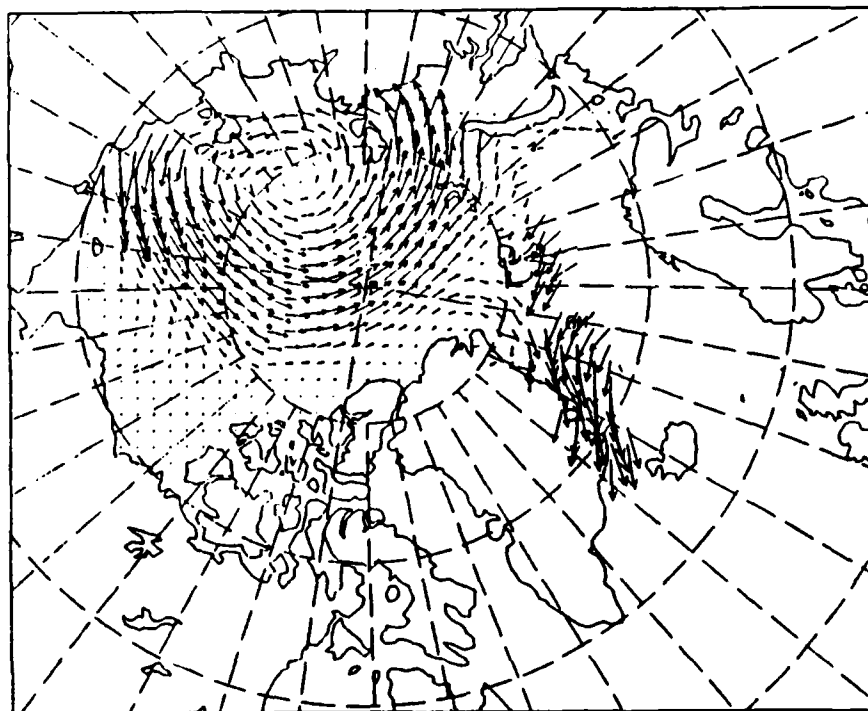
ICE VELØCITIES

Figure 52b. PIPS 15 April 90 ice velocities (maximum vector is 50 centimeters per second).

Figure 52c. PIPS 16 April 90 wind velocities (maximum vector is 50 meters per second).

ICE VELOCITIES

Figure 52d. PIPS 16 April 90 ice velocities (maximum vector is 50 centimeters per second).

Figure 52e. PIPS 17 April 90 wind velocities (maximum vector is 50 meters per second).

ICE VELOCITIES

Figure 52f. PIPS 17 April 90 ice velocities (maximum vector is 50 centimeters per second).

Appendix A.

The Hough Transform for the Analysis of Leads in Sea Ice Imagery

Introduction

The Hough transform is often used in computer vision for finding lines or shapes in images. Compared to other methods of shape detection such as template matching, the Hough transform is fast and relatively insensitive to noise in most applications. Recently, the Hough transform has found acceptance as a feature extraction tool for analysis of remote sensing imagery. Cross, for instance, uses the Hough transform to detect circular geological features such as salt domes and impact craters in Landsat MSS imagery (Cross, 1988). Skingley and Rye apply the Hough transform to airborne SAR imagery of a forest in order to detect faint lines in the imagery (Skingley and Rye, 1987). Here, sea ice leads are assumed to be linear features, and the Hough transform is employed as a line detector (Fetterer and Holyer, 1989).

The Hough transform for line detection

The Hough transform works on pixels which have already been tentatively classified as lead pixels. Each lead pixel in "image space" is mapped into a curve in "parameter space" (Fig. 1a), where parameters are rho, which is the normal distance from the image origin to a line, and theta, the orientation of the normal relative to horizontal (and therefore of the line relative to vertical). The transform uses the normal parameterization of a line:

$$\rho = x * \cos(\theta) + y * \sin(\theta)$$

Parameter space is represented as an accumulator array of discrete rho, theta values. To transform an (x,y) image pixel, theta is incremented from 0 to 180 in steps of 1° and rho calculated for each theta. Accumulator element (rho,theta) is incremented for each pair. Every lead point in the image is therefore transformed into a sinusoidal curve of 180 points in the accumulator, where each (rho,theta) element of the curve describes possible lines through that image point. If points in image space are members of the same line, curves formed by those points will cross in parameter space at the (rho,theta) element which describes the line (Fig. 1b). That element will have a higher value than surrounding elements in the accumulator array (Duda and Hart, 1972). If the line is straight, the value of the peak will equal the number of pixels on the line in the image.

Peaks in the accumulator array above a noise threshold correspond to lines in the image. Therefore, by finding peaks in the accumulator, lines in the image are known by their orientation and distance from the origin. The orientation in parameter space gives lead orientation relative to vertical in

the image, while the size of the peak is an indication of lead size. However, the (rho,theta) location of a peak in the accumulator gives no indication of whether points on the line are adjacent, or where the end points of the line are.

Refinements to the Hough transform method

The disadvantages of using the Hough transform for line detection in imagery lie in 2 areas: detecting peaks in the accumulator, and interpreting the peaks in a rigorous way. For an excellent survey of the Hough transform and how others have handled these difficulties, see Illingworth and Kittler (1988). The difficulties lie in the fact that the peaks in the accumulator may be quite sharp, but are more often spread over a cluster of accumulator elements. The height and spread of the peaks is a complicated function of:

(a)   the number of pixels on the image line (the line's length, if pixels are contiguous)
(b)   the width of the image line
(c)   the curvature of the image line (slight curvature will spread the peak, an abrupt change in curvature will produce two peaks)
(d)   the quantization of theta and rho
(e)   the shape of the image itself (its "retina")

Dr. Vivien Cambridge, of Sverdrup Technology, has developed a method of using the Hough transform for this project which simplifies peak finding in accumulator space, and which allows us to relate the value of the peaks to lead size. Gerig's method (1987) is used to simplify accumulator space. The result is peaks which occupy single elements in the accumulator, rather than a spread of elements. There is one high-valued element, or peak, for every set of colinear points more than a few pixels long. Peaks which are very close together in the new, simplified accumulator result from parallel sets of colinear points (i.e., leads more than 1 pixel wide) or from sets of colinear points which vary only slightly in orientation (i.e., leads which are composed of straight line segments but which have some slight curvature). These peak points are brought together by a clustering algorithm which replaces a cluster of peak points in the accumulator with a single peak point having the summed value of all the points which contributed to it. This value, then, is equal to the summed number of pixels in all the smaller line or lead segments which contribute to make a lead. Because 1 pixel is about 1 km^2, we can say that this value is the size of the lead in km^2. The orientation of the lead, relative to vertical, is simply equal to the value of theta for the column in which the peak point is found.

This method assumes that there are no false detections. False detections occur when points which are randomly colinear but which do not belong to the same lead are detected. The possibility of this happening is lessened if the Hough transform

is computed for small blocks of the image. False detections are not a problem in this work when a block size of 64 x 64 pixels is used.

Future work will continue the development of a new method whereby the positions of all points along a lead, as well as the lead's orientation, can be represented symbolically in Hough transform space. By transferring lead pixels from a raster-based representation to an object-based representation, rules can be written for the definition of leads and lead complexes, and lead statistics can be extracted directly from Hough transform space based on those definitions. While in this project lead statistics (other than orientation) are extracted from the binary lead image itself, the new method will make use of the object-based representation of leads in Hough transform space for lead statistics.

References

Cross, A.M. (1988). Detection of circular geological features using the Hough transform. International Journal of Remote Sensing 9:1519-1528.

Duda, R.O. and P.E. Hart (1972). Use of the Hough transform to detect lines and curves in pictures. Communications of the Association of Computing Machinery 15:11-15.

Fetterer, F.M. and R.J. Holyer (1989). A Hough transform technique for extracting lead features from sea ice imagery. Proceedings, International Geoscience and Remote Sensing Symposium, Vancouver, British Columbia, July 10-14.

Gerig, G. (1987). Linking image-space and accumulator-space: a new approach for object recognition. Proceedings, First International Conference on Computer Vision, June 8-11.

Illingworth, J. and J. Kittler (1988). A survey of the Hough transform. Computer Vision, Graphics, and Image Processing 44:87-116.

IMAGE SPACE

PARAMETER SPACE
(accumulator of elements ρ,θ)

$(0,0)$ $(n,0)$

θ

(a)

ρ

$(0,n)$ (n,n)

$-(\sqrt{2})n$

(b)

ρ

$(\sqrt{2})n$

0   180

θ
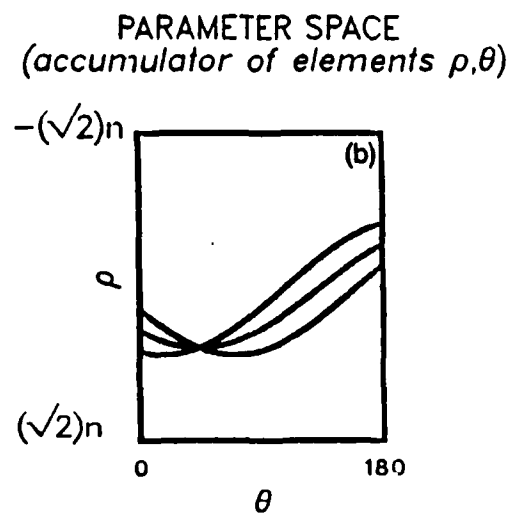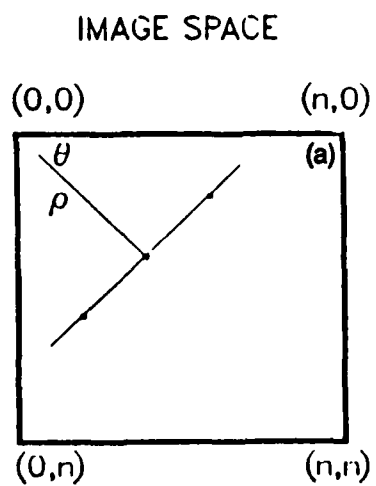
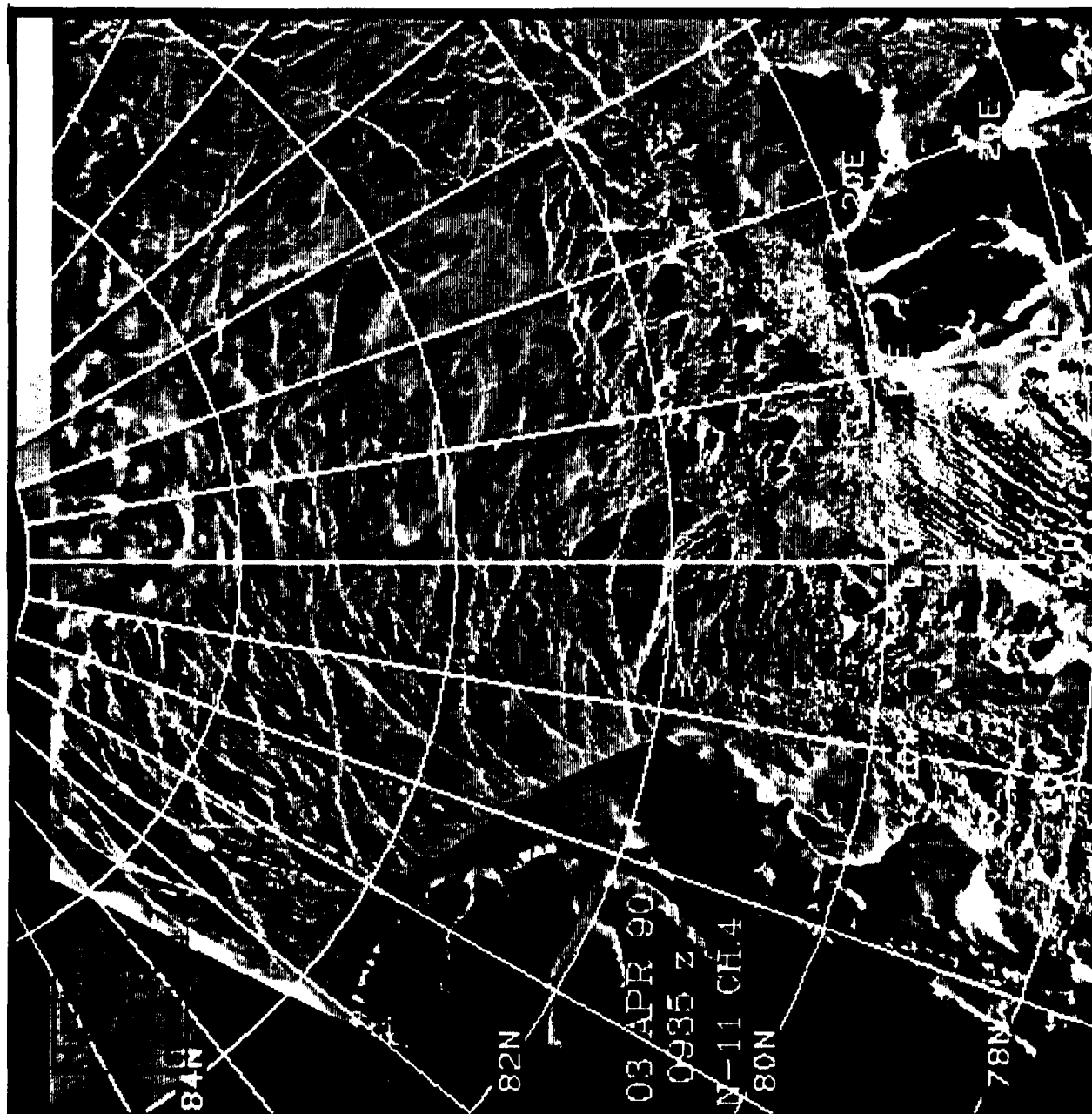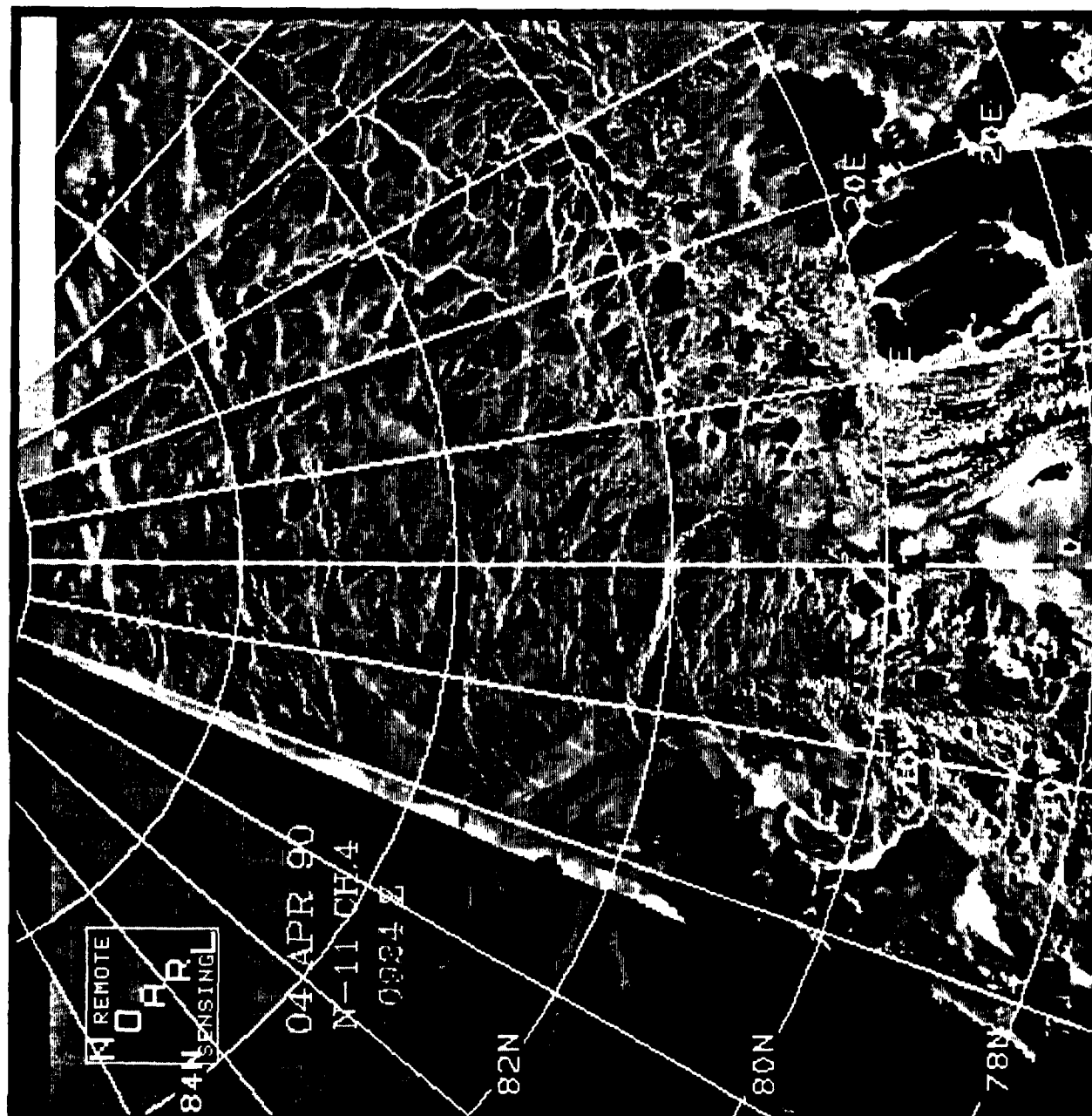Figure 1a and 1b. The Hough transform maps points from image space (1a) into parameter space (1b). See text for explanation.

Appendix B.

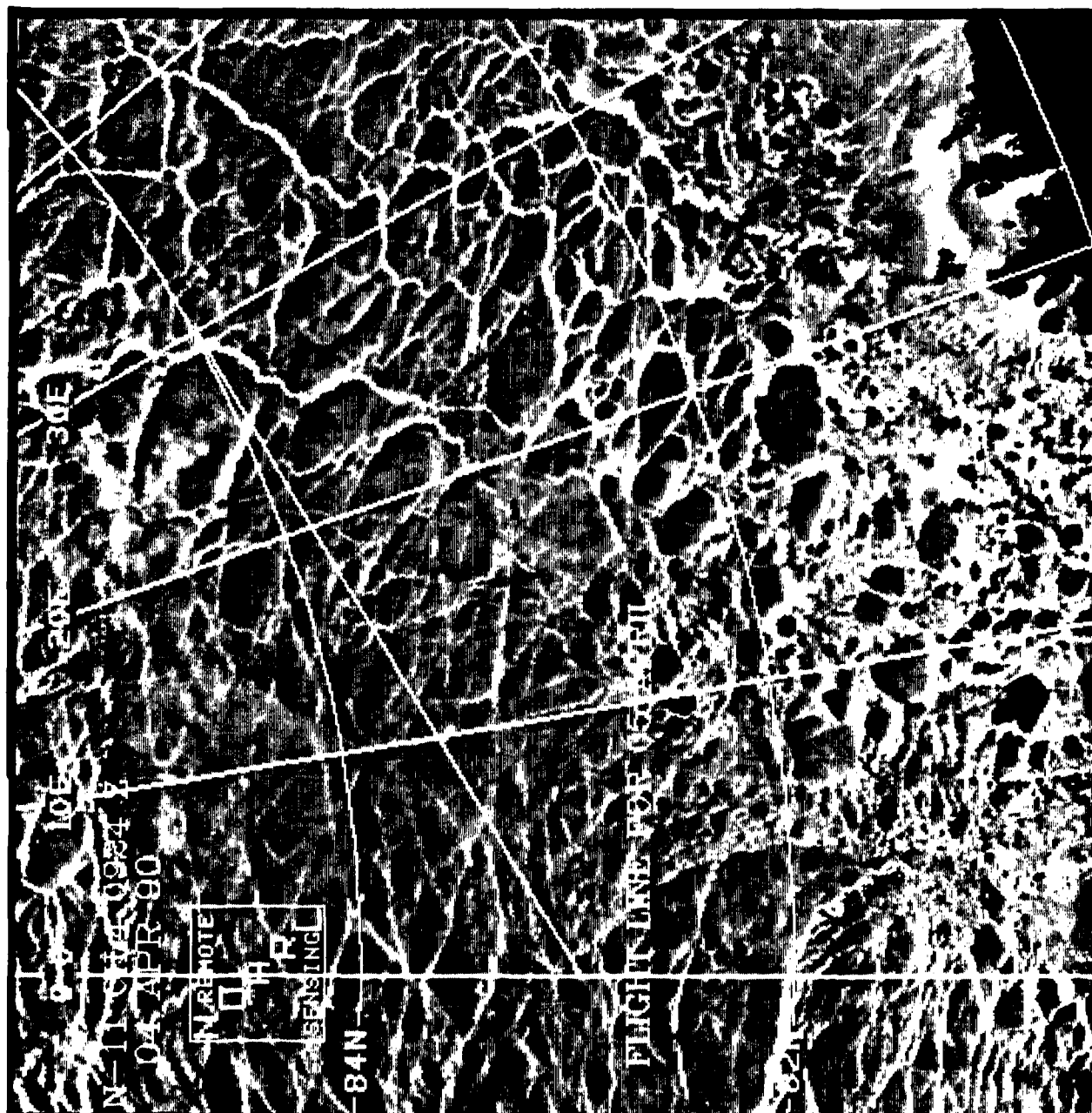**Fram Strait Imagery**

     Imagery of the Fram Strait was processed and sent from the Naval Oceanographic and Atmospheric Research Laboratory to a PC-based image processor at Thule, Greenland, where the imagery was used to assist flight planning during ICEX. That imagery, covering the period from 01 to 12 April 1990, is reproduced on the following pages.
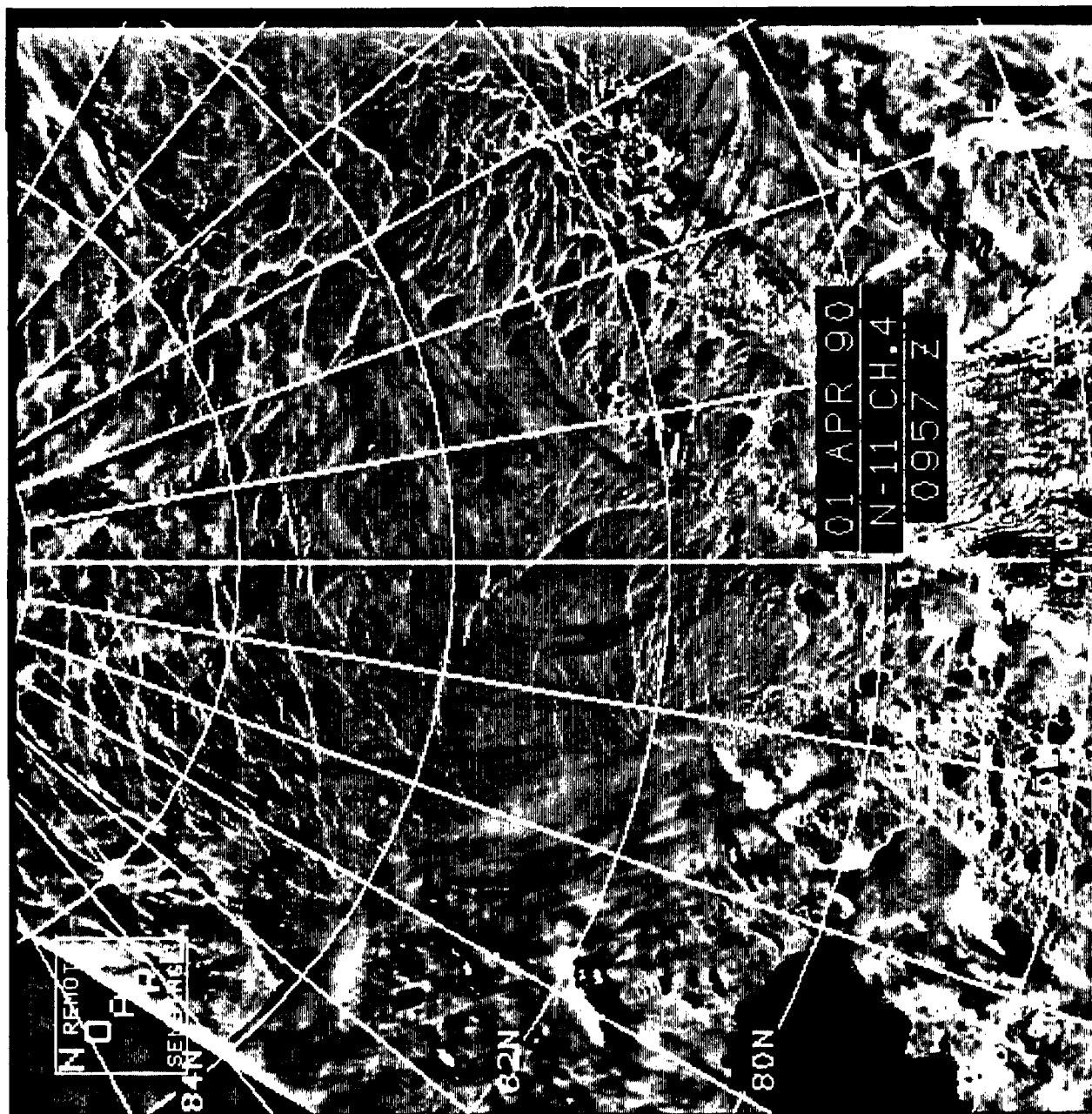
01 APR 90
N-11 CH.4
0957 Z

N REMOTE
S E
SENSING
84N
82N
80N

03 APR 90
0935 Z
N-11 CH.4

84N

82N

80N

78N

REMOTE
□ R. R.
84N SENSING
04 APR 90
N-11 CH 4
0934 Z
82N
80N
78N

04 APR 90
0924 Z
N-11 CH.4

N REMOTE
O A R
SENSING L

REMOTE SENSING

84N
82N
05 APR 91
1055 Z
N-11 CH.4
80N
78N
30E

REMOTE
O R
SENSING

82N
N-11 CH
07 APR 90
1034 Z
80N
78N

82N

08 APR 90
1023 Z
N-11 CH.4

80N

78N

N-1 CH4
11 APR 90
80N 0949
20W
78N

REMC

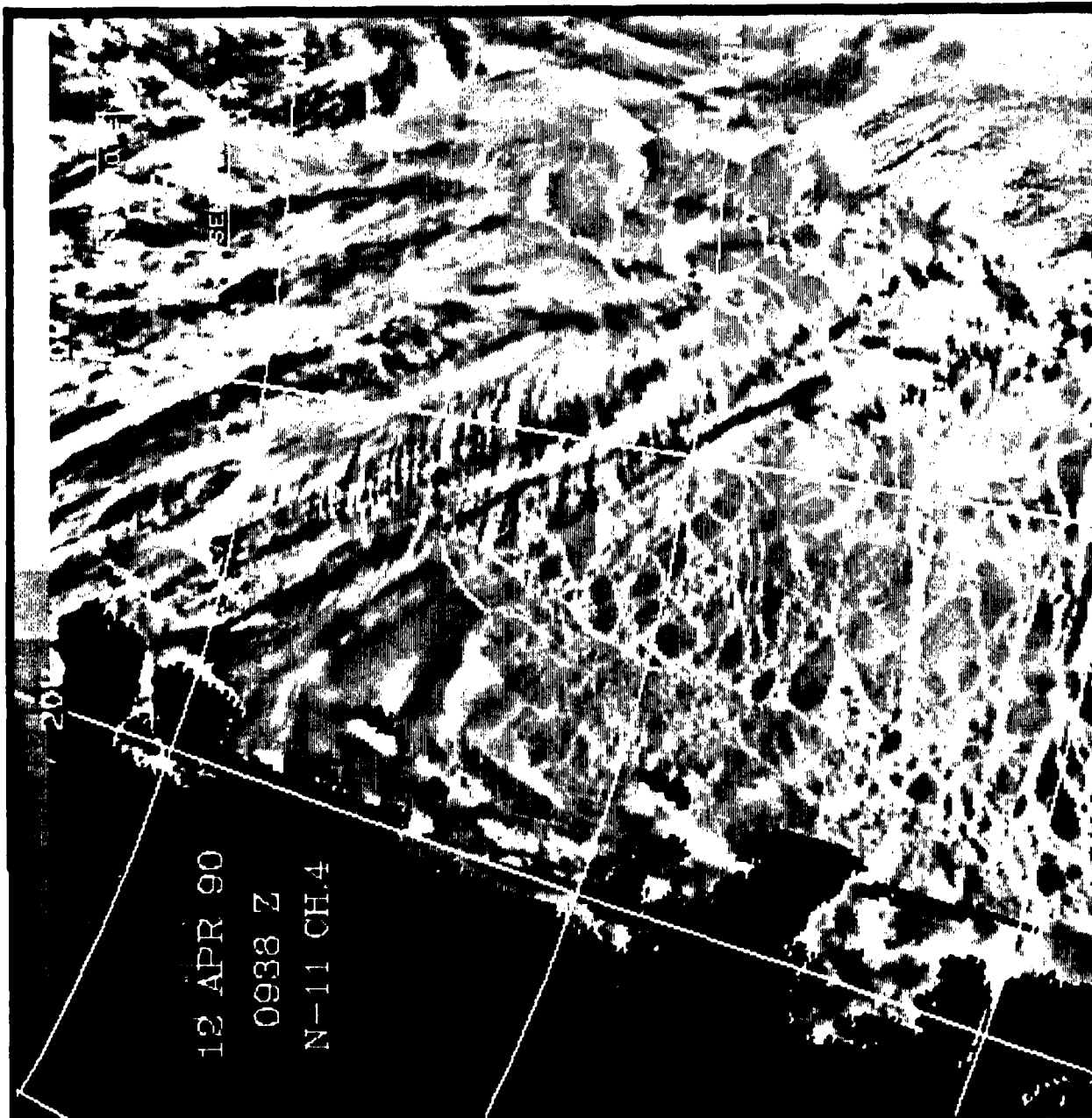12 APR 90
09 38 Z
N-11 CH
7BN

12 APR 90
0938 Z
N-11 CH.4
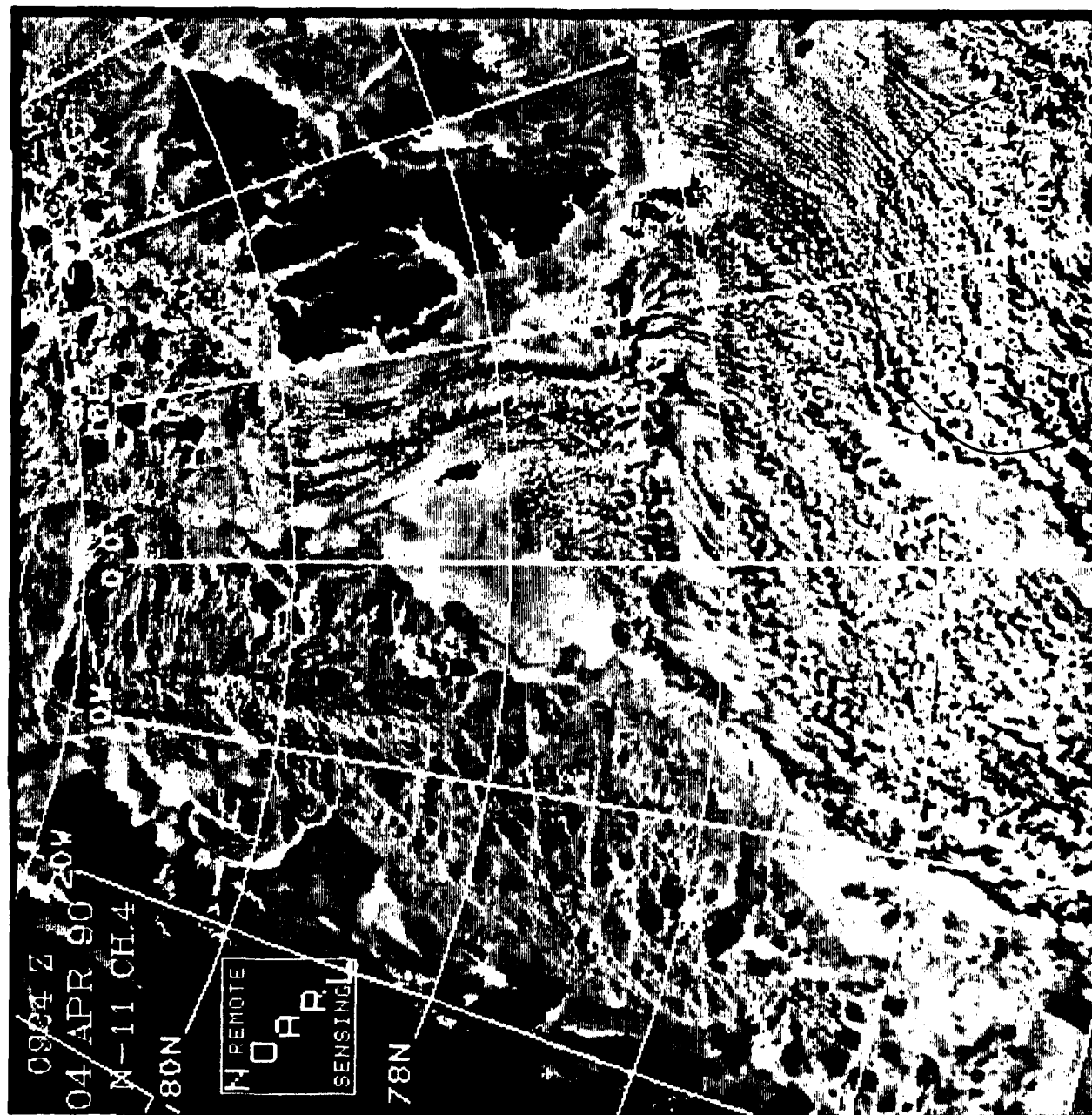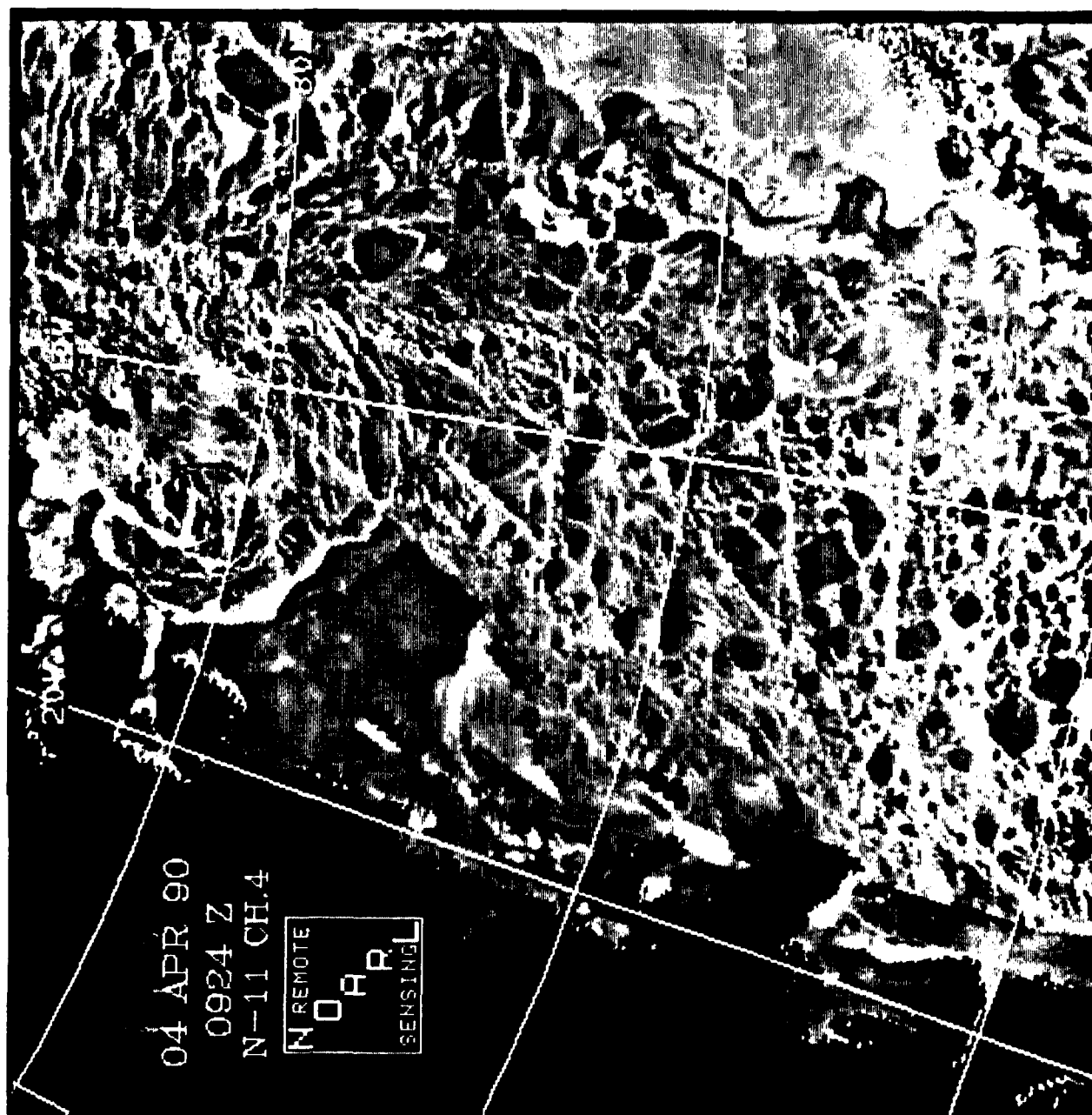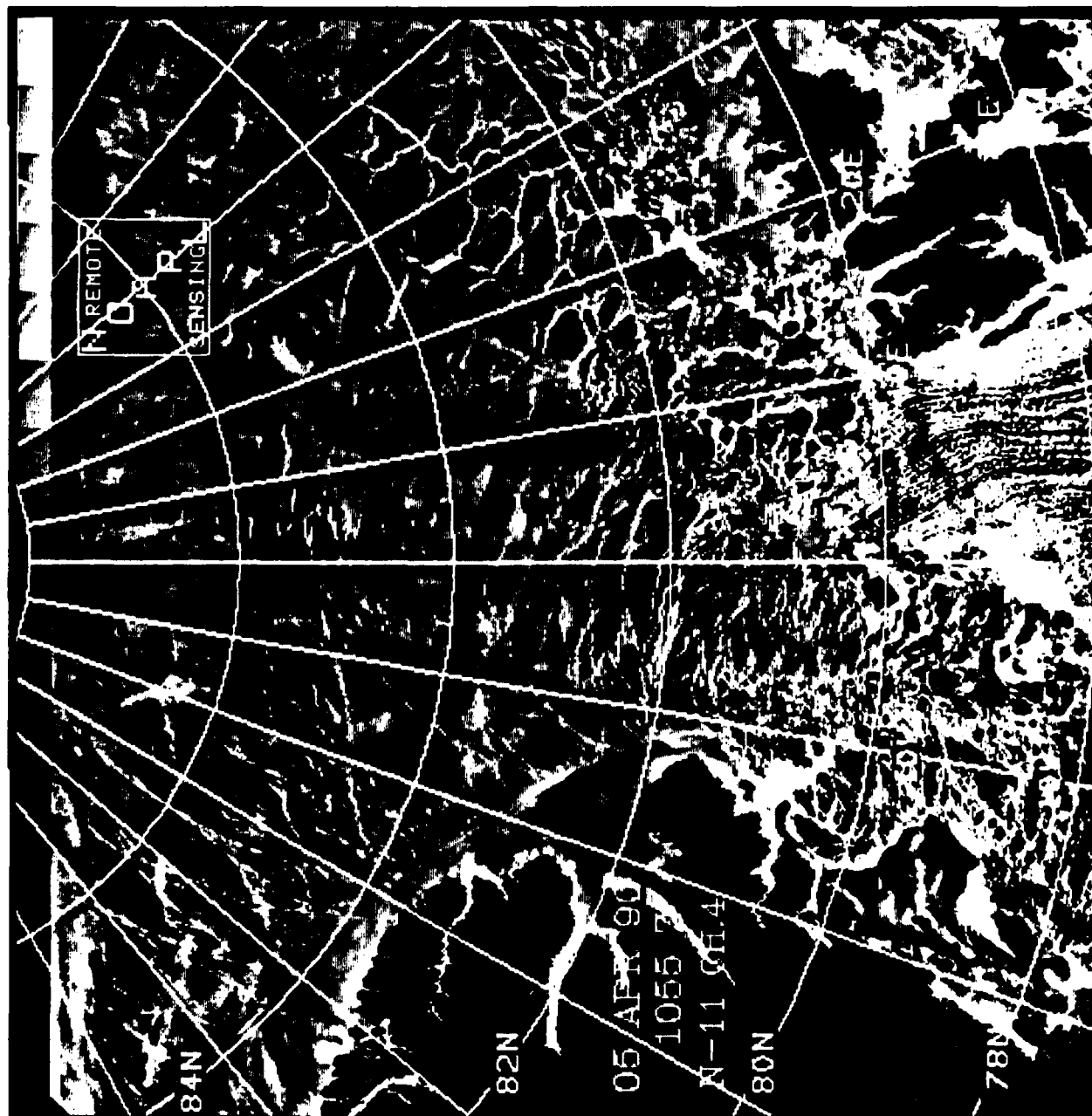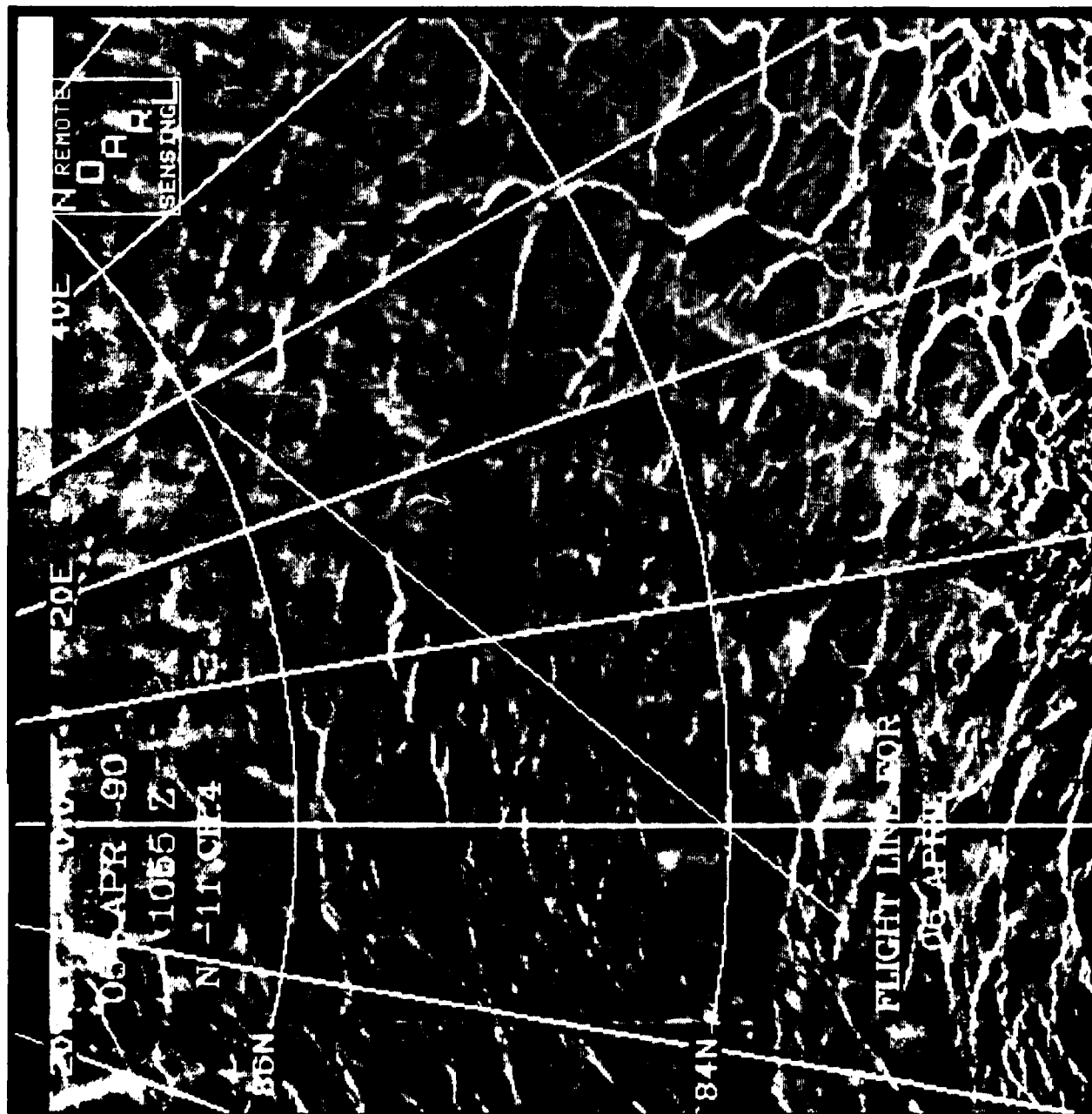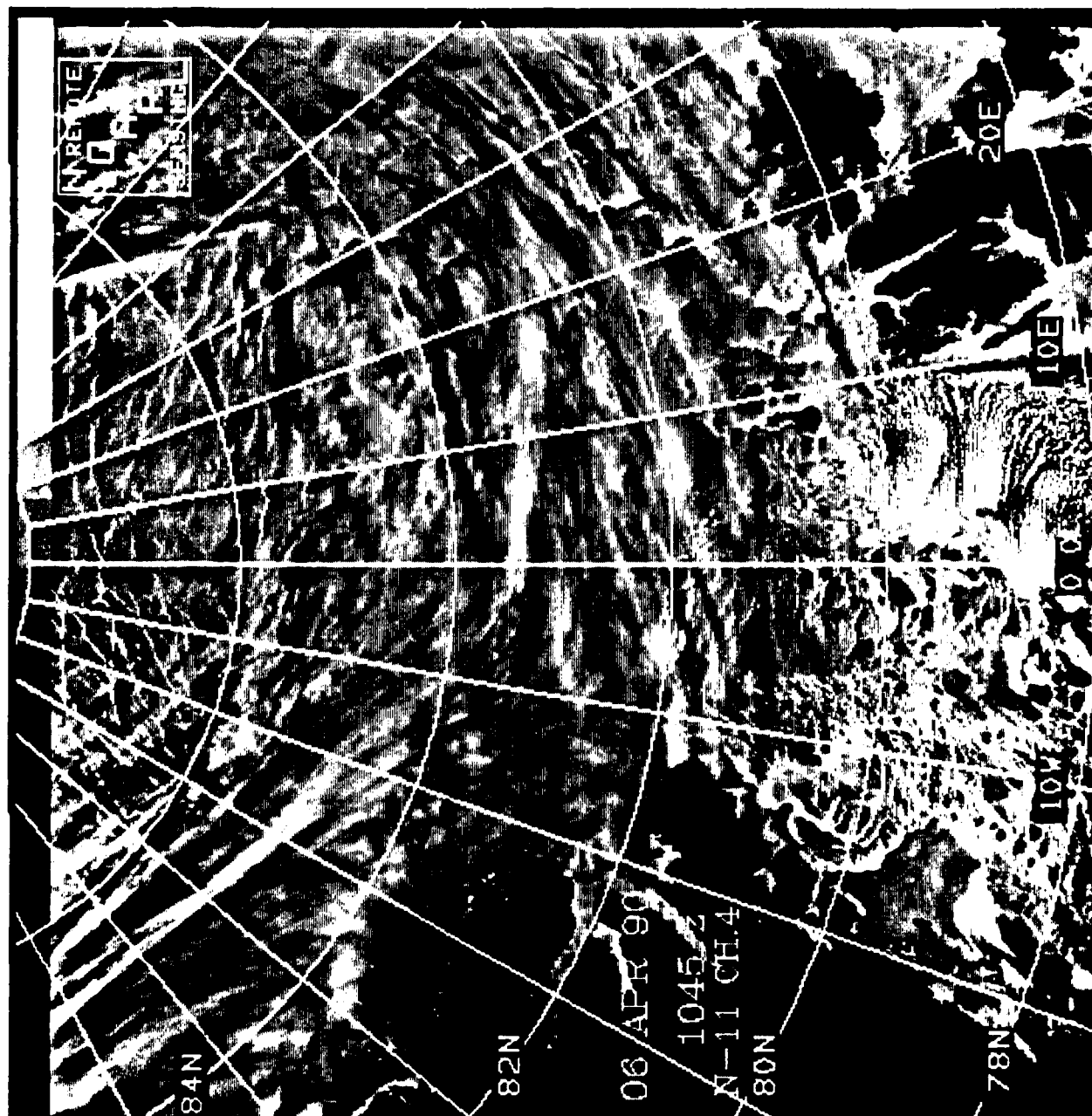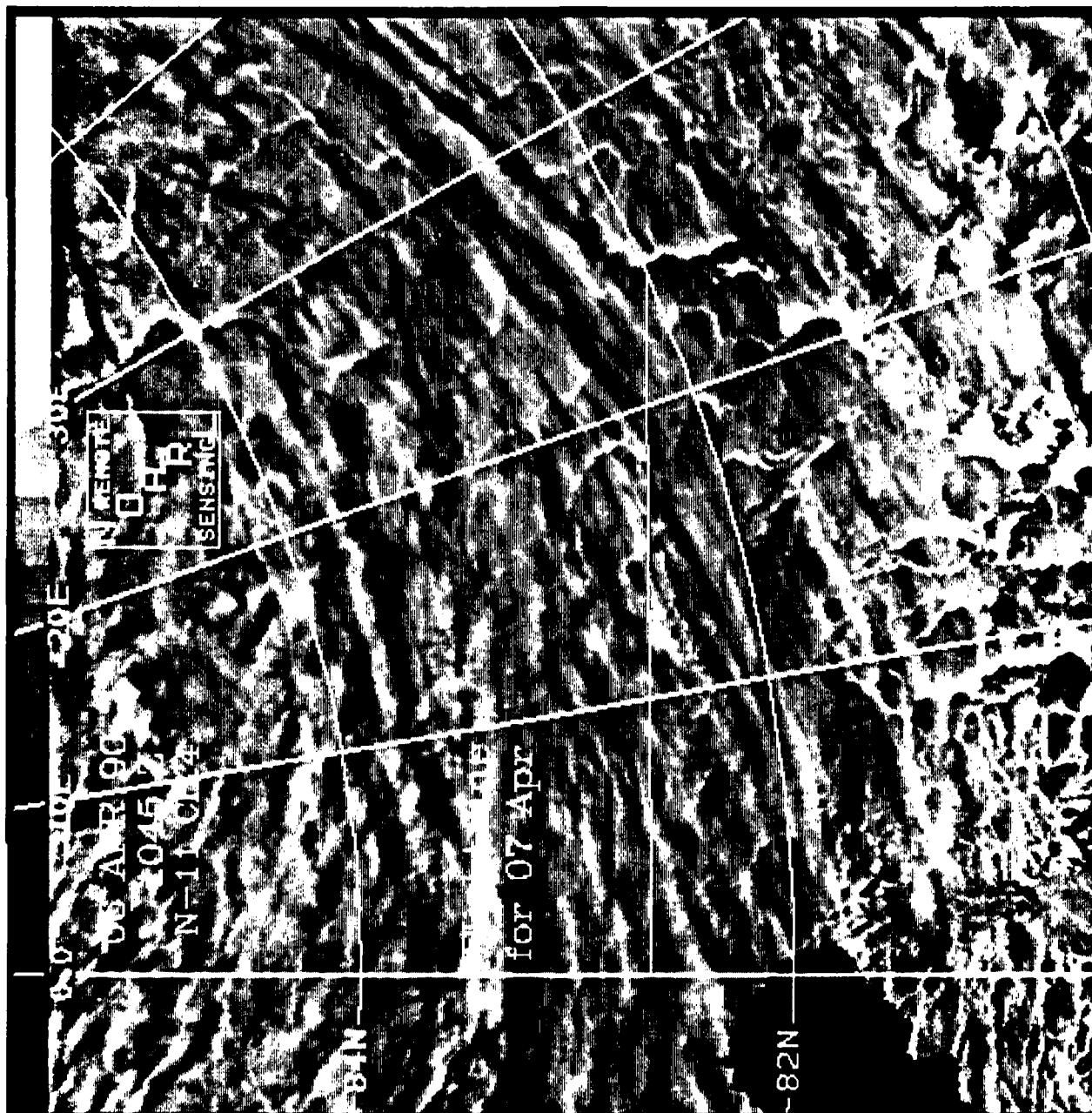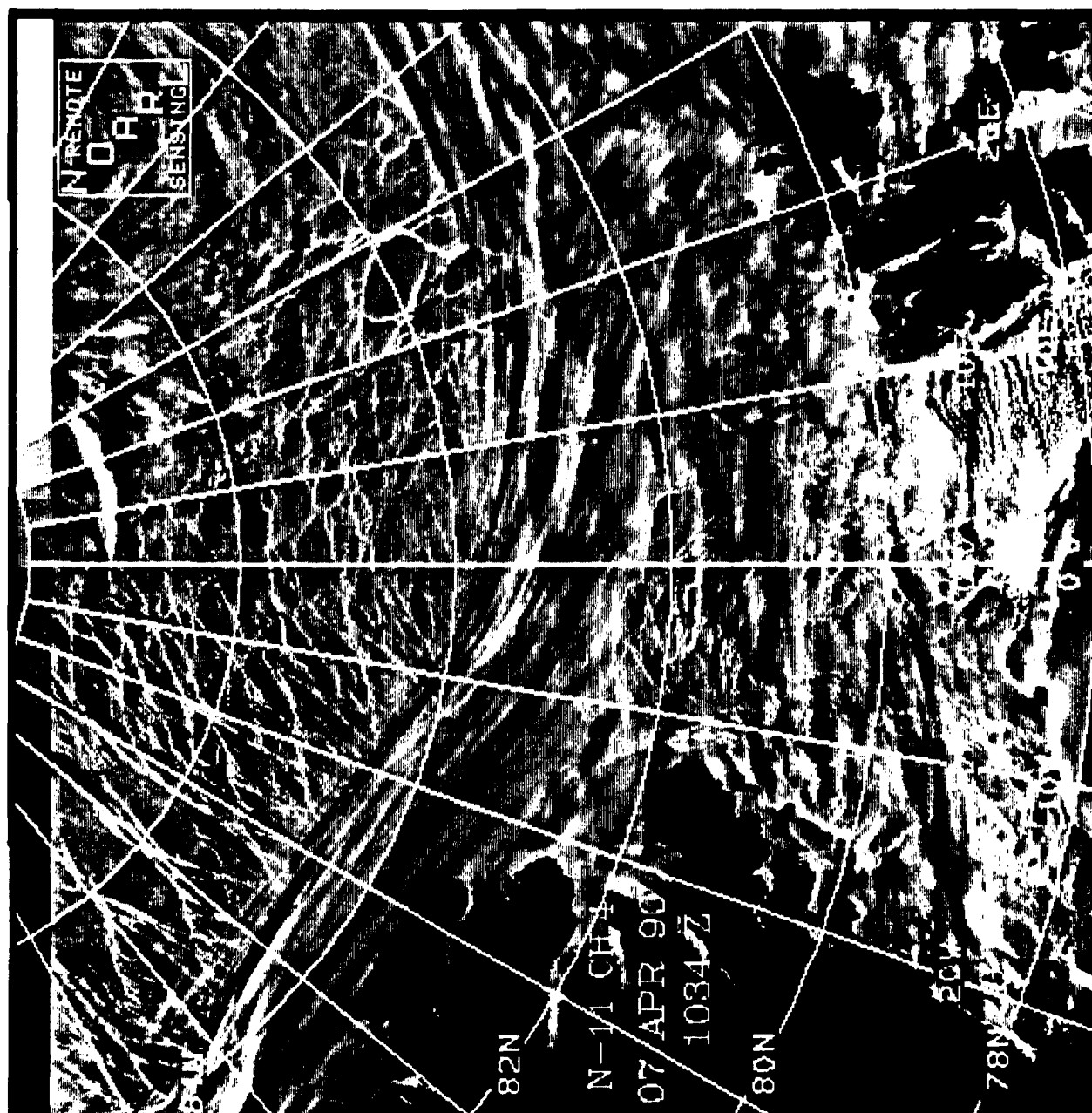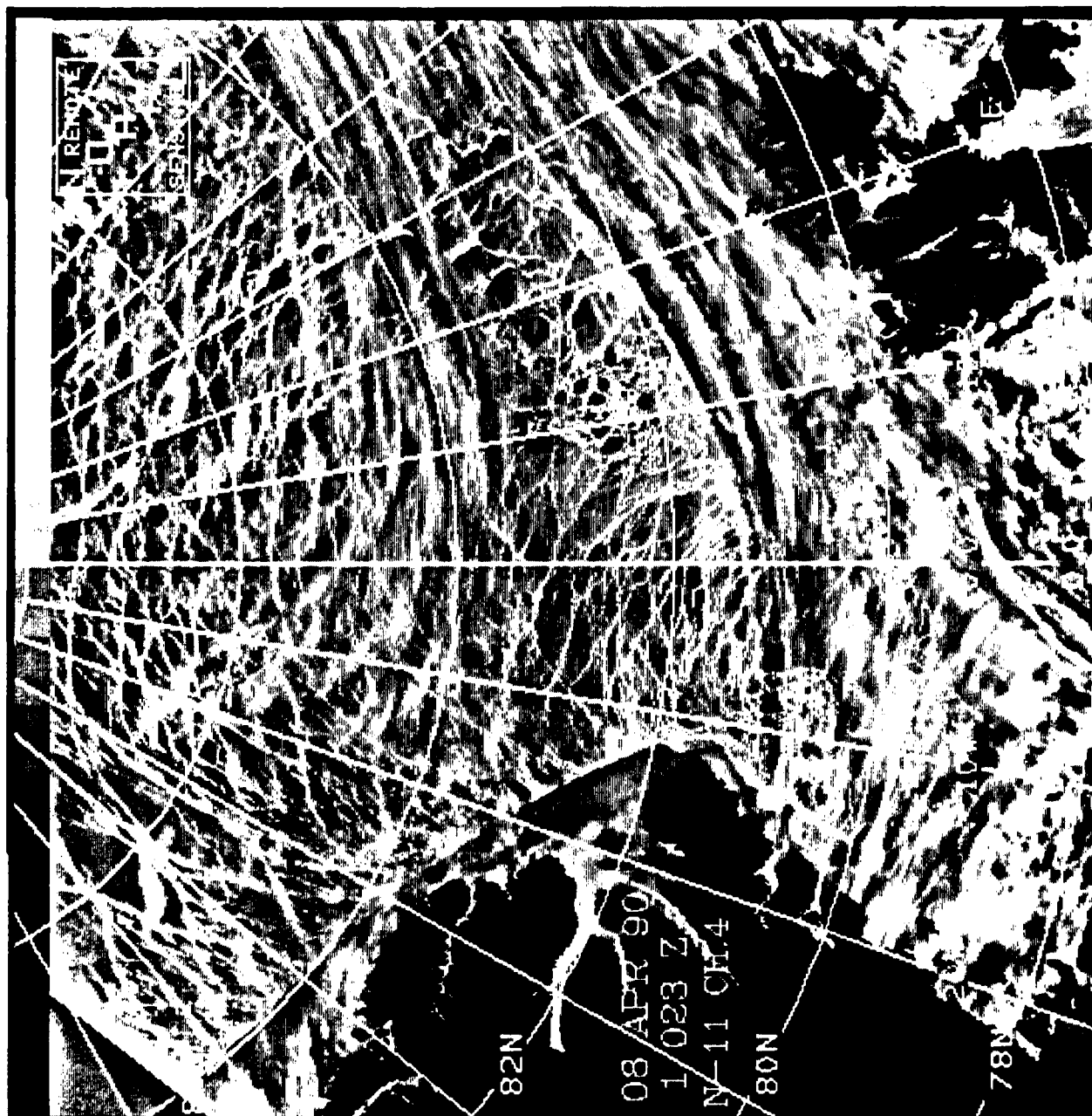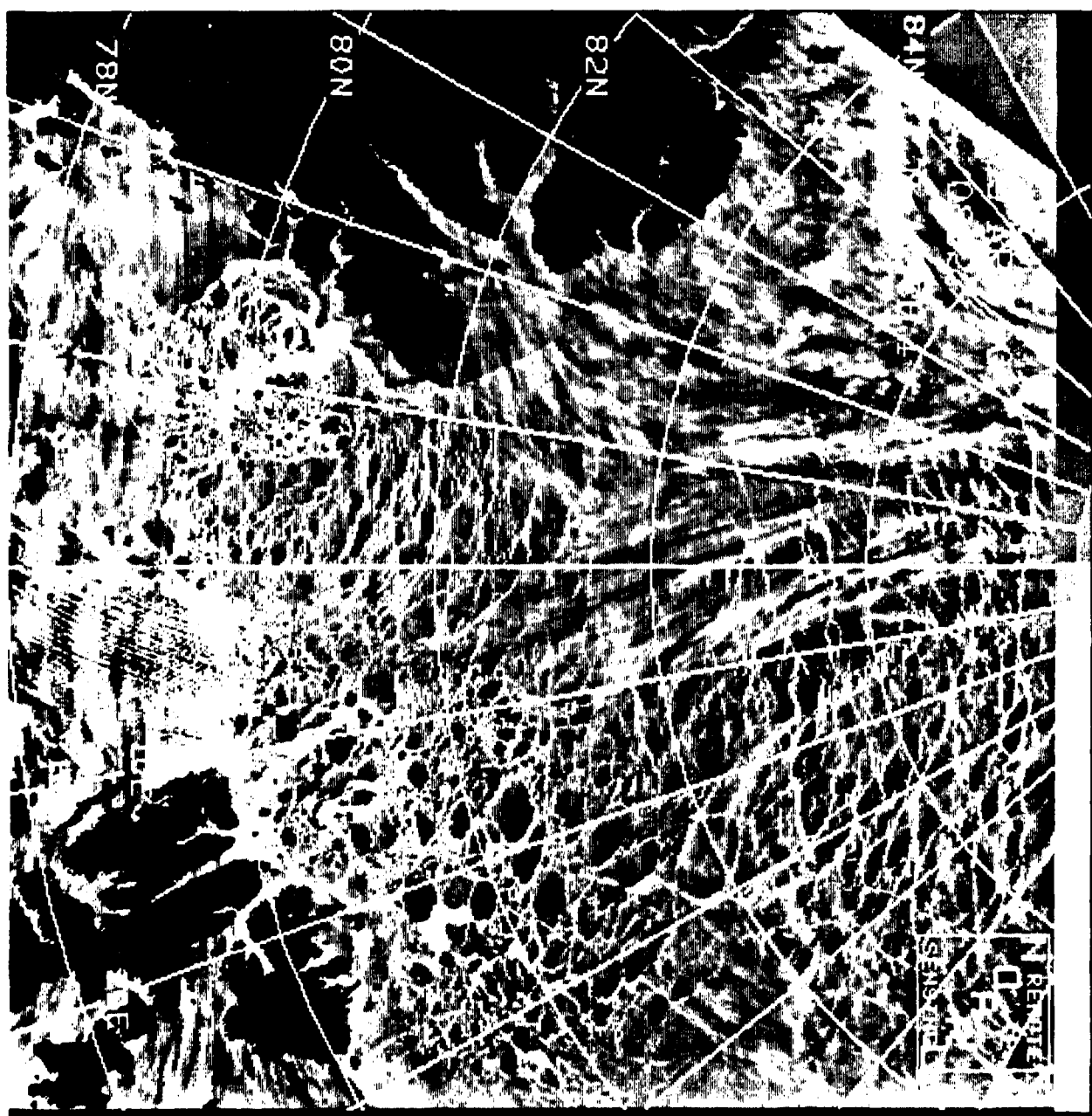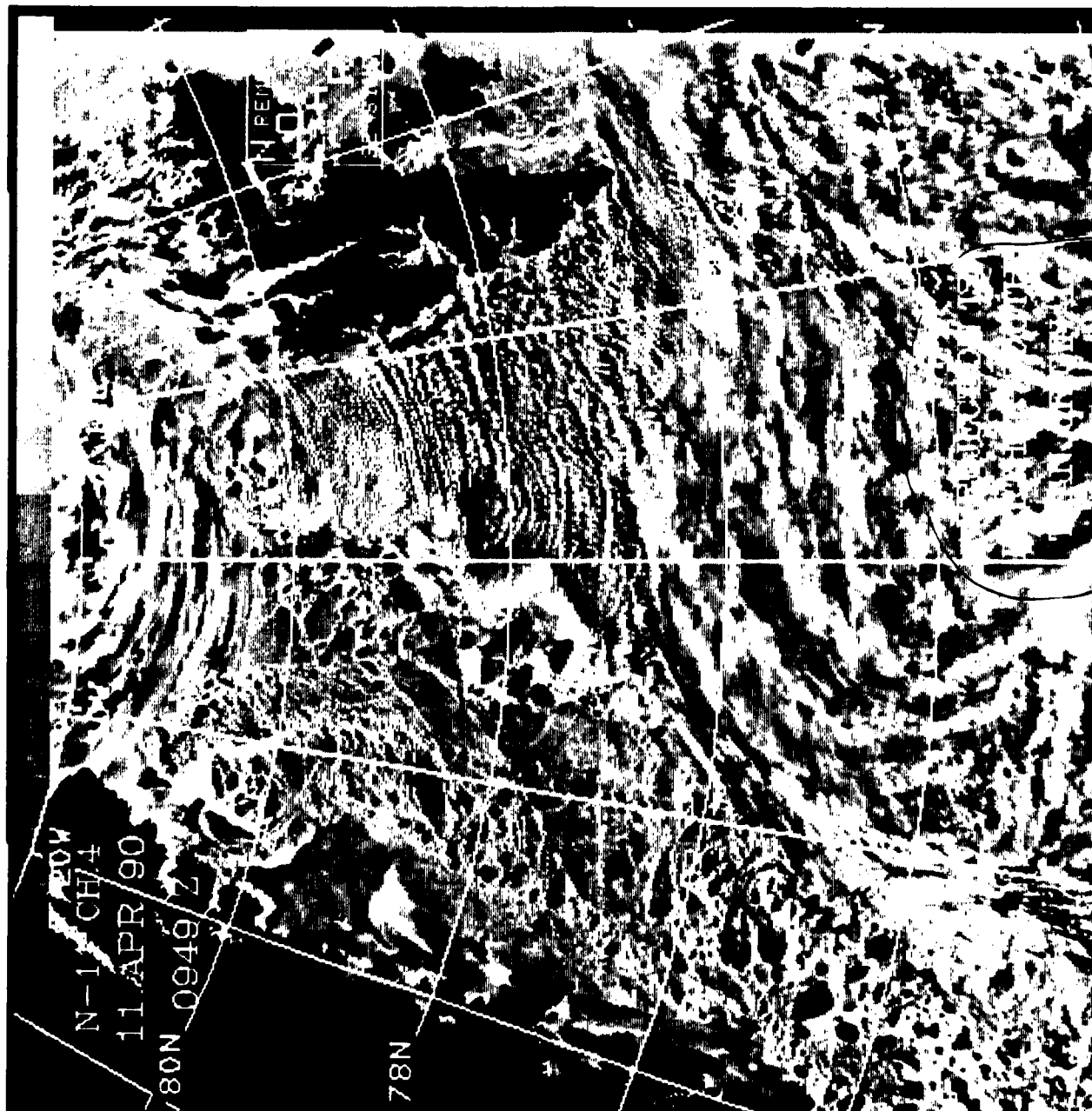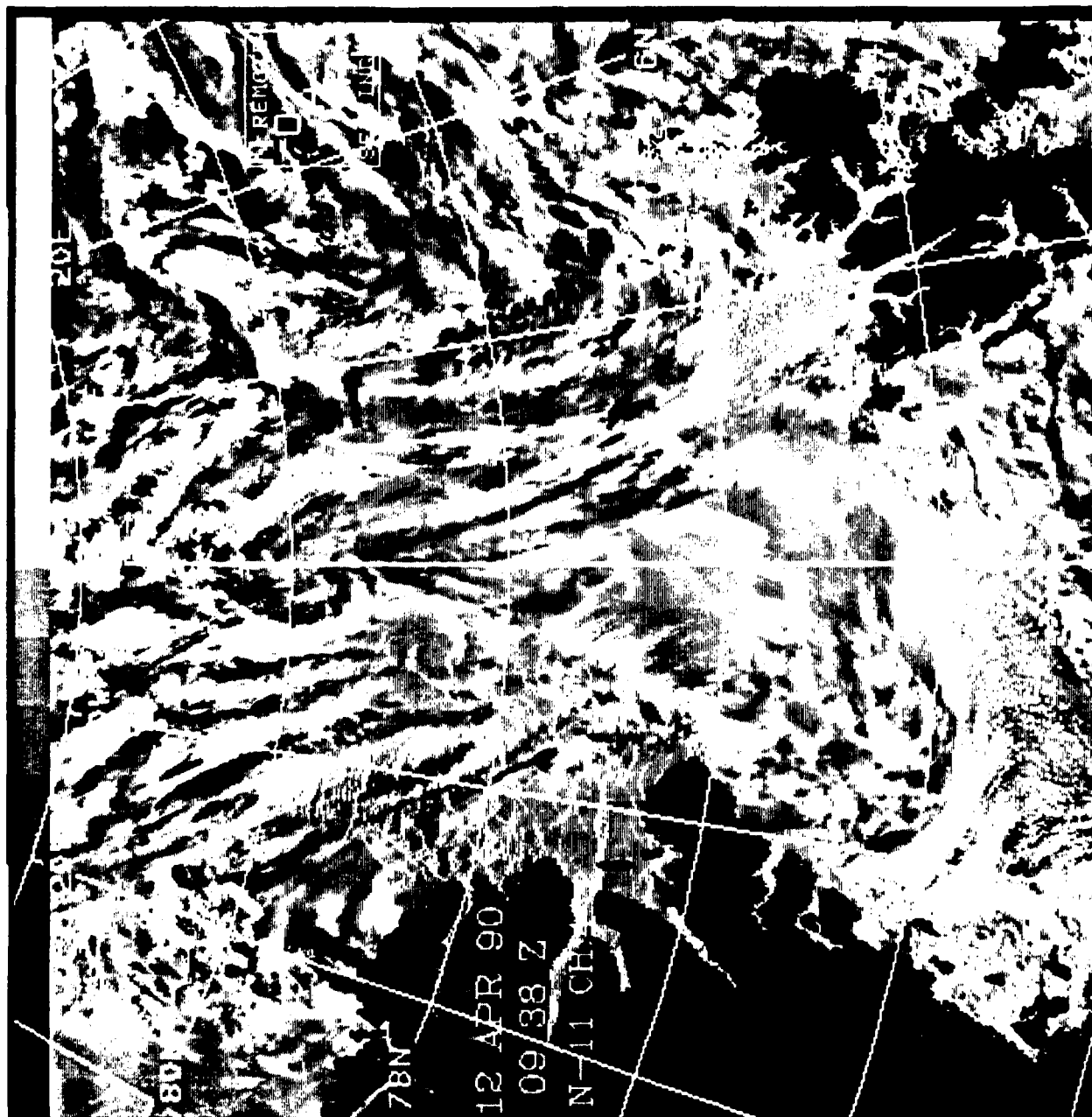
DISTRIBUTION LIST

Commander
Space and Naval Warfare Sys Com
Attn: CAPT Carl Hoffman
Code PMW-141
2511 Jefferson Davis Highway
Washington, DC 20363-5100

Oceanographer of the Navy
Chief of Naval Operations
Attn: OP-096B (R. Feden)
       OP-961E2 (J. Malay)
U.S. Naval Observatory
34th and Massachusetts Ave., NW
Washington, DC 20390-1800

Space and Naval Warfare Sys Com
Attn: LCDR Bill Cook
2511 Jeff Davis Hwy
Washington, DC 20363-5100

Naval Oceanography Command
Attn: Dr. Paul Moersdorf
Stennis Space Center, MS 39529

Commanding Officer
Fleet Numerical Oceanography Center
Attn: Capt Jack Jensen
Monterey, CA 93943-5004

Naval Oceanographic Office
Attn: Capt Charles A. Martinek
Stennis Space Center, MS 39529

Planning Systems, Inc.
Attn: Dr. R.L. Crout
115 Christian Lane
Slidell, LA 70458

BDM
Attn: Max Coon
16300 Christensen Road
Seattle, WA 98188

Navy/NOAA Joint Ice Center
Attn: Mr. Gary Whol
4301 Suitland Road
Washington, DC 20395

NOARL Liaison Office
Attn: Mr. Brooke Farquhar
Crystal Plaza #5, Room 802
2211 Jefferson Davis Highway
Arlington, VA 22202-5000

NOARL
Code 100
     105
     115
     125L (10)
     125P
     200
     300
     320
     321 (25 - 4 color)
     242 (C. Mire)
     322 (R. Preller)
     222 (P. Bucca)

Naval Postgraduate School
Attn: Dr. Curtis A. Collins, Chairman
Dept. of Oceanography, Code 68
Monterey, CA 93943

Commander
Naval Ocean Systems Center
Attn: Dr. Barbara Sotirin
San Diego, CA 92152-5000

NOARL Code 332
Attn: Dr. Duane Eppler
72 Lyme Road
Hanover, NH 03755-1290

Naval Oceanographic Office (MT)
Attn: Mr. Andrew Johnson
Stennis Space Center, MS 39529

Naval Oceanographic Office (MTR)
Attn: Mr. James Rigney
Stennis Space Center, MS 39529

Applied Physics Laboratory
Polar Science Center
Attn: Dr. R.A. Rothrock
1013 NE 40th Street
Seattle, WA 98105

NOARL West
Attn: Mr. Robert W. Fett
Code 441
Monterey, CA 93943-5006

Naval Polar Oceanography Center
Attn: Mr. David Benner
4301 Suitland Road
Washington, DC 20390

U.S. Naval Observatory
Attn: Mr. Donald Montgomery
34th and Massachusetts Ave., NW
Washington, DC 20392-1800

Applied Research Laboratories
Attn: Dr. Nancy Bedford
P.O. Box 8029
University of Texas at Austin
Austin, TX 78713-8029

Director
Office of Naval Technology
Attn: Dr. C.V. Votaw, Code 234
      Dr. M. Briscoe, Code 228
800 N. Quincy Street
Arlington, VA 22217-5000

Commanding Officer
Naval Research Laboratory
Attn: CAPT John J. Donegan, Jr.
Washington, DC 20375

Institute of Naval Oceanography
Attn: Dr. John Leese
Stennis Space Center, MS 39529

Naval Research Laboratory
Attn: Dr. Vincent Noble
Washington, DC 20375-5000

Naval Polar Oceanography Center
Attn: LCDR Kathy Garcia
4301 Suitland Road
Washington, DC 20390

Commander
Naval Oceanography Command
Attn: W. Shutt
Stennis Space Center, MS 39529

Sverdrup Technology, Inc.
Applied Math & Physics Section
Attn: Dr. Vivien Cambridge
Bldg. 2109
Stennis Space Center, MS 39529

Director
Office of Naval Research
Attn: Dr. E. Hartwig, Code 112
      Dr. E. Silva, Code 10D/10P
      Dr. C. Luther, Code 112D1
      Dr. T. Curtin
800 N. Quincy Street
Arlington, VA 22217-5000

Director
National Ocean Data Center
WSC1 Rm 103
6001 Executive Blvd
Attn: G.W. Withee
Rockville, MD 20852

Commander
Naval Oceanography Command
Attn: RADM J.E. Koehr
Stennis Space Center, MS 39529

NOARL
Attn: Dr. John Hovermale
Code 400
Monterey, CA 93943-5006

Naval Postgraduate School
Attn: Dr. C. Wash
Monterey, CA 93943

REPORT DOCUMENTATION PAGE

1. Agency Use Only (Leave blank).	2. Report Date. July 1990	3. Report Type and Dates Covered. Interim

4. Title and Subtitle.
Sea Ice Lead Statistics from Satellite Imagery of the Lincoln Sea during the ICESHELF Acoustic Exercise, Spring 1990

6. Author(s).
F. M. Fetterer, A. E. Pressman and R. L. Crout*

5. Funding Numbers.

Program Element No. 63704N

Project No.

Task No

Accession No. DN250003

7. Performing Organization Names(s) and Address(es).
Naval Oceanographic and Atmospheric Research Laboratory
Ocean Science Directorate
Stennis Space Center, Mississippi 39529-5004

8. Performing Organization Report Number.
NOARL Technical Note 50

9. Sponsoring/Monitoring Agency Name(s) and Address(es).
Space and Naval Warfare Systems Command
Washington, DC

10. Sponsoring/Monitoring Agency Report Number.
NOARL Technical Note 50

11. Supplementary Notes.
*Planning Systems Incorporated
Slidell, Louisiana

12a. Distribution/Availability Statement.

Approved for public release; distribution is unlimited.

12b. Distribution Code.

13. Abstract (Maximum 200 words).

During March and April of 1990, the Naval Oceanographic and Atmospheric Research Laboratory's (NOARL) Remote Sensing Branch collected Advanced Very High Resolution Radiometer (AVHRR) satellite imagery of the Lincoln Sea and Fram Strait in support of the ICESHELF and ICEX acoustic exercises. The Lincoln Sea imagery was analyzed for sea ice lead statistics using a new method based on the Hough transform. Products of the analysis such as lead orientation rose diagrams, lead spacing statistics, and the area covered by leads, are presented here along with the imagery from which the products were derived. Ice motion vectors for three time periods produced by an automated ice motion algorithm are also shown. Imagery of the Fram Strait is included in the appendix.

14. Subject Terms.
(U) Acoustic, (U) Satellite, (U) Exercises

15. Number of Pages.
136

16. Price Code.

17. Security Classification of Report. Unclassified	18. Security Classification of This Page. Unclassified	19. Security Classification of Abstract. Unclassified	20. Limitation of Abstract. SAR